

# Electro-Hydrostatic Actuator (EHA) Position Tracking and Correction

Electro-Hydrostatic Actuator (EHA) Position Tracking and Correction

A Thesis Submitted to the School of Graduate Studies in Partial Fulfillment of the  
Requirements for the Degree of Master of Applied Science in the Department of  
Mechanical Engineering, McMaster University, Hamilton, Canada

By  
Xiang Hu

Copyright Xiang Hu, December 2014. All rights reserved.

MASTER OF APPLIED SCIENCE (2014)      McMaster University  
(Mechanical Engineering)                      Hamilton

TITLE:                                      Electro-Hydrostatic Actuator (EHA) Position Tracking  
and Correction

AUTHOR:                                    Xiang Hu, B.ENG (McMaster University)

SUPERVISOR:                              Dr. Saeid R. Habibi, Professor  
Department of Mechanical Engineering

NUMBER OF PAGES:                      xii, 110

## **Permission to Use**

In presenting this thesis in partial fulfillment of the requirements for a Postgraduate degree from McMaster University, I agree that the Libraries of this University may make it freely available for inspection. I further agree that the permission for copying this thesis in any manner, in whole or in part for scholarly purposes, may be granted by the professors who supervised my thesis work or, in their absence, by the Head of the Department or the Faculty Dean in which my thesis work was conducted. It is understood that any copying or publication or use of this thesis or parts thereof for financial gain shall not be allowed without my written permission. It is also understood that due recognition shall be given to me and McMaster University in any scholarly use which may be made of any material in my thesis. Requests for permission to copy or to make other use of material in this thesis, in whole or part, should be addressed to:

Head of the Department of Mechanical Engineering

McMaster University

Faculty of Engineering

1280 Main Street West

Hamilton, Ontario L8S 4L6

Canada

## **Abstract**

The Electro-Hydrostatic Actuator (EHA) is a self-contained and modular hydraulic actuation system using feedback control. EHAs are being increasingly used in engineering and industrial systems that require high precision and efficiency such as aircrafts (Airbus 380), off-highway hydraulic hybrids and construction machineries. In this research, mathematical models (linear and nonlinear) with different control strategies (that include PID, PID with feedforward compensation, and Sliding Mode Control (SMC)) are developed and experimentally applied to an EHA prototype. These methods are then compared to a new control strategy that is a combination of Interacting Multiple Model concept, Sliding Mode Control (IMM-SMC) and the Smooth Variable Structure Filter (SVSF). The IMM and the SMC strategies are also applied with the Kalman Filter (KF) for comparison.

The above mentioned control strategies were implemented on an EHA prototype for position control under a range of fault conditions that were physically simulated. Both simulation and experimental results showed that the new IMM-SMC with SVSF outperformed all the other control strategies in terms of robustness and precision in trajectory tracking.

## **Acknowledgements**

The author would like to express his gratitude to his supervisor, Professor S.R. Habibi, for his guidance, advice and support during the course of this research and the writing of this dissertation. Special appreciations go to Dr. Dhafar Al-Ani for his dedication and tutoring throughout my research and writing the thesis. Also many thanks to all fellows in my research group, in particular Dr. Andrew Gadsden and Mr. Yu Song for assistance and support during my studies.

Financial support provided by the School of Graduate Studies, the Department of Mechanical Engineering and the Ontario Government's Graduate Scholarship Program is acknowledged and appreciated.

I would also like to express my gratitude to my parents for their encouragement and support.

## Table of Contents

Abstract .....	v
Acknowledgements .....	vi
Table of Contents .....	vii
List of Figures .....	x
List of Tables .....	xii
Chapter 1 .....	1
Introduction .....	1
1.1 Plan of Master Research .....	1
1.2 Problem Statement .....	2
1.3 Objective .....	3
1.4 Contribution .....	3
1.5 Summary of All Chapters .....	4
Chapter 2 .....	5
Literature Review .....	5
2.1 Sliding Mode Control (SMC) .....	5
2.1.1 Introduction to SMC .....	5
2.1.2 History of SMC .....	8
2.1.3 Lyapunov Stability Analysis in SMC .....	8
2.2 Filters (Estimation Techniques) .....	11
2.2.1 Kalman Filtering (KF) .....	11
2.2.2 The Smooth Variable Structure Filter (SVSF) .....	15
2.3 Multiple Model (MM) .....	21
2.3.1 Static Multiple Model .....	21
2.3.2 Dynamic Multiple Model .....	24
2.3.3 The Interacting Multiple Model Strategy .....	25
Chapter 3 .....	30
Electro -Hydrostatic Actuator (EHA) Introduction, Setup, and Models .....	30
3.1 Brief History on Aircraft Flight Surface Control .....	30

3.1.1.	Mechanical Linkages .....	31
3.1.2.	Flight Surface Control by Hydro-Mechanical Actuators .....	32
3.1.3.	Hydraulic Systems Incorporating the Fly-by-Wire Strategy.....	33
3.1.4.	Power-by-Wire strategy (PBW).....	33
3.2.	Electro Hydrostatic Actuation and the Experimental Prototype. ....	34
3.2.1.	Introduction to Hydraulic Systems.....	34
3.2.2.	The Basic EHA Structure.....	36
3.2.3.	McMaster`s EHA Prototype Overview .....	36
3.2.4.	Cause of Failure and Effects .....	38
3.2.5.	The EHA Configuration used in this Research Setup.....	39
3.3.	EHA Physical Fault Conditions Simulation.....	41
3.3.1.	Leakage Fault.....	42
3.3.2.	Friction Fault.....	44
3.4.	EHA Modeling.....	46
3.4.1.	Leakage Model.....	46
3.4.2.	Friction Model.....	48
Chapter 4.....		51
Control Strategies.....		51
4.1.	Existing controller: Misawa Based Sliding Mode Control Strategy .....	51
4.2.	New Design: Slotine and Li Based SMC Strategy.....	53
4.3.	IMM with SMC Strategy .....	58
4.4.	PID Control.....	61
4.5.1.	PID for EHA .....	63
4.5.2.	PID with Equivalent Control.....	63
Chapter 5.....		65
Experiment Results .....		65
5.1.	Initial Experiment Setup .....	65
5.1.1.	EHA Input and its Simulated Fault Conditions.....	66
5.1.2.	EHA Mathematic Models .....	67
5.2.	IMM Implementation.....	71

5.3. Controllers Simulation Results ..... 77

5.4. Controllers Experimental Results ..... 90

5.5. Conclusion ..... 104

Chapter 6..... 105

Remark Conclusions and Future Work..... 105

    Future Work Recommendation..... 106

Bibliography ..... 107

## List of Figures

Figure 1.1: Research Flowchart .....	2
Figure 2.2: SVSF State Estimation Concept, [4] .....	16
Figure 2.3: Proper Smoothing Boundary Layer, [24] .....	18
Figure 2.4: Improper Smoothing Boundary Layer, Chattering, [24] .....	18
Figure 2.5: VBL Working Concept, [24] .....	19
Figure 2.6: Static MM For $r = 2$ Fixed Models, [18] .....	21
Figure 3.1: Primary Flight Surfaces Control for Different Types of Motion, [31] .....	30
Figure 3.2: Flight Surface Controlled by Mechanical Linkages, [32] .....	32
Figure 3.3: Hydro-Mechanical Flight Surface, [33].....	32
Figure 3.4: Valve Controlled Hydraulic System, [35] .....	35
Figure 3.5: Pump Controlled Hydraulic System, [35] .....	35
Figure 3.6: Basic Structure of EHA, [37] .....	36
Figure 3.7: EHA Prototype Apparatus.....	37
Figure 3.8: EHA Basic Scheme Plot.....	37
Figure 3.9: EHA Simplified Diagram, [4] .....	41
Figure 3.10: Actuator Velocity vs. Throttling Valve Input.....	43
Figure 3.11: Differential Pressures vs. Throttling Valve Input.....	45
Figure 3.12: Actuator Flow Rate vs. Differential Pressure .....	47
Figure 3.13: Friction Force vs. Actuator Velocity .....	49
Figure 4.1: IMM Overall Concept .....	27
Figure 4.2: SMC-IMM Basic Structure .....	58
Figure 4.3: IMM-SMC Flowchart.....	61
Figure 4.4: PID Control .....	63
Figure 4.5: PID with Equivalent Control .....	64
Figure 5.1: EHA Input Motor Angular Velocity.....	66
Figure 5.2: Position Plot .....	70
Figure 5.3: Velocity Plot.....	70
Figure 5.4: Acceleration Plot .....	70
Figure 5.6: Leakage Condition with Nonlinear Model .....	72
Figure 5.7: Friction Condition with Nonlinear Model .....	73
Figure 5.8: Combined Condition with Nonlinear Model .....	73
Figure 5.9: Normal Condition with Linear Model .....	74
Figure 5.10: Leakage Condition with Linear Model.....	74
Figure 5.11: Friction Condition with Linear Model.....	75
Figure 5.12: Combined Condition with Linear Model.....	75
Figure 5.13: Misawa based SMC Simulation .....	80
Figure 5.14: Misawa based IMM-SMC-KF Simulation .....	81

Figure 5.15: Misawa based IMM-SMC-SVSF Simulation.....	82
Figure 5.16: Slotine and Li based SMC Simulation .....	83
Figure 5.17: Slotine and Li based IMM-SMC-KF Simulation .....	84
Figure 5.18: Slotine and Li based IMM-SMC-SVSF Simulation.....	85
Figure 5.19: Simulation Position Errors of Misawa based SMC, IMM-SMC-KF and IMM-SMC-SVSF .....	87
Figure 5.20: Simulation Position Errors of Slotine and Li based SMC, IMM-SMC-KF and IMM-SMC-SVSF .....	88
Figure 5.21: PID Controller .....	91
Figure 5.22: PID Controller with Equivalent Control.....	92
Figure 5.23: Misawa Based SMC Experimental Result.....	93
Figure 5.24: Misawa Based IMM-SMC-KF Experimental Result .....	94
Figure 5.25: Misawa Based IMM-SMC-SVSF Experimental Result.....	95
Figure 5.26: Slotine and Li Based SMC Experimental Result.....	96
Figure 5.27: Slotine and Li Based IMM-SMC-KF Experimental Result .....	97
Figure 5.28: Slotine and Li Based IMM-SMC-KF Experimental Result .....	98
Figure 5.29: Position Errors of PID, PID Equivalent Control and SMCs.....	100
Figure 5.30: Position Errors of Misawa Based SMC, IMM-SMC-KF and IMM-SMC-SVSF....	101
Figure 5.31: Position Errors of Slotine and Li Based SMC, IMM-SMC-KF and IMM-SMC-SVSF .....	102

**List of Tables**

Table 3.1: Actuator Velocity vs. Throttling Valve Input ..... 44

Table 3.2: Differential Pressure vs. Throttling Valve Input..... 46

Table 5.1: EHA Fault Conditions ..... 66

Table 5.2: EHA Nonlinear Model Parameters ..... 68

Table 5.3: EHA Nonlinear Model Leakage Coefficients ..... 68

Table 5.4: EHA Nonlinear Model Friction Coefficients..... 68

Table 5.5: EHA Linear Model Leakage Coefficients ..... 69

Table 5.6: EHA Linear Model Friction Coefficients ..... 69

Table 5.7: Simulation Root Mean Square Errors ..... 89

Table 5.8: Experimental Root Mean Square Errors ..... 103

## **Chapter 1**

### **Introduction**

Hydraulic systems have been widely used in modern engineering applications; including aircraft flight control, vehicle suspension and brake, and construction machinery. Hydraulic systems are even being considered for futuristic technologies, such as powered exoskeletons for potential military and civilian usage, [1, 2]. Hydraulic systems have the advantage of higher torque to mass ratio at the actuator level compared to mechanical (i.e., traditional or conventional) systems; a feature that makes them suitable for heavy duty applications.

#### **1.1 Plan of Master Research**

The general overview of the research is shown in Figure 1.1. The research uses an Electro-Hydrostatic actuator (EHA) prototype designed and developed by K. McCullough, [3]. The experimental studies reported in this thesis have all been implemented on this prototype. These studies pertain to the implementation of trajectory tracking control strategies under normal and fault conditions. Previously, EHA fault conditions were studied and characterized by Y. Song, [4]. He also implemented a fault detection and diagnosis (FDD) strategy using the Interacting Multiple Model (IMM) concept. In this research, Song's FDD method was used in conjunction with two control strategies that were Proportional-Integral-Derivative (PID) and Sliding Mode Control

(SMC). Moreover, different filtering techniques have been implemented with these control strategies to improve the control as well as the fault detection and diagnosis performance of EHA systems. Figure 1.1 illustrates the flowchart of the research.

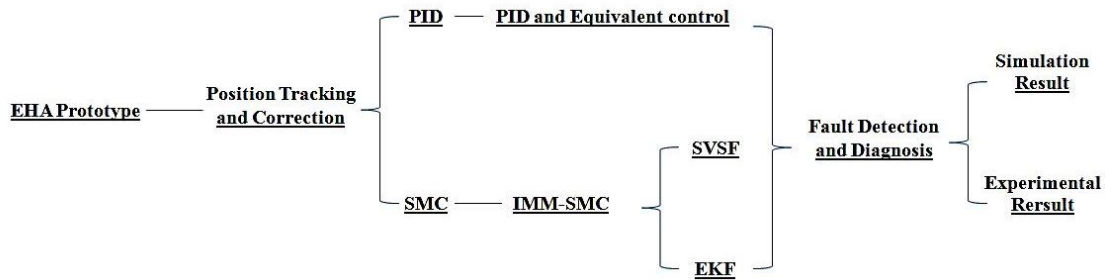


Figure 1.1: Research Flowchart

## 1.2 Problem Statement

In any type of systems, unexpected fault conditions may occur. A minor fault situation may cause the system efficiency and performance to deviate from norm and/or deteriorate; a major fault condition may cause a system failure. Fault detection and diagnosis and fault tolerant strategies are two important concepts that need to be considered in hydraulic systems to enhance their safety. This thesis considers a form of hydraulic actuation known as Electro-Hydrostatic Actuation (EHA) systems and uses a prototype of an EHA to implement novel fault tolerant control strategies. This EHA prototype has been specifically designed for research into flight control actuation. An EHA is a self-contained modular closed circuit hydraulic system that is based on the concept of displacement control. Generally speaking, an EHA consists of a controller, a motor, a pump, a hydraulic circuit, and an actuator. The main objective of this research is

to investigate the effects of different fault conditions on the EHA and to implement a novel robust control strategy.

### **1.3 Objective**

The goal of this research is to maintain the EHA's closed loop performance when there are unexpected fault conditions. To fulfill this objective, a robust control strategy using Sliding Mode Control (SMC) combined with the Interacting Multiple Model (IMM) concept referred to as IMM-SMC has been proposed, designed and implemented on the above mentioned EHA prototype. The performance of the IMM-SMC has also been comparatively evaluated.

### **1.4 Contribution**

A real time SMC strategy has been developed in this thesis. This SMC strategy is based on Slotine and Li's SMC method. By providing robustness control performance under leakage fault and friction fault conditions, this strategy demonstrate higher accuracy in trajectory tracking application than other investigated methods in this research such as PID, PID with feedforward compensation and E. A. Misawa's SMC theory based controller. Also, a combined control strategy IMM-SMC is studied, which improves the SMC tracking performance further.

## **1.5 Summary of All Chapters**

The thesis is structured as follows: Chapter 2 provides a literature review on sliding mode control, estimation techniques, and the multiple model concept. Flight control actuation developments, overview of an EHA prototype used in this research and its fault conditions, and EHA prototype model are provided in Chapter 3. The control strategies including the new SMC strategy with feedforward compensation, and IMM are explained in Chapter 4. These control strategies have been applied to the EHA prototype; their design and implementation results are presented in Chapter 5. Chapter 6 provides the conclusions from this research with future work and recommendations.

## Chapter 2

### Literature Review

Chapter 2 briefly provides a literature review on Sliding Mode Control (SMC) as well as robust estimation techniques (such as the Kaman Filter (KF) and the Smooth Variable Structure Filter (SVSF)). The chapter starts with a history of the SMC, its background, and its basic concepts. The Lyapunov stability criterion is then reviewed and the stability issues associated with designing and implementing SMCs on real-world engineering systems are discussed. Two well-known and commonly used estimation techniques: the Kalman filter (KF) and the Smooth Variable Structure Filter (SVSF) are briefly reviewed. The Multiple Model (MM) concept and its applications to the EHA are also considered.

#### 2.1. Sliding Mode Control (SMC)

##### 2.1.1. Introduction to SMC

Variable Structure Systems (VSS) are systems that have a discontinuity in their state space, [8]. In either side of the discontinuity, the system can be modeled by a continuous and differentiable function. Consider the following VSS:

$$\dot{x} = \Phi(x, u, t) \tag{2.1}$$

$$\Phi(x, t) = [\varphi_1(x, u, t), \varphi_2(x, u, t), \dots, \varphi_n(x, u, t)]^T \tag{2.2}$$

where  $x$  is the state vector,  $u$  is the control input, and  $t$  is the time variable.

$\varphi_n(x, u, t)$  are differentiable functions describing the state space regions segmented by discontinuity surfaces. At the boundary between two  $\varphi_n(x, u, t)$ , the behavior is discontinuous, and  $\Phi(x, t)$  is not differentiable.

By extending the study into Variable Structure Control (VSC), a special form of VSC is created by forcing the states to move towards a discontinuity surface and to sliding along it. This special form is called sliding mode control (SMC), [9]. SMC forces the system to behave under a reduced order form that is robust to bounded disturbances. There are two key elements in a SMC design that are the switching hyper-plane and the discontinuous control input.

The Switching hyper-plane can be defined as:

$$s(x) = 0 \quad (2.3)$$

where  $s$  is the distance of the state trajectory from the hyper-plane that under ideal circumstances would be zero. The discontinuous control input  $u$  forces the states to converge and then slide along the hyper-plane by using a switching action. It is defined as:

$$\begin{aligned} u(t) &= u^+(t), \text{ if } s(x) > 0 \\ &= u^-(t), \text{ if } s(x) < 0 \end{aligned} \quad (2.4)$$

Under sliding mode, the switching occurs at a high frequency, resulting in an unwanted effect known as chattering. Eqs. (2.1), (2.3) and (2.4) are the general form of SMC system, [8]:

$$\begin{aligned} \dot{x} &= \Phi(x, u, t) \\ s(x) &= 0 \end{aligned} \quad (2.5)$$

$$\begin{aligned}
 u(t) &= u^+(t), \text{ if } s(x) > 0 \\
 &= u^-(t), \text{ if } s(x) < 0
 \end{aligned}$$

SMC has two phases: the reaching mode and the sliding mode. During the reaching phase, the system states are forced to move toward the hyper-plane. Eq. (2.6) specifies the reaching condition that guarantees the reachability and stability, [10]:

$$\begin{aligned}
 \dot{s} < 0, \text{ if } s(x) > 0 \quad \text{or} \quad \dot{s}s < 0 \\
 \dot{s} > 0, \text{ if } s(x) < 0
 \end{aligned} \tag{2.6}$$

The reaching condition determines the manner of how the sliding surface is reached; there are three different ways of determining this as follows, [11]:

(1) - Constant approaching law: switching function reaching zero with constant velocity as:

$$\dot{s} = -\epsilon * \text{sgn}(s) \tag{2.7}$$

where  $\epsilon$  is a constant positive number.

(2) - Proportional approaching law: on the basis of Eq. (2.7), adding another proportional gain to the distance to the hyper-plane:

$$\dot{s} = -\epsilon * \text{sgn}(s) - k * s \tag{2.8}$$

where  $\epsilon$  and  $k$  are constant positive numbers.

(3) - Exponential approaching law:

$$\dot{s} = -k * |s|^\alpha, k > 0, 1 > \alpha > 0 \tag{2.9}$$

where  $k$  is a constant positive number,  $\epsilon$  is a constant positive number less than 1.

After reaching the switching surface, the system changes to a sliding mode. In this step, the system dynamic is governed by its reduced order form and is robust to disturbances.

### 2.1.2. History of SMC

The development of SMC algorithms has progressed through four stages: the originating stage, the early stage, the multi-input stage and the advanced stage, [11].

(1) - The originating stage is from 1930s to 1957. During this period, the basic concept of SMC was developed, [8].

(2) - During the early stage of SMC (1957-1970), high order, linear differential equations were studied with switching surface being defined as second order, [8].

(3) - From 1970 to 1980, SMC theory evolved to include general multi-input systems using a state space form:  $\dot{x} = Ax + Bu$ .

(4) - In the 1980s, the SMC studies gained acceptance in the west. A number of researchers worked on SMC theory with excellent achievements; these included the work by E. Misawa, [5, 6], J.J. E. Slotine, and Weiping Li, [7], S.J. Zhu, [8], H. Asada and J.J. E. Slotine, [12], E. Bailey and A. Arapostathis, [13], C. M. Dorling and A. S. Zinober, [14], , C. M. Dorling, [15], S.R. Habibi and R. J. Richards, [16], W. B. Gao and J. C. Hung, [17], M. Chaouki and G. Moncef, [18].

### 2.1.3. Lyapunov Stability Analysis in SMC

An important consideration for control systems is stability. Systems may be classified into stable, unstable, or marginally-stable categories. According to N.S. Nise, [19], if the natural response goes to zero as time goes to infinity, then it is said that the system is stable; if the natural response goes to infinity as time goes to infinity, then the system is unstable; and if the natural response does not go to zero or infinity, but oscillates at its natural frequency as time goes to infinity, then it is said to be marginally-stable. By

treating natural response and forced response as total response, stability can be defined as: “for every bounded input comes with a bounded output (BIBO)”, the system is stable; while “for a bounded input provides an unbounded output”, the system is unstable.

There are different methods used for assessing a system's stability, such as the Routh Hurowitz's stability, [19], and Nyquist stability [20] criteria. However, these criteria are only applicable to linear systems. For a nonlinear or time-varying system, other stability criteria are needed. The second method of Lyapunov is a general tool used for proving the stability of nonlinear systems, [20]. The Lyapunov's first method is relatively complex and requires an explicit form of solution for the system model expressed as differential equations. The second method is easier since it can determine stability using a simpler form using a Lyapunov function that is basically a measure of energy. Starting with a basic nonlinear/time-varying system, [20]:

$$\dot{\mathbf{x}} = \mathbf{f}(\mathbf{x}, t)$$

where  $\mathbf{x}$  is the state vector,  $t$  is time, and  $\mathbf{f}$  is a function of  $\mathbf{x}$  and  $t$ . Let the initial conditions be defined as the initial state vector  $\mathbf{x}_0$  and initial condition  $\Phi(t, (\mathbf{x}_0, t_0))$ .

- **Equilibrium State**

A state  $\mathbf{x}^*$  is an equilibrium state (equilibrium point) of the system if once  $\mathbf{x}(t)$  is equal to  $\mathbf{x}^*$ , it remains equal to  $\mathbf{x}^*$  for all future time (which means  $\mathbf{x}^*$  must satisfy  $\mathbf{0} = \mathbf{f}(\mathbf{x}^*)$ ), [7].

For a linear, time-invariant system,  $\dot{\mathbf{x}} = \mathbf{A}\mathbf{x}$ , it has a single equilibrium point (the origin  $\mathbf{0}$ ) if  $\mathbf{A}$  is non-singular. If  $\mathbf{A}$  is singular, it has an infinity many of equilibrium points, which are contained in the null-space of the matrix  $\mathbf{A}$  (i.e.,  $\mathbf{A}\mathbf{x} = \mathbf{0}$ ).

- **Stability in the Sense of Lyapunov**

For an equilibrium state  $x_e$ , assume a spherical region with radius  $r$  around it:

$$\|x - x_e\| = [(x_1 - x_{1e})^2 + (x_2 - x_{2e})^2 + \dots + (x_n - x_{ne})^2]^{1/2} \leq r$$

Let  $S(\delta)$  consist of all initial states  $x_0$  that satisfy  $\|x_0 - x_e\| \leq \delta$ , then, let  $S(\varepsilon)$  consist of all points that satisfy  $\Phi(t, (x_0, t_0)) - x_e \leq \varepsilon$  for any time  $t > t_0$ . For any equilibrium state  $x_e$  (is called stable in the sense of Lyapunov), *if* for any given  $\varepsilon$ , there is an  $S(\delta)$ , so that any trajectories that start in  $S(\delta)$  will not leave  $S(\varepsilon)$ , as time  $t$  goes to infinity, [20].

- **Asymptotic Stability**

For any equilibrium state  $x_e$  to be asymptotically stable, the state  $x_e$  must satisfy the stability in the sense of Lyapunov. Furthermore, for every solution of  $\Phi(t, (x_0, t_0))$  that starts in  $S(\delta)$  converges  $x_e$  as  $t$  goes to infinity. Asymptotic stability is also known as local stability, since only trajectories starting within the region of attraction converge to the origin. If the region of attraction expands to all of the state space, then asymptotic stability becomes global stability, [8].

- **Second Method of Lyapunov**

The Lyapunov's Second method is based on three theorems as follows, [7, 20].

**Theorem 1:** For the system:  $\dot{x} = f(x, t)$  with  $f(0, t) = 0$  for all  $t > t_0$ , *if* there exists a scalar function  $V(x, t)$  having continuous, first partial derivatives and satisfying the conditions:  $V(x, t)$  is positive definite and  $\dot{V}(x, t)$  is negative definite, the equilibrium state at the origin is uniformly asymptotically stable.

**Theorem 2:** For the system:  $\dot{x} = f(x, t)$  with  $f(0, t) = 0$  for all  $t > t_0$ , *if* there exists a scalar function  $V(x, t)$  having continuous, first partial derivatives and satisfying the

conditions:  $V(x, t)$  is positive definite and  $\dot{V}(x, t)$  is negative semi-definite for any initial state  $(x_0 (\neq 0), t_0)$ , then the equilibrium state at the origin of the system is uniformly asymptotically stable in the large.

**Theorem 3:** For the system:  $\dot{x} = f(x, t)$  with  $f(0, t) = 0$  for all  $t > t_0$ , if there exists a scalar function  $V(x, t)$  having continuous, first partial derivatives and satisfying the conditions:  $V(x, t)$  is positive definite in some region about the origin and  $\dot{V}(x, t)$  is positive definite in the same region, the equilibrium state at the origin unstable.

## 2.2. Filters (Estimation Techniques)

### 2.2.1. Kalman Filtering (KF)

The Kalman filter (KF) ranks amongst the most important contributions to the field of control engineering. It is an estimation and filtering strategy for stochastic system that was proposed by Rudolph Kalman in 1960.

The Kalman filter is an optimal strategy if the system model is known and, noise is white, [21, 22]. The Kalman filter has been applied to many problems, such as process control, flood prediction, tracking and navigation. Successful applications of the Kalman filter include NASA's lunar and Apollo missions, [23].

Figure 2.1 is a flowchart of the Kalman filter in a summarized form. At every estimation interval, an a priori state estimate is calculated using the system model. The estimated states are then projected to a priori output estimates and, then the error between the measured and the estimated a priori system output is calculated, referred to as the filter innovation. An optimal correction is applied to the a priori state estimates to form

improved a posteriori estimates using the filter innovation. This process is repeated at every sampling interval. An outcome of the process is also an error covariance matrix that provides a measure of the filter's performance.

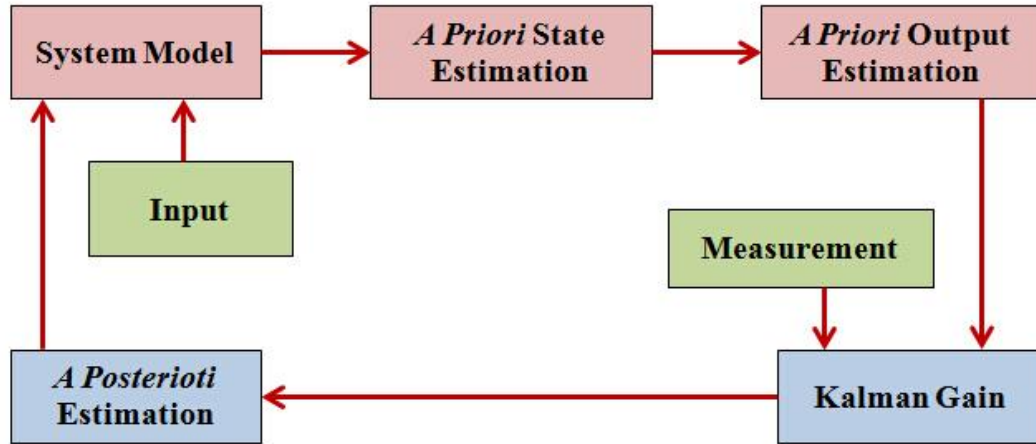


Figure 2.1: Flowchart of Kalman Filter, [4]

### 2.2.1.1. Linear System

For a discrete linear system, the Kalman filter process is illustrated in Figure 2.1 and is formulated as follow. Let the system model be defined in a state space form as:

$$x_{k+1} = Ax_k + Bu_k + w_k \quad (2.10)$$

$$z_{k+1} = Hx_k + v_k \quad (2.11)$$

The matrices  $A$ ,  $B$ , and  $H$  are the system matrix, the input matrix, and the measurement matrix, respectively.  $x$  represents the states of the system.  $u$  is the system input. The subscripts  $k$  and  $k + 1$  represent the  $k^{th}$  and  $k + 1^{th}$  step of the process.  $z$  is the measurement.  $w_k$  and  $v_k$  are the system and measurement noise and they are assumed to be independent, white, and with normal probability distributions:

$$p(w) \sim \mathcal{N}(0, Q) \quad (2.12)$$

$$p(v) \sim \mathcal{N}(0, R) \quad (2.13)$$

The Kalman Filter procedural steps are as follows:

(1) - The “a priori” predictions of the states and outputs are calculated using the system model and the previous estimates.

$$\hat{x}_{k+1|k} = A\hat{x}_{k|k} + Bu_k \quad (2.14)$$

$$\hat{z}_{k+1|k} = H\hat{x}_{k+1|k} \quad (2.15)$$

$\hat{x}$  and  $\hat{z}$  represent the state and the output vector estimates. The subscript  $k + 1|k$  signifies a prediction at moment  $k + 1$  based on information from time step  $k$ .

(2) - The "a priori" error covariance  $P_{k+1|k}$  is calculated as:

$$P_{k+1|k} = AP_{k|k}A^T + Q \quad (2.16)$$

(3) - The Kalman gain  $K_k$  is then obtained as:

$$K_k = P_{k+1|k}H^T(H P_{k+1|k}H^T + R)^{-1} \quad (2.17)$$

(4) - The a priori estimates are refined into the “a posteriori” form by using the Kalman gain:

$$\hat{x}_{k+1|k+1} = \hat{x}_{k+1|k} + K_k(z_{k+1} - \hat{z}_{k+1|k}) \quad (2.18)$$

(5) - The “a posteriori” estimation error covariance  $P_{k+1|k+1}$  is calculated as following:

$$P_{k+1|k+1} = (I - K_kH)P_{k+1|k} \quad (2.19)$$

Eqs. (2.14) to (2.19) are repeated for at every time interval.

### 2.2.1.2. Nonlinear System

The Kalman filter was formulated for linear systems. A number of modified strategies that are used for nonlinear systems, albeit in a sub-optimal form they are: the Extended Kalman Filter (EKF), the Unscented Kalman Filter (UKF), and the Cubature Kalman Filter (CKF), [24]. In this research, the EKF strategy will be used. The EKF was the first successful application of the Kalman filter, notably in the Apollo Mission to the moon. Since then, EKF has been successfully applied for estimation in many other nonlinear problems.

The EKF has a similar structure as the Kalman filter. Let the nonlinear system be:

$$x_{k+1} = f(x_k, u_k) + w_k \quad (2.20)$$

$$z_{k+1} = h(x_{k+1}) + v_k \quad (2.21)$$

where  $f$  and  $h$  are nonlinear functions associated with the state and the measurement vectors, respectively. Similarly to the Kalman filter, the nonlinear model of Eqs. (2.20) and (2.21) is first used to calculate the a priori state and output estimates:

$$\hat{x}_{k+1|k} = f(\hat{x}_{k|k}, u_k) \quad (2.22)$$

$$\hat{z}_{k+1|k} = h(\hat{x}_{k+1|k}) \quad (2.23)$$

The nonlinear model is then linearized around the last a posteriori state estimate such that:

$$F = \left. \frac{\partial f(x)}{\partial x} \right|_{x=\hat{x}_{k|k}, u_k} \quad (2.24)$$

$$H = \left. \frac{\partial h(x)}{\partial x} \right|_{x=\hat{x}_{k+1|k}} \quad (2.25)$$

Using  $F$  and  $H$ , the error covariance matrix  $P_{k+1|k}$  and the Extended Kalman gain  $K$  are obtained as:

$$P_{k+1|k} = FP_{k|k}F^T + Q \quad (2.26)$$

$$K_{k+1} = P_{k+1|k}H^T(H_kP_{k+1|k}H^T + R)^{-1} \quad (2.27)$$

The “a posteriori” estimates are then calculated:

$$\hat{x}_{k+1|k+1} = \hat{x}_{k+1|k} + K_{k+1}(z_{k+1} - \hat{z}_{k+1|k}) \quad (2.28)$$

$$P_{k+1|k+1} = (I - K_{k+1}H)P_{k+1|k} \quad (2.29)$$

Eqs. (2.20) to (2.29) summaries the steps taken in one time interval of the EKF iteration.

## 2.2.2. The Smooth Variable Structure Filter (SVSF)

### 2.2.2.1. Fixed Boundary Layer

The variable structure filter (VSF) was presented in 2003 by S. R. Habibi and R. Burton, [25]. The VSF has since evolved into a smooth variable structure filter (SVSF) by Habibi in 2007, [26]. SVSF is a state estimation strategy that can be applied to either linear or nonlinear systems, with robustness to disturbances. The basic concept (Figure 2.2) is based on the sliding mode theory. The SVSF has been further developed in the past few years by contributions from several other researchers, [24].

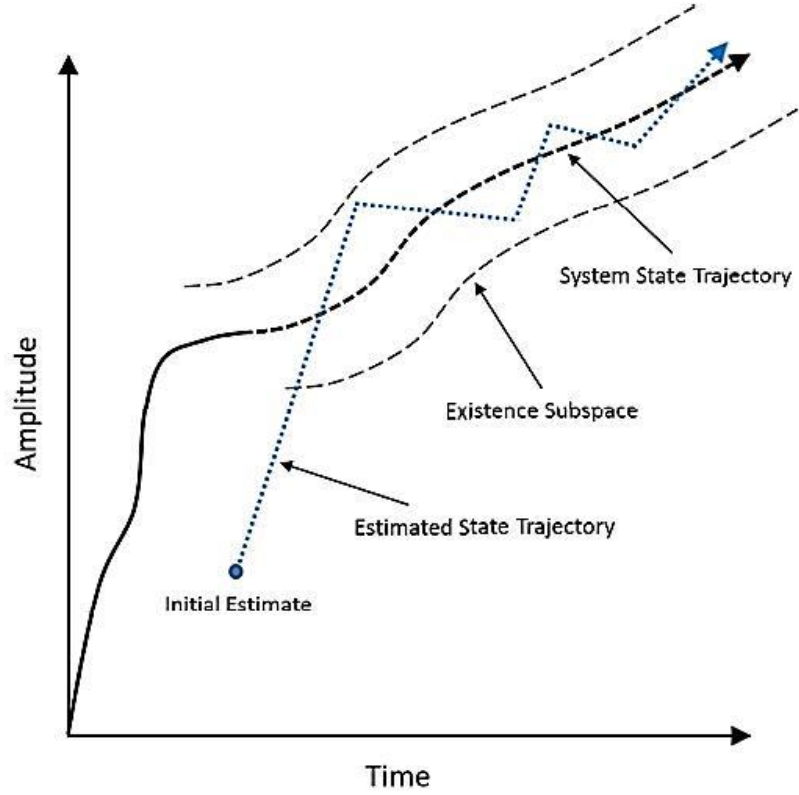


Figure 2.2: SVSF State Estimation Concept, [4]

For a system represented by Eqs. (2.20) and (2.21), the system model  $f$  could be either linear or nonlinear, and the measurement matrix  $H$  is assumed to be linear, positive definite, and pseudo diagonal. Similarly to the KF, "a priori" predicted state and measurement estimations are calculated as:

$$\hat{x}_{k+1|k} = f(x_{k|k}, u_k) \quad (2.30)$$

$$\hat{z}_{k+1|k} = H\hat{x}_{k+1|k} \quad (2.31)$$

The output estimation error vector  $e_{z,k+1}$  or filter innovation is then calculated:

$$e_{z,k+1|k} = z_{k+1} - \hat{z}_{k+1|k} \quad (2.32)$$

Then SVSF gain  $K_{k+1}^{SVSF}$  has been defined in [26] as:

$$K_{k+1}^{SVSF} = H^+ (|e_{z,k+1|k}| + \gamma |e_{z,k|k}|) * \text{sat}\left(\frac{e_{z,k+1|k}}{\psi}\right) \quad (2.33)$$

where

$$\text{sat}\left(\frac{a}{b}\right) = \begin{cases} \text{if } |a| > b; \text{sat}\left(\frac{a}{b}\right) = \text{sgn}(a) \\ \text{if } |a| < b; \text{sat}\left(\frac{a}{b}\right) = \frac{a}{b} \end{cases} \quad (2.34)$$

and  $e_{z,k|k}$  is the "a priori" measurement error,  $\gamma$  is the memory convergence rate ( $0 < \gamma < 1$ ), and  $\psi$  is a smoothing boundary layer width. The "a posteriori" state and measurement estimated are obtained as:

$$\hat{x}_{k+1|k+1} = \hat{x}_{k+1|k} + K_{k+1}^{SVSF} \quad (2.35)$$

$$\hat{z}_{k+1|k+1} = H \hat{x}_{k+1|k+1} \quad (2.36)$$

The measurement error is then updated:

$$e_{z,k+1|k+1} = z_{k+1} - \hat{z}_{k+1|k+1} \quad (2.37)$$

The existence subspace is a neighborhood around the actual state trajectory as shown in Figure 2.2 with a width that is a function of the modeling uncertainties. The estimated state converges to this region and then after switches back and forth across the state trajectory within this subspace for bounded disturbances. The width of the existence subspace reflects the amount of uncertainties in the estimation process, which is not exactly known.

Within the existence boundary subspace, high frequency switching of estimated states may cause chattering, which is undesirable. This chattering can be removed by using a smoothing boundary layer  $\psi$  with a width that would encompass the existence subspace as shown in Figure 2.3. If the width of the existence subspace is greater than the

smoothing boundary layer as shown in Figure 2.4, then chattering would remain, but with a reduced amplitude.

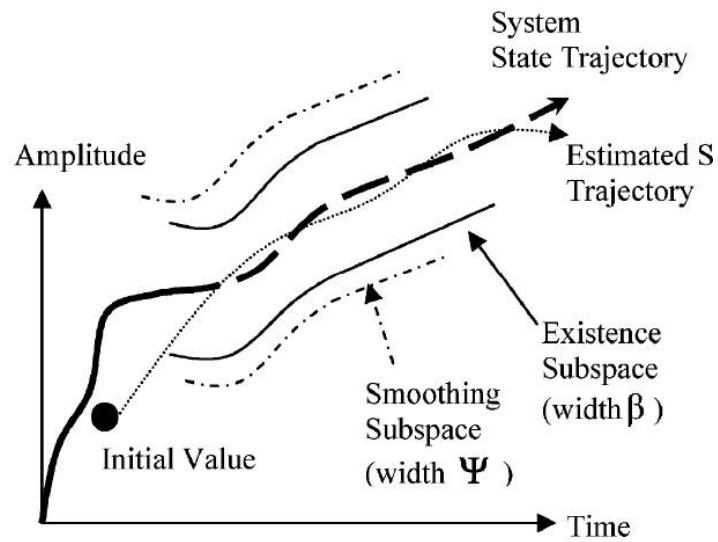


Figure 2.3: Proper Smoothing Boundary Layer, [24]

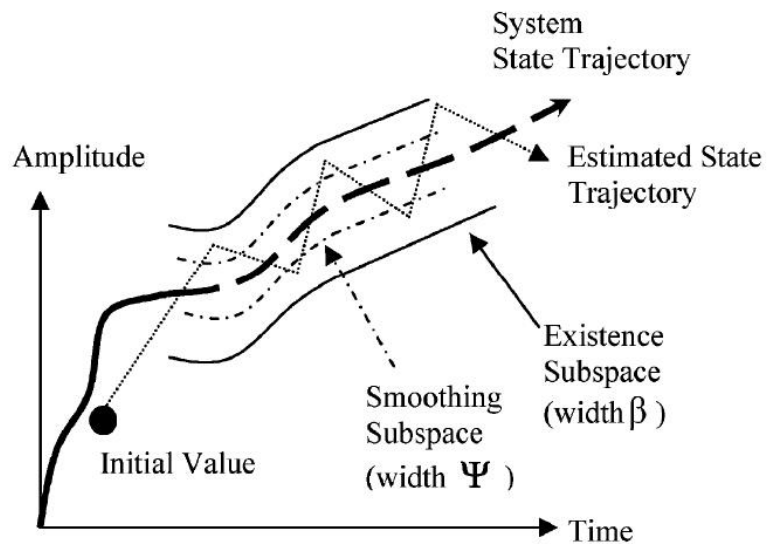


Figure 2.4: Improper Smoothing Boundary Layer, Chattering, [24]

### 2.2.2.2. Varying Boundary Layer

When setting smoothing boundary layer  $\psi$  to a fixed value, it should be based on the upper bound of modeling uncertainties in order for the chattering effect to be avoided. However, this could compromise the accuracy of the SVSF if the smoothing boundary width is overestimated. S.A. Gadsden, [24], proposed a new strategy that overcomes this problem. This is done by creating a time varying boundary layer (VBL) that can adjust the boundary width with respect to disturbances. Figure 2.5 shows the working concept of VBL. The original SVSF has a smooth boundary layer term  $\psi$  for each estimate and these boundary layer terms are independent of each other. In a matrix form, this amounts to a pseudo-diagonal representation. In order to have an optimal derivation, a full matrix of smoothing boundary layers needs to be considered, [24].

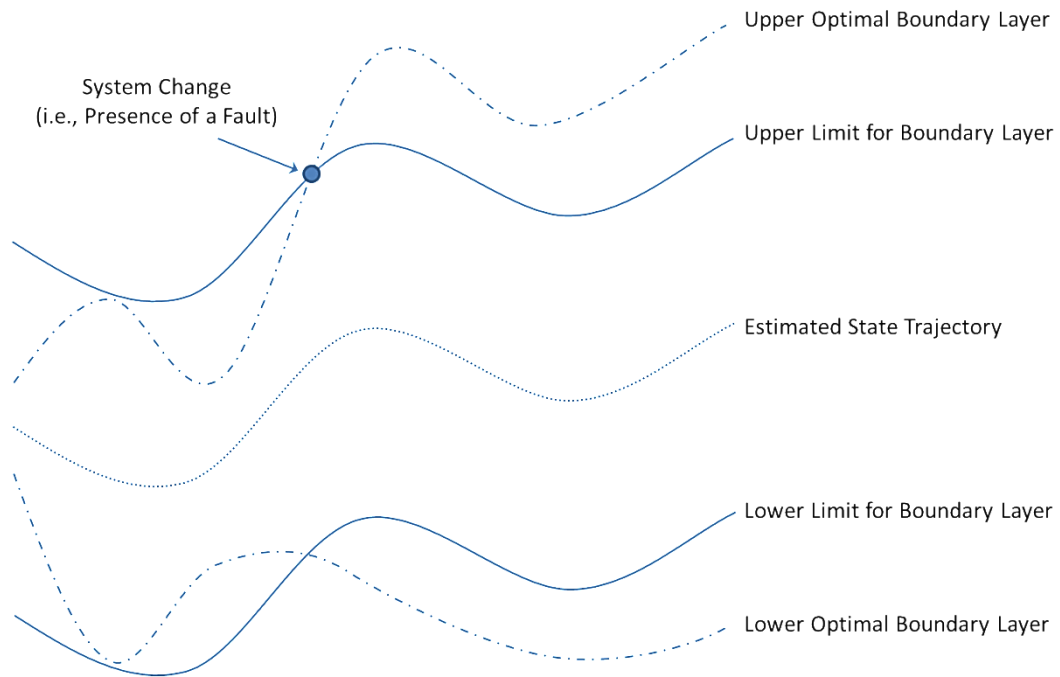


Figure 2.5: VBL Working Concept, [24]

In Gadsden's method, the VBL is obtained through optimization by minimizing the estimation error covariance with respect to the smoothing boundary layer width such that:

$$\frac{\partial \left( \text{trace}(P_{k+1|k+1}) \right)}{\partial \psi} = 0 \quad (2.38)$$

Eqs. (2.33) and (2.35) become:

$$K_{k+1}^{SVSF} = H_{sys}^+ (|e_{z,k+1|k}| + \gamma |e_{z,k|k}|) \circ \text{sat} \left( \frac{e_{z,k+1|k}}{\psi} \right) \text{diag}(e_{z,k+1|k})^{-1} \quad (2.39)$$

$$\hat{x}_{k+1|k+1} = \hat{x}_{k+1|k} + K_{k+1}^{SVSF} e_{z,k+1|k} \quad (2.40)$$

The covariance and posteriori state error covariance are obtained as:

$$P_{k+1|k} = F P_{k|k} F^T + Q_k \quad (2.41)$$

$$P_{k+1|k+1} = (I - K_{k+1}^{SVSF} H) P_{k+1|k} (I - K_{k+1}^{SVSF} H)^T + K_{k+1}^{SVSF} R_{k+1} K_{k+1}^{SVSF,T} \quad (2.42)$$

Taking Eqs. (2.40) to (2.43) into Eq.(2.39), yields:

$$S_{k+1} = H P_{k+1|k} H^T + R_{k+1} \quad (2.43)$$

$$\psi_{k+1} = \left( \text{diag}(|e_{z,k+1|k}| + \gamma |e_{z,k|k}|) \right)^{-1} H P_{k+1|k} H^T S_{k+1}^{-1} \quad (2.44)$$

Given a known mathematical model subject to white noise, SVSF with VBL collapses to be the same as the Kalman filter, indicating a loss of robustness to modeling uncertainty as a trade-off to optimality. To overcome this drawback, a saturation limit ( $\psi_{max}$ ) is set for achieving both robustness and performance, [24].

In the SVSF-VBL the estimates are optimal while the smoothing boundary layer is less than the salutation limit ( $\psi_{max}$ ). Once uncertainties presents in the system cause the VBL to go outside the saturation limit ( $\psi_{max}$ ), then the filter reverts to the original SVSF

maintaining its robustness to uncertainties, In this way, the estimated states are forced to follow the actual state trajectories. This is summarized as:

$$\begin{aligned} \psi_{k+1} &= \psi_{max}, \text{ if } abs(\psi_{k+1}) \geq \psi_{max}; \\ \psi_{k+1} &= \psi_{k+1}, \text{ if } abs(\psi_{k+1}) < \psi_{max}. \end{aligned} \quad (2.45)$$

### 2.3. Multiple Model (MM)

A system behavior may vary with time; different models may better represent its dynamics according to its mode of operation. The Multiple Model (MM) approach is a strategy that can be used in such circumstances. MM assumes that the system behavior fits into one of a set of predefined system models, [27]. The MM strategy is often used for fault detection and diagnosis studies, [4]. The two basic MM approaches are static MM and dynamic MM.

#### 2.3.1. Static Multiple Model

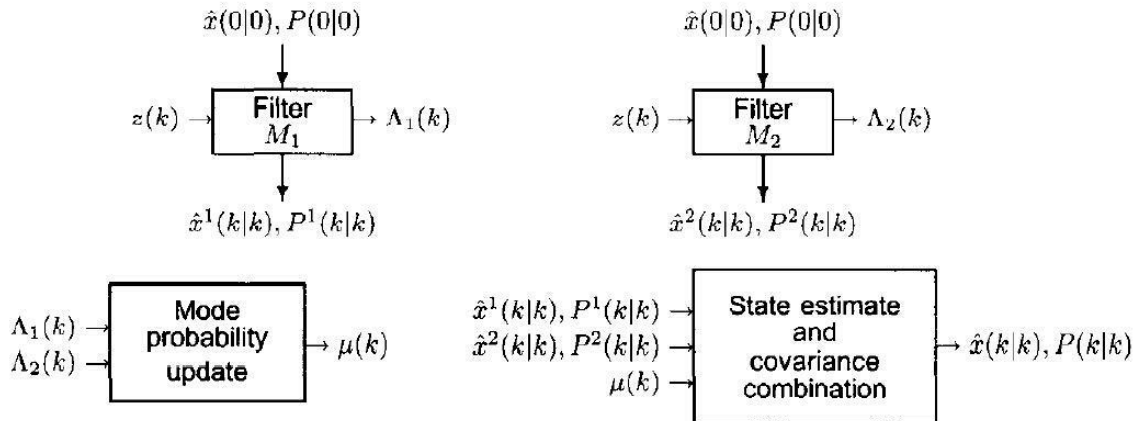


Figure 2.6: Static MM For  $r = 2$  Fixed Models, [18]

Figure 2.6 shows one iteration of the static MM estimator. Static MM assumes that the system behavior ( $M$ ) is described by one of the system models ( $M_j$ ), and its behavior remains unchanged at all time (one of the  $r$  modes):

$$M \in \{M_j\}_{j=1}^r \quad (2.46)$$

The prior probability of the  $M_j$  is correct (i.e., the system behaviors can be described by a particular mode  $j$  of  $r$  modes) is:

$$P\{M_j|Z^0\} = \mu_j(0) \quad (2.47)$$

$$\sum_{j=1}^r \mu_j(0) = 1 \quad (2.48)$$

where  $j = 1, \dots, r$ , and  $Z^0$  is prior information.

Next, the posteriori probability  $\mu_j(k)$  of mode  $j$  being correct with measurements up to moment  $k$ :

$$\mu_j(k) = \frac{p[z(k)|Z^{k-1}, M_j] \mu_j(k-1)}{\sum_{i=1}^r p[z(k)|Z^{k-1}, M_i] \mu_i(k-1)} \quad (2.49)$$

The posteriori probability is the updated probability, which provides more accurate mode estimation than the prior probability, since it has more information  $Z^j$  than  $Z^0$ . The posterior probability will be used for updating state and covariance estimation later.

On the right hand side of above equation, the first term of numerator part is a likelihood function of mode  $j$  at time  $k$ , under the assumption of linear-Gaussian, it has the following form:

$$\Lambda_j(k) \triangleq p[z(k)|Z^{k-1}, M_j] = p[v_j(k)] = \mathcal{N}[v_j(k); 0; S_j(k)] \quad (2.50)$$

where  $v_j$  and  $S_j$  are the innovation (i.e.,  $v_j = z_{k+1} - \hat{z}_{k+1|k}$  from Eq.(2.18)) and covariance (i.e.,  $S_j = HP_{k+1|k}H^T + R$  from Eq.(2.17)) of the mode-matched filter

corresponding to mode  $j$  (means one filter only operate under one mode condition, for  $r$  modes there are  $r$  filters), respectively. A filter matched to each mode is set up yielding mode-conditioned state estimation and covariances. Figure 2.6 shows the illustration of a bank of filters for  $r = 2$ .

Outputs from each filters are mode-conditioned state estimate  $\hat{x}^j$  and covariance  $P^j$  and likelihood  $\Lambda_j$  under the assumption that mode  $j$  is corrected.

The pdf (probability density function) of the state has the form:

$$p[x(k)|Z^k] = \sum_{j=1}^r \mu_j(k) \mathcal{N}[x(k); \hat{x}^j(k|k); P^j(k|k)] \quad (2.51)$$

Finally the combined mode-conditioned estimate state and covariance are given as follow:

$$\hat{x}(k|k) = \sum_{j=1}^r \mu_j(k) \hat{x}^j(k|k) \quad (2.52)$$

$$P(k|k) = \sum_{j=1}^r \mu_j(k) \{P^j(k|k) + [\hat{x}^j(k|k) - \hat{x}(k|k)][\hat{x}^j(k|k) - \hat{x}(k|k)]'\} \quad (2.53)$$

For a static MM, the assumption is that the correct model is among the  $r$  models and no model changes occur after the initial time. If the system behavior changes during any point of time after, the static MM will not detect that. So, the static MM accuracy is relatively low.

### 2.3.2. Dynamic Multiple Model

The Dynamic MM is more flexible than the static MM. It allows for the system behavior to change at any point in time. As such, the Dynamic MM switches between system models accordingly. Let the system be modeled as:

$$x(k) = F[M(k)]x(k-1) + v[k-1, M(k)] \quad (2.54)$$

$$z(k) = H[M(k)]x(k) + w[k, M(k)] \quad (2.55)$$

where  $M(k)$  is the model at time  $k$ . The mode at  $k$  is assumed to be one of the  $r$  modes:

$$M(k) \in \{M_j\}_{j=1}^r \quad (2.56)$$

The  $l^{th}$  mode history through time  $k$  is:

$$M^{k,l} = \{M_{i_{1,l}}, \dots, M_{i_{k,l}}\}, \text{ where } l = 1, \dots, r^k \quad (2.57)$$

It is clear that the number of histories increases exponentially for every iteration. The  $i_{\kappa,l}$  is the model index at  $\kappa$  from history  $l$  where:

$$1 \leq i_{\kappa,l} \leq r, \kappa = 1, \dots, k$$

The mode switching process is assumed a Markov chain with mode transition probabilities defined as:

$$p_{ij} \triangleq P\{M(k) = M_j | M(k-1) = M_i\} \quad (2.58)$$

The conditional pdf of the state is calculated as:

$$p[x(k)|Z^k] = \sum_{j=1}^{r^k} p[x(k)|M^{k,l}, Z^k] P\{M^{k,l}, Z^k\} \quad (2.59)$$

The probability of mode history is calculated if the current mode probability only depends on previous one step:

$$\mu^{k,l} = P\{M^{k,l}|Z^k\} = \frac{1}{c}p[z(k)|M^{k,l}, Z^{k-1}]p_{ij}\mu^{k-1,s} \quad (2.60)$$

where  $c$  is the normalization constant,  $i = s_{k-1}$  is the last model of parent sequence  $s$ . The above equation indicates that conditioning on the entire past history is needed (which means this method is impractical).

The Dynamic MM gives more accurate calculations than the static MM under mode switching situations. The drawback of the dynamic MM is that for each iteration, mode histories increase exponentially, adding to complexity.

From a practical perspective, suboptimal techniques are used. For example, the Generalized Pseudo-Bayesian (GPB) approach, keeps probabilities to the last one or two sampling time to reduce the amount of calculations. Also, the interacting multiple model (IMM) algorithms, which combine the simplicity of the static MM and the accuracy of the dynamic MM are commonly applied.

### 2.3.3. The Interacting Multiple Model Strategy

In real applications, system behaviour may change and the system models must change accordingly. For example, in target tracking applications, a particle may travel with a constant speed, a changing speed or changing direction, [27], and each different motion has a different model associated with it. It is necessary to implement an adaptive estimation algorithm that adapts to different models and will minimize state error. “Interacting Multiple Model” (IMM) is the adaptive estimation technique that has often been used. IMM is an improvement over the “multiple model” (MM) techniques described earlier, [28]. A probability-based (Bayesian) framework is used. Initially using

prior probabilities of each model being correct (system behaviours are modelled by a finite number of modes and models), and updated probabilities are calculated and implemented (system behaviours switch from one mode to another), [27].

By taking measurements of the system at each time step, the model probabilities are calculated, which gives us an understanding of the system behaviour with respect to time.

IMM has been successfully applied on the EHA actuator in several studies, [4, 28, 29].

And the results from the IMM strategy have been used for fault detection and diagnosis.

In practical applications, system measurements have a certain level of noise. As such, the IMM concept is often used with filtering and estimation strategies such as the Kalman filter (KF) or the smooth variable structure filter (SVSF); these are, referred to in this thesis as IMM-KF or IMM-SVSF.

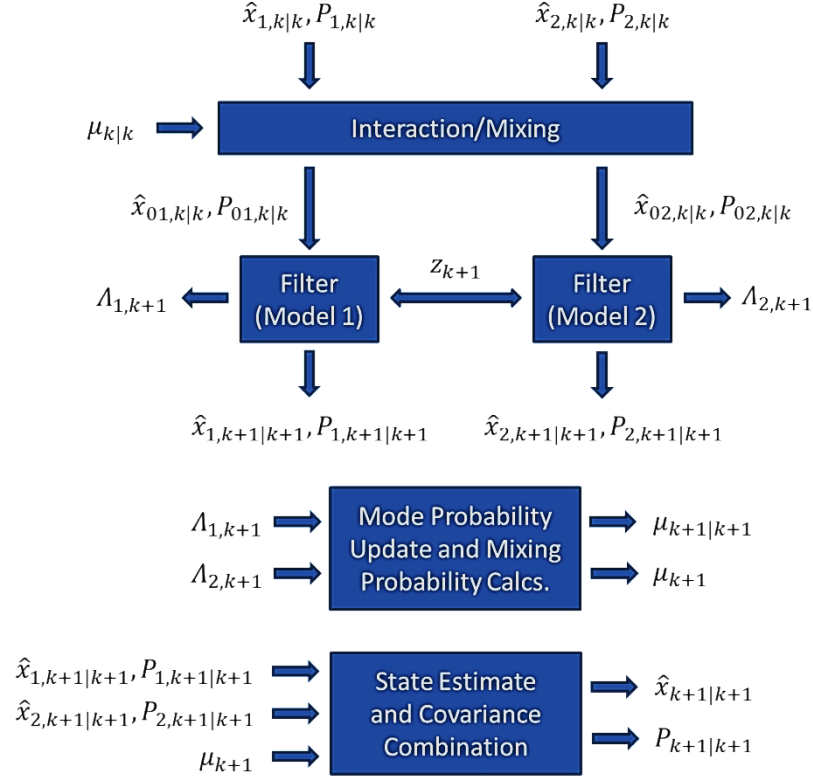


Figure 4.1: IMM Overall Concept

Figure 4.1 shows the basic flow chart of IMM over one sample time and iteration. IMM techniques include five basic steps, [28]: (1) - initial mixing probabilities, (2) - mixing stage, (3) - mode matched filtering, (4) - mode probability update, and (5) - state and covariance estimation. These steps are listed and explained as follows:

(1) - Mixing probabilities are calculated. These terms represent the probabilities of current modes  $i$  turning into mode  $j$  in the next time step, as follows:

$$\mu_{i|j,k|k} = \frac{1}{\bar{c}_j} p_{ij} \mu_{i,k|k} \quad (2.61)$$

$$\bar{c}_j = \sum_{i=1}^r p_{ij} \mu_{i,k|k} \quad (2.62)$$

$p_{ij}$  is the pre-defined parameter, which is the mode transition probabilities.  $\mu_{i,k}$  is the probability of mode  $i$  being correct.

(2) - Mixing stage: mixing probabilities  $\mu_{i|j,k|k}$ , mode-matched states  $x_{i,k|k}$ , and covariance  $p_{i,k|k}$  are used to calculate the mixed initial state and the covariance.

$$\hat{x}_{0j,k|k} = \sum_{i=1}^r \hat{x}_{i,k|k} \mu_{i|j,k|k} \quad (2.63)$$

$$P_{0j,k|k} = \sum_{i=1}^r \mu_{i|j,k|k} \left\{ P_{i,k|k} + (\hat{x}_{i,k|k} - \hat{x}_{0j,k|k})(\hat{x}_{i,k|k} - \hat{x}_{0j,k|k})^T \right\} \quad (2.64)$$

(3) - Mode matched filtering: The third step involves using the outputs of step two, and the mixed initial states and covariances, with measurements  $z_{k+1}$  and input  $u_k$ , to calculate likelihood values, and use these for updating the mode probabilities. Note that, the actual calculation of the likelihood function requires a covariance matrix from a filtering algorithm such as the KF or the SVSF as follows:

$$\Lambda_{j,k+1} = \frac{1}{\sqrt{|2\pi S_{j,k+1}|}} \exp\left(\frac{-\frac{1}{2} e_{j,z,k+1|k}^T e_{j,z,k+1|k}}{S_{j,k+1}}\right) \quad (2.65)$$

$e_{j,z,k+1|k}$  is the measurements innovations, and  $S_{j,k+1}$  is the error covariance.

(4) - Mode probability update: With the likelihood values of each mode, the mode probabilities can be updated with the following equations.  $c$  is the normalizing constant which is used for updating states and covariances'.

$$u_{j,k+1} = \frac{1}{c} \Lambda_{j,k+1} \sum_{i=1}^r p_{ij} u_{i,k} \quad (2.66)$$

$$c = \sum_{j=1}^r \Lambda_{j,k+1} \sum_{i=1}^r p_{ij} u_{i,k} \quad (2.67)$$

(5) - State estimation and covariance combination: Finally, the mixed overall state and covariance estimations are calculated.

$$\hat{x}_{k+1|k+1} = \sum_{j=1}^r \hat{x}_{j,k+1|k+1} u_{j,k+1} \quad (2.68)$$

$$P_{k+1|k+1} = \sum_{j=1}^r u_{j,k+1} \left\{ P_{j,k+1|k+1} + (\hat{x}_{j,k+1|k+1} - \hat{x}_{k+1|k+1})(\hat{x}_{j,k+1|k+1} - \hat{x}_{k+1|k+1})^T \right\} \quad (2.69)$$

Eqs. (2.61) to (2.69) summarize the basic process for the IMM mode probability calculation. Eqs. (2.68) and (2.69) are applied if there are uncertainties associated with measurements and when filter estimation is necessary, [28].

## Chapter 3

### Electro -Hydrostatic Actuator (EHA) Introduction, Setup, and Models

The motion of an aircraft is controlled by flight control surfaces. In early aircraft, only a few control surfaces were used for relatively simple aircraft motion control. Nowadays, more and more complex motions are needed by modern aircrafts, requiring a larger number of control surfaces to work together.

#### 3.1. Brief History on Aircraft Flight Surface Control

Primary flight surfaces include ailerons, elevators and rudders, which provide the basic motion of roll, pitch and yaw. While secondary flight surfaces provide improved performance, [30]. Figure 3.1 shows the primary flight surfaces control for different motions of an aircraft.

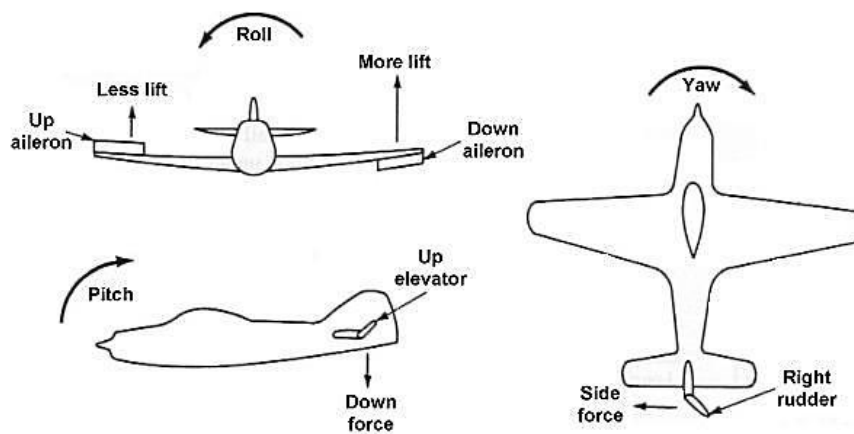


Figure 3.1: Primary Flight Surfaces Control for Different Types of Motion, [31]

Researchers working on actuators have been focused mainly on the primary flight surfaces, since they are more important to the safety and reliability of aircrafts. There are four considerations pertaining to the development of aircraft flight surfaces that are, [3]:

- Pure Mechanical Linkages,
- Hydro-Mechanical Actuators,
- Fly-By-Wire (FBW) Strategy, and
- Power-By-Wire (PBW) Strategy.

### **3.1.1. Mechanical Linkages**

In the early stages of aircraft development in the early 20<sup>th</sup> century, mechanical linkage control schemes, as a very simple and reliable method, were successfully used since aircrafts at that time were relatively small and slow. The control force was applied by a pilot through a joystick and foot pedals in the cockpit that was connected through linkages, wires, and pulleys to the flight surface. Figure 3.2 shows a basic structure of flight surface with the mechanical linkage control. This method was limited to the size and the performance of the aircraft since the power needed to move the flight surface is solely provided by the human operator. With the development of larger aircrafts, new methods with extra power were needed.

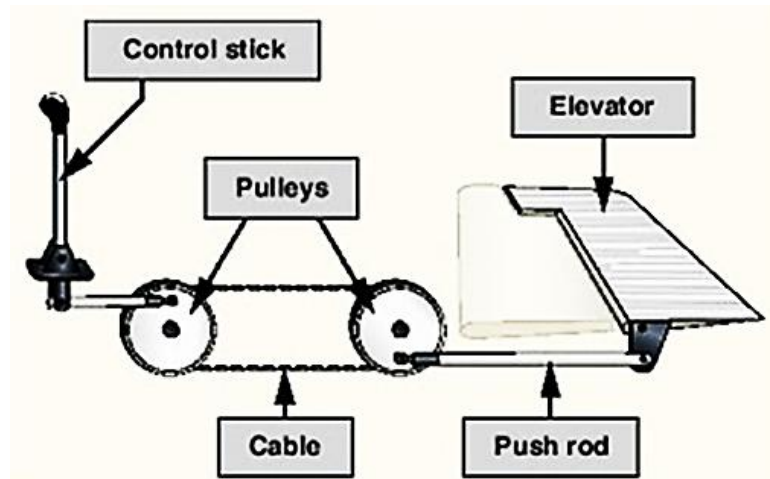


Figure 3.2: Flight Surface Controlled by Mechanical Linkages, [32]

### 3.1.2. Flight Surface Control by Hydro-Mechanical Actuators

From the 1930s on, hydraulic systems were introduced into flight surface control. Instead of using mechanical linkage alone on flight surfaces, the control scheme incorporated a centralized hydraulic system (i.e., using directional valves) which allowed for the fluid to move the actuator. Large flight surfaces can be actuated by hydro-mechanical actuators.

A basic example is shown in Figure 3.3.

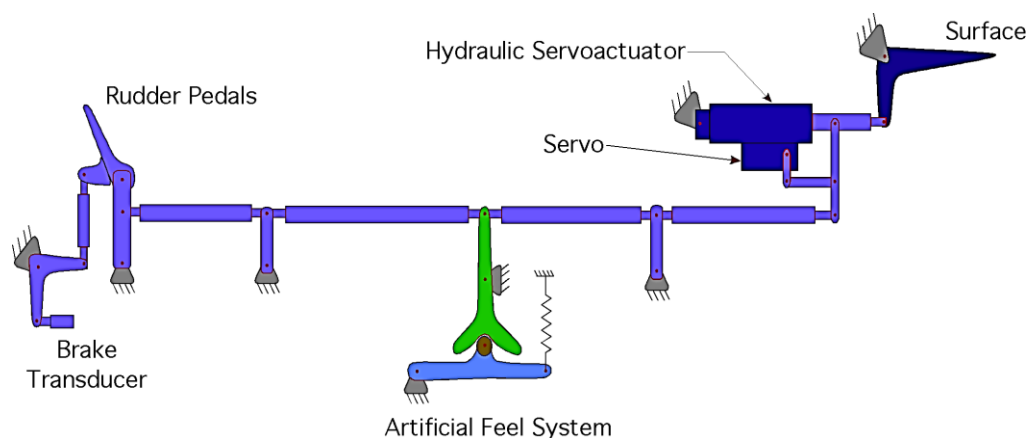


Figure 3.3: Hydro-Mechanical Flight Surface, [33]

Figure 3.3 shows a common hydro-mechanical control surface with a feedback feel system. Pilot input demand transfers from the pedal through linkages to a hydraulic system, the servomotor will then push fluid in the actuator in the desired direction as well as the flight surface. At the same time, the artificial feel system will provide a force feedback through the pedal to the pilot.

### **3.1.3. Hydraulic Systems Incorporating the Fly-by-Wire Strategy**

In the 1970s, mechanical linkage controls started to be replaced by distributed centralized electrical signals and wires. This new method was called Fly-By-Wire (FBW). Its advantages were:

- Weight reduction due to replacing mechanical linkages.
- Computerized control could be implemented to improve stability.

Its disadvantages were:

- A fault in one of the hydraulic lines potentially could lead to a complete hydraulic system failure.
- Hydraulic pressure had to be maintained (21-42 MPa) at all times, regardless of demand.
- Higher complexity.

### **3.1.4. Power-by-Wire strategy (PBW)**

This technology has been considered as a replacement to the traditional centralized hydraulic actuation systems, by using modular subsystems. Instead of using a centralized hydraulic circuit and power lines through the aircraft, modular actuators with

electric signal wires are used. The aircraft flight control system consists of a number of electrically driven Electro-Mechanical actuators (EMA) or Electro-Hydrostatic actuators (EHA), [34]. The advantages are:

- Reduced overall weight.
- Reduced complexity.
- Modularity.
- Power on demand leading to better overall energy efficiency.

In this thesis the control of EHA systems is considered.

### **3.2. Electro Hydrostatic Actuation and the Experimental Prototype.**

This section goes over the necessary information that are related to EHA study. First, the hydraulic circuit is introduced. Then general EHA components and structure are explained. An experimental EHA prototype has been previously designed and was used in this research. The EHA prototype is described and its model is presented in this section.

#### **3.2.1. Introduction to Hydraulic Systems**

Two main types of hydraulic transmission systems are used in applications; they are valve controlled and pump controlled hydraulic systems, [35, 16]. Figures 3.4 and 3.5 show the outline of each system.

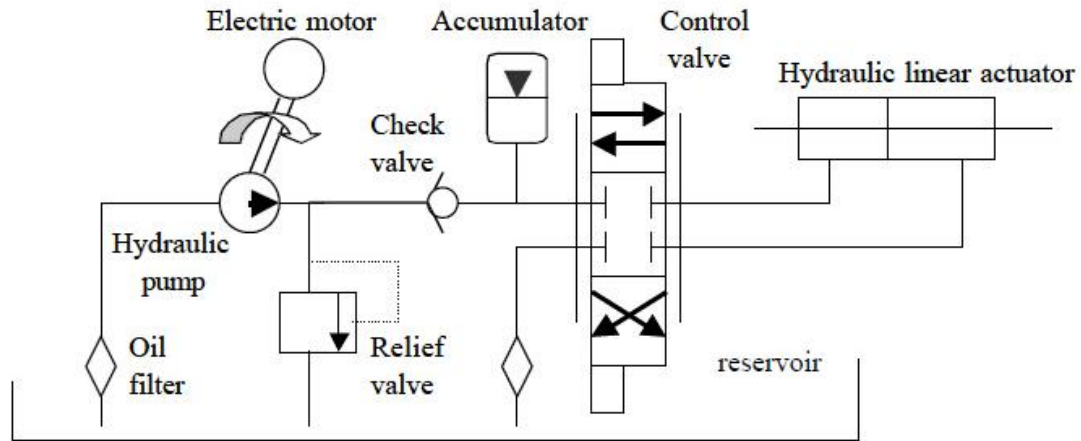


Figure 3.4: Valve Controlled Hydraulic System, [35]

In valve controlled hydraulic systems, a motor driven pump provides fluid maintained at constant pressure. A valve controls the flow that enters the actuator. This type of hydraulic system has a very good performance, and it is widely used in industry. The disadvantages of centralized valve controlled systems are: a large and often bulky oil reservoir is needed; the energy efficiency is very poor, and higher cost if servo-valves are used, [35].

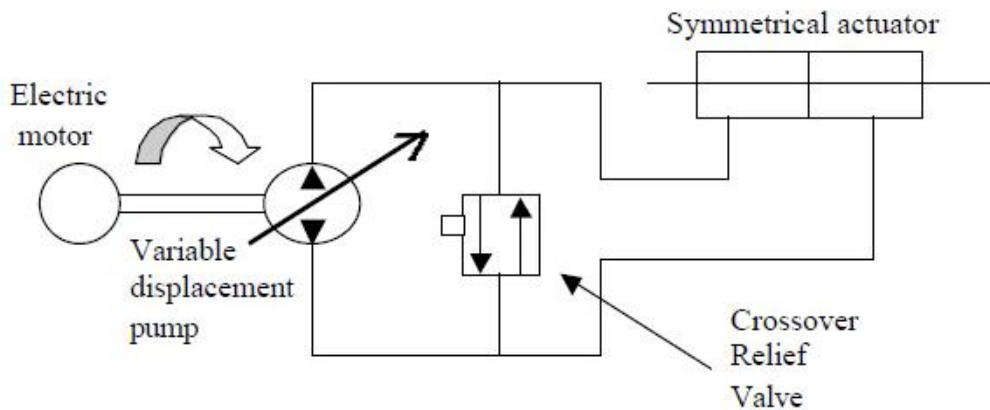


Figure 3.5: Pump Controlled Hydraulic System, [35]

Another option is to use a displacement pump controlled hydraulic system; hydrostatic systems fall within this category. With this option, the servo-valve unit is no longer

needed, and the pump directly controls the amount and direction of flow that moves the actuator. In Figure 3.5, a fixed speed motor drives a variable displacement pump; alternatively a variable speed motor can drive a fixed displacement pump. The fluid in the system does not go back to the reservoir; instead the fluid goes through the pump from one actuator chamber to the other, [35].

### 3.2.2. The Basic EHA Structure

An example of an EHA system is shown in Figure 3.6. It consists of a controller, motor, pump, an inner hydraulic circuit to prevent cavitation and an actuator. The motor-pump is the heart, and provides power to the system. The actuator is the muscle, which does the movement. Sensors work as the nervous system, providing feedback. The controller is the brain, giving commands and taking feedback, [36].

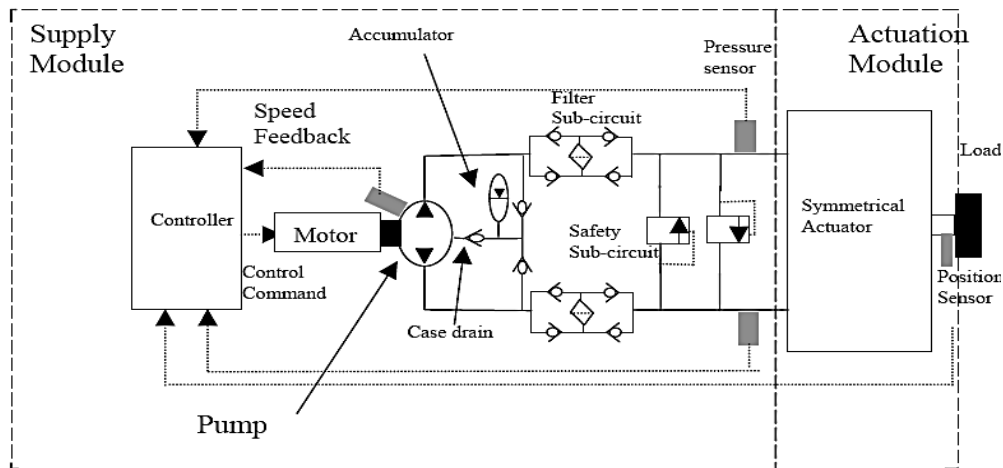


Figure 3.6: Basic Structure of EHA, [37]

### 3.2.3. McMaster's EHA Prototype Overview

The EHA prototype developed at McMaster University for experimentation is shown in Figure 3.7. It was designed and built by Kelvin McCullough, [3]. Figure 3.8 shows the

basic circuit of this EHA. The initial setup included two EHAs arranged in tandem with two motors/pumps and two symmetrical linear actuators. Other components include sensors, pressure relief valves, an accumulator, and check valves.

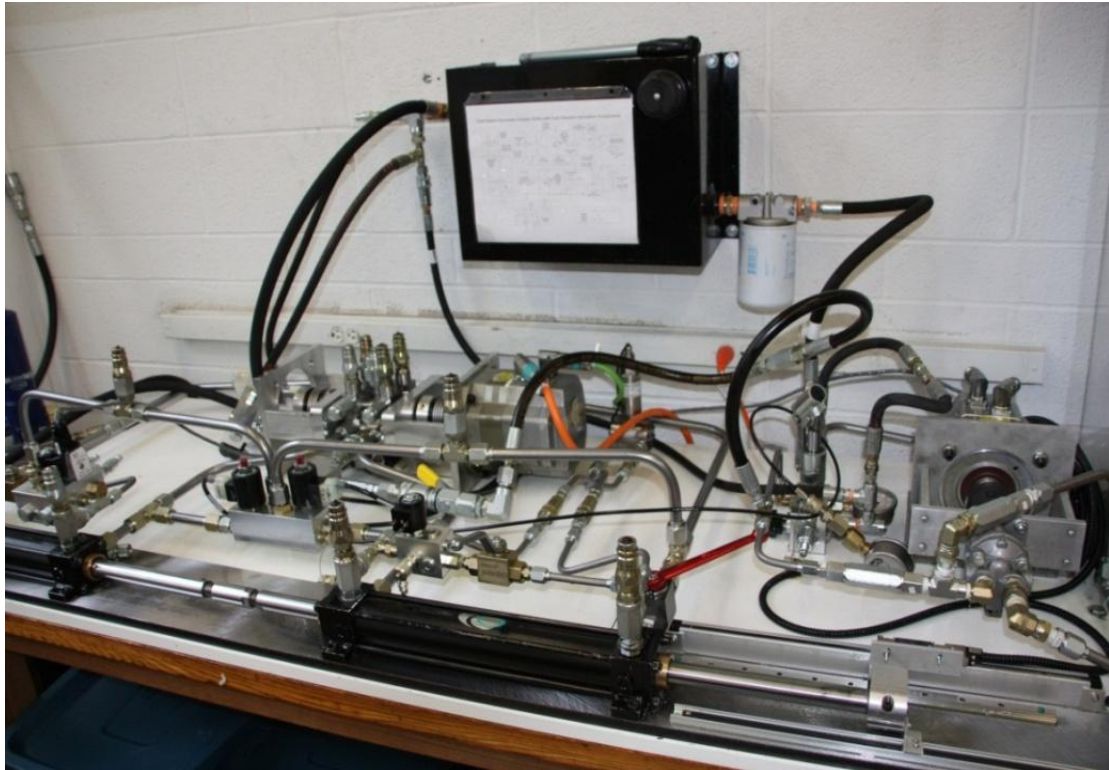


Figure 3.7: EHA Prototype Apparatus

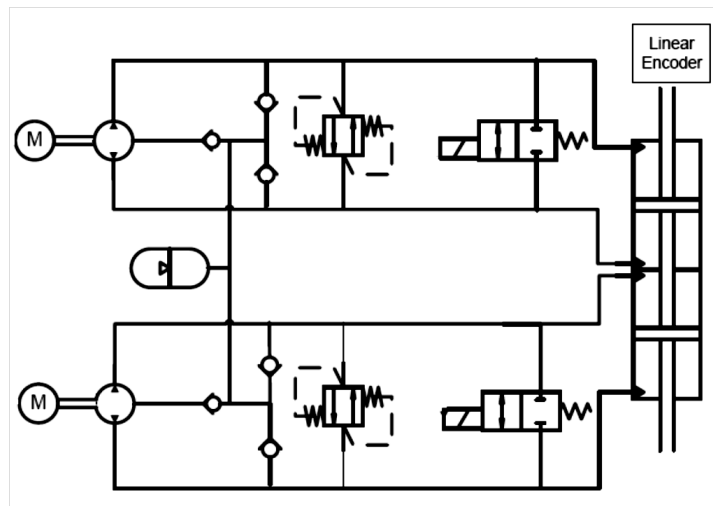


Figure 3.8: EHA Basic Scheme Plot

### 3.2.4. Cause of Failure and Effects

According to research performed by Chinniah [35], the causes of EHA faults and failures are the following.

- Motor

Cause	Effect
Overload/overheating. Electric motor has a regular working range, and a protection function regulates the motor input in a safety range	Motor shuts down

- Pump

Cause	Effect
1) Gear wear	1) Lower efficiency and more noise
2) Seal wear	2) Leakage along motor and coupling shaft
3) Case drain seal failure	3) Leakage into accumulator, and a rise in accumulator pressure, lower actuator velocity

- Coupling between motor and pump

Cause	Effect
Fatigue/wear	Increase vibration; failure

- Actuator

Cause	Effect
Seal wear	Leakage coefficient increases; also may change

	friction characteristics
--	--------------------------

- Connection

Cause	Effect
External leakage	Increase in the leakage coefficient, system failure

- Relief valve

Cause	Effect
Stuck, not fully open or closed	Fluid temperature rise, lower actuator velocity

- Check valve

Cause	Effect
Fail to maintain pressure	Large amount of leakage

- Oil

Cause	Effect
Air trapped in the hydraulic circuit, mixes with the hydraulic fluid, and changes the bulk modulus	Lower efficiency, change in the system behaviors

### 3.2.5. The EHA Configuration used in this Research Setup

The EHA prototype was modified for studying fault conditions and correction strategies.

In order to do that, the second motor-pump circuit was disabled. As such, one side of the

EHA prototype was operated as a single motor-pump system while the second circuit was

used for physically simulating fault conditions. This section explains the modified EHA prototype for fault condition simulation.

EHA has several key features that need to be mentioned, [3, 4]. Figure 3.9 shows the simplified EHA prototype configuration with the important features labeled.

The red solid line indicates the main driven circuit. The motor (see ① in Figure 3.9) is a Siemens 1FK7080-5AF71-1AG2 servomotor. It has a maximum speed of 3000 rpm (314.58 rad/s), nominal torque of 6.8 Nm and a nominal power of 2.14 kW. The pump housing was machined in house and the pump gears (②) were purchased as Marzocchi ALP-5 with a volumetric displacement of  $5.57 \times 10^{-7} \text{ m}^3/\text{rad}$ . The shaft coupling that connects the motor and pump is a R+W America BK2/60/83, and it is assumed that the coupling can make sure both motor and pump rotate perfectly in the same speed.

The EHA has an inner circuit that is emphasized by a red dash line in Figure 3.9. The inner circuit serves to prevent cavitation and to contain the case drain leakage. The accumulator (⑩) maintains the pressure above 40 Psi, if pressure drops below 40 Psi, the check valves (③) open to avoid cavitation. The case drain is used also to replenish the accumulator.

A differential pressure relief valve (④) is active when the pipe pressure exceeds 500 Psi, allowing the fluid to bypass. This component prevents excessive pressure build up and is for safety.

Two types of sensors are employed, an absolute pressure sensor (⑤) and a linear encoder (⑪). These sensors measure the pressures at the two chambers of the linear actuator and its position. The pressure sensors have a working range of  $\pm 2500$  Psi and an error band

of 1%. The linear encoder is a Fagor Automation MX-35-5, with an accuracy of  $\pm 5\mu\text{m}$ , resolution of  $1\mu\text{m}$ , maximum speed of  $1\text{m/s}$ , and a working range of  $0.35\text{m}$ . Also, actuator velocity and acceleration values are calculated by taking the derivative of the actuator position.

The double rod (⑥) are rigidly connected.

Two electrically controlled throttling valves (⑧, ⑨), and two manually controlled ball valves (⑦) are used for physically simulating friction and leakage fault conditions. .

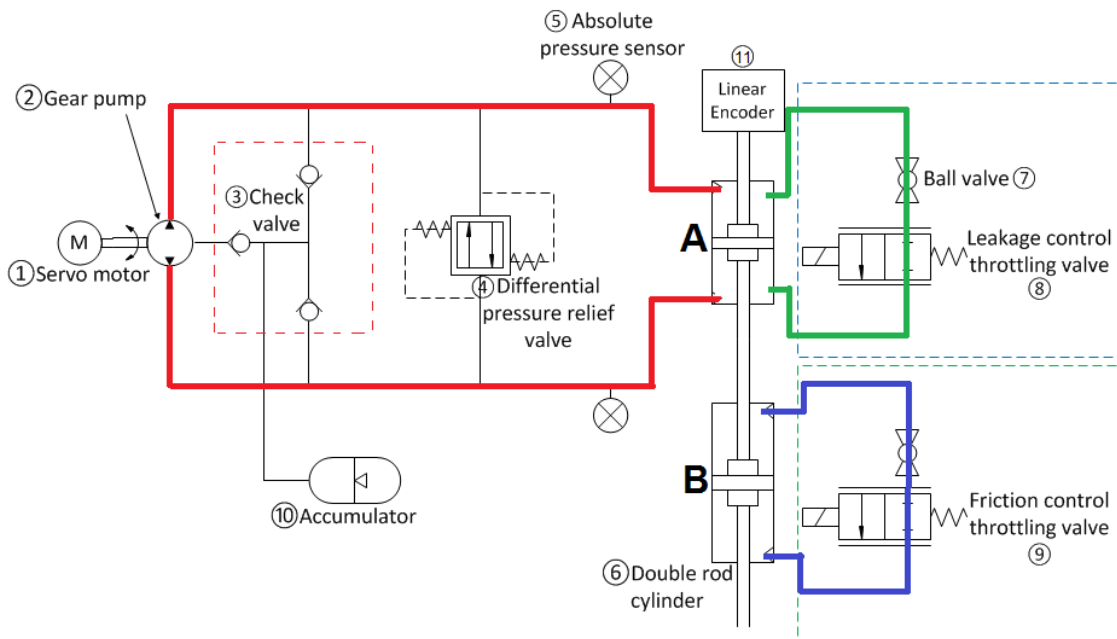


Figure 3.9: EHA Simplified Diagram, [4]

### 3.3. EHA Physical Fault Conditions Simulation

Leakage and friction fault conditions can be physically simulated on the EHA prototype. Figure 3.9 shows the EHA circuit with the leakage simulation sub-circuit (green line) and the load (friction simulation) sub-circuits (blue line). The pump provides fluid power in

either clockwise or counter-clockwise direction according to the desired motion of the actuator. The hydraulic fluid pushes the top actuator (A) directly, and the bottom actuator (B) (⑥) constitutes the load.

Each actuator has a parallel loop connected, which allows the fluid bypass the actuator. The two bypass circuits allow physical simulation of leakage and friction fault conditions. Each bypass is controlled by a throttling valve (⑧, ⑨). By controlling the opening of throttling valves, different combinations and levels of severity of fault conditions can be simulated. The throttling valves are a HydraForce SP08-25, 2-way, normally open, bi-directional type, [8]. The valve opening level is proportional to the input voltage. The input range is 0-10 VDC; with 10 VDC the valve is fully closed and with 0 VDC the valve is fully open.

### **3.3.1. Leakage Fault**

The consequences of a leakage fault are that the actuator velocity is reduced and the system efficiency is lowered, [4]. There are two kinds of leakage: external and internal, [38]. External leakage occurs when there is: a crack on the outside of the hydraulic pipe; an external seal failure; or an improper connection of the pipes. External leakage is easy to detect visually. However, internal leakage occurs inside the actuator in the actuator cylinder and piston, or within the pump, and cannot be easily detected, [38]. In our study, internal leakage is considered as a type of leakage fault.

By allowing a portion of the fluid from the driven hydraulic circuit to pass through the green solid bypass in Figure 3.9, internal leakage is physically simulated. Based on the study by Y. Song, in [4], leakage fault has large impact on actuator velocity. Figure 3.8 is

a plot of actuator velocity versus the throttling valve voltage. All tests have been done with the same pump speed of 900 RPM (94.25 rad/s).

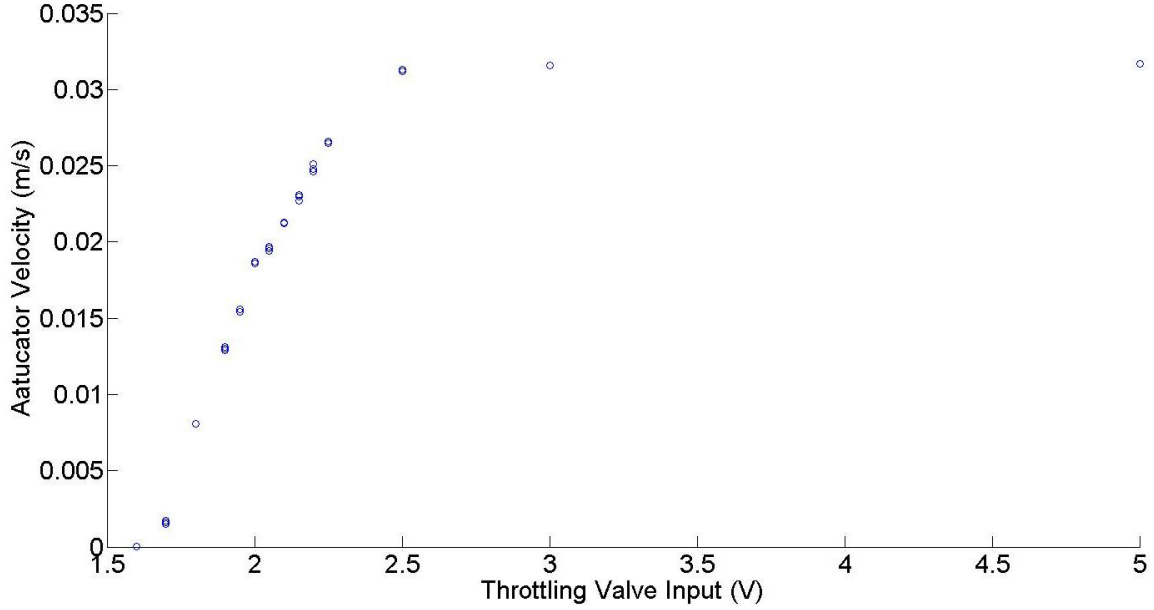


Figure 3.10: Actuator Velocity vs. Throttling Valve Input

For the throttling valve inputs above 3 V, The actuator velocity remains at the same level.

The actuator velocity has notable changes between 1.5 V to 2.5 V. According to Song model's Eqs. (4.1) and (4.2) in [8], the leakage level under steady state conditions can be defined as provided in Table 3.1.

$$Q_{leakage} = A * \dot{x}_{NC} - A * \dot{x} \quad (3.1)$$

$$\%_{leakage} = \frac{Q_{leakage}}{A * \dot{x}_{NC}} = 1 - \left( \frac{\dot{x}}{\dot{x}_{NC}} \right) \quad (3.2)$$

where  $Q_{leakage}$  is leakage flow rate,  $A$  is the actuator piston area, and  $\dot{x}_{NC}$  is the normal actuator velocity. The percentage of leakage rate,  $\%_{leakage}$  can be calculated. At throttling valve inputs of 1.8 V, a leakage level of 74.39 % is set as leakage conditions, (see Table 3.1).

Table 3.1: Actuator Velocity vs. Throttling Valve Input

Throttling valve input (V)	Actuator velocity (m/s)	Percentage leakage
10	0.0316	0.00%
5	0.0316	0.00%
3	0.0316	0.11%
2.5	0.0312	1.16%
2.25	0.0265	16.12%
2.2	0.0248	21.50%
2.15	0.0229	27.50%
2.1	0.0212	32.88%
2.05	0.0195	38.15%
2	0.0186	41.10%
1.95	0.0154	51.11%
1.9	0.0130	58.90%
<b>1.8</b>	<b>0.0081</b>	<b>74.39%</b>
1.7	0.0016	94.94%
1.6	0.0001	99.84%

### 3.3.2. Friction Fault

The actuator's piston seal conditions affect the friction level, [4]. Large friction may accelerate the piston's wear and cause the piston seal to fail, which may also lead to leakage fault, [39, 40]. Applying the blue solid bypass in Figure 3.9, the bottom actuator (B) and friction bypass forms a small closed-loop. By varying the opening of the throttling valve, friction faults can be physically simulated Figure 3.11 is a plot of differential pressure versus throttling valve input value. All tests have been done with the same pump speed at 900 RPM (94.25 rad/s).

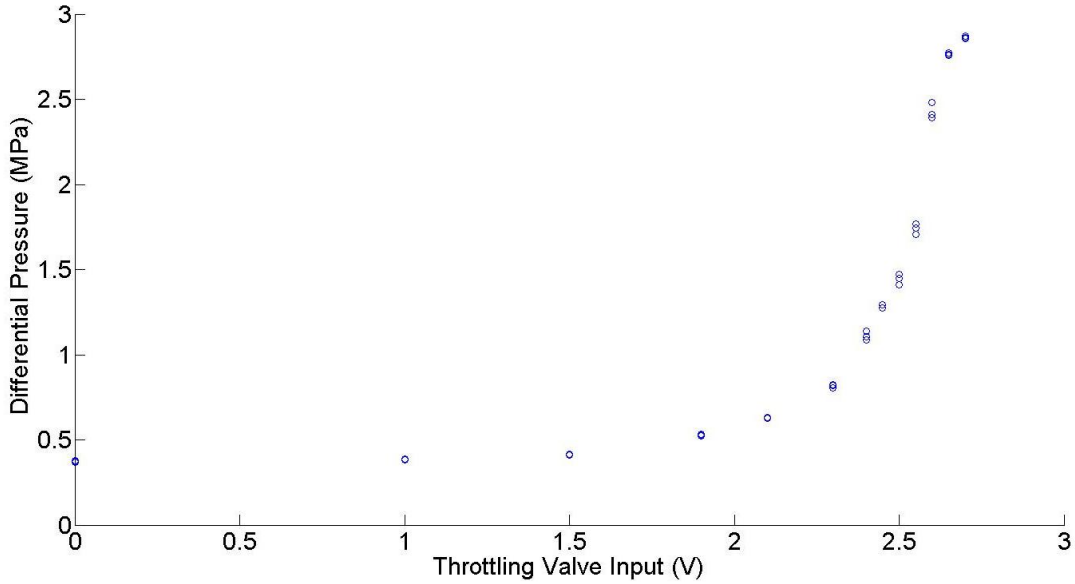


Figure 3.11: Differential Pressures vs. Throttling Valve Input

The differential pressure remains at a relatively low level from 0-2 V throttling valve input, and increases to a high level when the throttling valve input is about 2.5 V. Referring to Song's model [4] of Eqs. (4.3) and (4.4), the friction level under steady state conditions can be defined as shown in Table 3.2.

$$F_f = A * \Delta P - A * \Delta P_{nc} \quad (3.3)$$

$$\%_{friction} = \frac{F_f}{A * \Delta P_{nc}} = \left( \frac{\Delta P}{\Delta P_{nc}} \right) - 1 \quad (3.4)$$

$F_f$  is friction force,  $\Delta P_{nc}$  is the differential pressure at normal conditions,  $\%_{friction}$  is percentage of friction force compared to the normal condition. Setting the throttling valve input at 2.45 V, the friction forces at this level is treated as the friction fault conditions.

Table 3.2: Differential Pressure vs. Throttling Valve Input

Throttling valve input (V)	Differential pressure (MPa)	Percentage friction
0	0.3749	0.00%
1	0.3837	2.33%
1.5	0.4124	9.99%
1.9	0.5279	40.80%
2.1	0.6299	67.99%
2.3	0.8155	117.50%
2.4	1.1109	196.29%
<b>2.45</b>	<b>1.2876</b>	<b>243.41%</b>
2.5	1.4435	285.00%
2.55	1.7393	363.88%
2.6	2.4285	547.68%
2.65	2.7646	637.34%
2.7	2.8616	663.19%

### 3.4. EHA Modeling

Based on the fault simulation results, EHA physical models are created, [4]. Physical models can provide an understanding of the system. A well-developed model library is able to describe EHA dynamics for fault detection studies.

#### 3.4.1. Leakage Model

An EHA leakage model is first developed. The EHA uses a gear pump with constant displacement. The pump flow rate can be modelled as following:

$$D_p \omega_p = A \dot{x} + \frac{V_0}{\beta} \left( \frac{dP_1}{dt} - \frac{dP_2}{dt} \right) + L_t (P_1 - P_2) \quad (3.5)$$

According to Eq. (3.5), [8], the ideal pump flow  $D_p \omega_p$  is a function of three terms: actuator motion, compressibility, and leakage. Where  $D_p$  is the pump's volumetric displacement,  $\omega_p$  is the pump's angular speed,  $A$  is the actuator piston area,  $\dot{x}$  is the

actuator speed,  $V_0$  is the nominal volume of the actuator chamber,  $\beta$  is the effective bulk modulus,  $L_t$  is the leakage coefficient, and  $P_1$  and  $P_2$  are the chamber pressures.

Under ideal steady state flow, pressure is unchanged and  $\frac{dP_1}{dt} - \frac{dP_2}{dt} = 0$ . Eq. (3.5) can be simplified and rearranged as:

$$Q_L = D_p \omega_p - A \dot{x} = L_t (P_1 - P_2) \quad (3.6)$$

where  $Q_L$  is the total leakage flow rate.

Yu developed a process to determine the leakage coefficient, [4] by running the EHA in a steady state mode under different pressure conditions with constant pump speed. The pressure changes were controlled by the friction throttling valve (⑨ in Figure 3.9); during experimentation, the actuator speed,  $\dot{x}$ , and the differential pressure ( $P_1 - P_2$ ) were recorded. Figure 3.12 shows the actuator flow rate versus differential pressure.

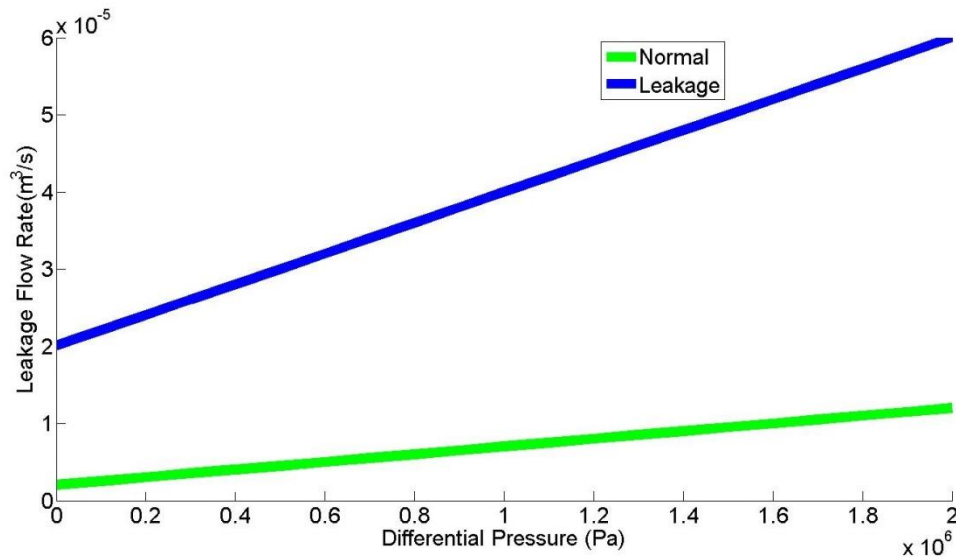


Figure 3.12: Actuator Flow Rate vs. Differential Pressure

In Figure 3.12, two lines represent normal and leakage conditions. For the purpose of this thesis, the green line will be set as the normal condition, the blue is the leakage fault

condition. In characterizing the leakage faults, Song used an offset  $Q_L$ , at zero differential pressure under leakage condition as shown in Eq. (3.6):

$$Q_L = D_p \omega_p - A\dot{x} = L_t(P_1 - P_2) + Q_{L0} \quad (3.7)$$

Rearranging Eq. (3.7):

$$D_p \omega_p = A\dot{x} + \frac{V_0}{\beta} \left( \frac{dP_1}{dt} - \frac{dP_2}{dt} \right) + L_t(P_1 - P_2) + \text{sgn}(P_1 - P_2)Q_{L0} \quad (3.8)$$

with  $L_t$  and  $Q_{L0}$  as leakage coefficients, Eq. (3.8) is the leakage model for the EHA, [4].

### 3.4.2. Friction Model

Friction model is designed in this section. By looking at the general force equation, and assuming no external load is applied to EHA at all time.

$$F = (P_1 - P_2)A = M\ddot{x} + F_f \quad (3.9)$$

Eq. (3.9) is the EHA actuator output force function, [4]. Where  $M$  is the actuator's mass,  $\ddot{x}$  is the actuator acceleration, and  $F_f$  is the friction force. The friction force term  $F_f$  can be described by a second order function:

$$F_f = a_2\dot{x} + (a_1\dot{x}^2 + a_3)\text{sgn}(\dot{x}) \quad (3.10)$$

where  $a_1$ ,  $a_2$ , and  $a_3$  are friction coefficients. At steady state  $\ddot{x} = 0$ , by combining Eqs. (3.9) and (3.10):

$$(P_1 - P_2)A = a_2\dot{x} + (a_1\dot{x}^2 + a_3)\text{sgn}(\dot{x}) \quad (3.11)$$

In order to determine friction fault coefficients, the EHA was operated at different speeds ( $\dot{x}$ ), and at each speed, the differential pressure ( $P_1 - P_2$ ) across the actuator chambers was measured, [4]. Figure 3.13 shows the plot of actuator speed versus Friction force ( $(P_1 - P_2)A$ ).

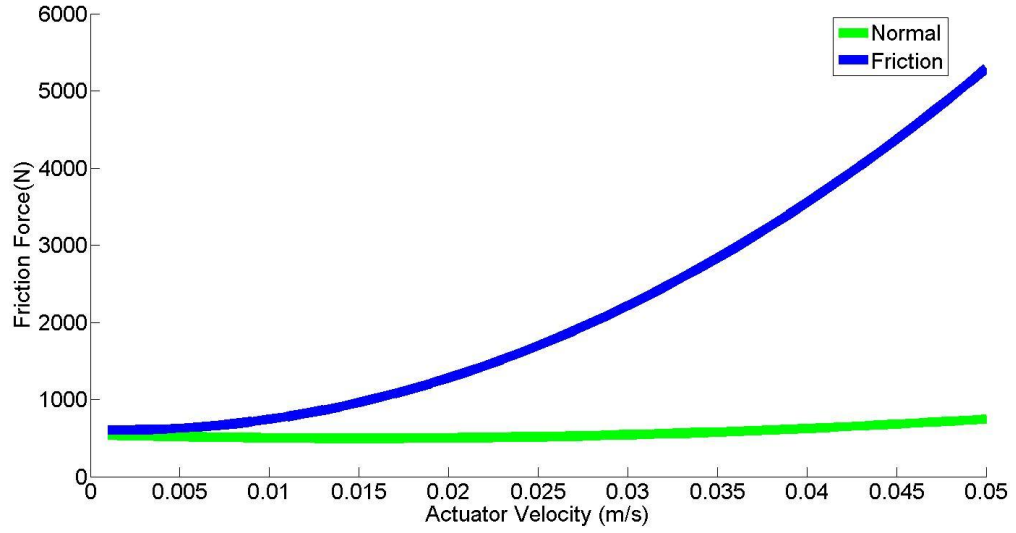


Figure 3.13: Friction Force vs. Actuator Velocity

In Figure 3.13, two line represent the normal and the friction fault conditions. For the purpose of this thesis, the green line is the normal condition, and the blue line is the friction fault. By dividing A from both side of Eq. (3.11):

$$P_1 - P_2 = \frac{M}{A} \ddot{x} + \frac{a_2}{A} \dot{x} + \frac{a_1 \dot{x}^2 + a_3}{A} \operatorname{sgn}(\dot{x}) \quad (3.12)$$

Taking the derivative of Eq. (3.12), and assuming that the sign function  $\operatorname{sgn}(\dot{x})$  is not continuous when  $\dot{x} = 0$ ,  $\frac{dP_1}{dt} - \frac{dP_2}{dt}$  is obtained as:

if  $\dot{x} > 0$

$$\frac{dP_1}{dt} - \frac{dP_2}{dt} = \frac{M}{A} \ddot{x} + \frac{a_2}{A} \ddot{x} + \frac{2a_1 \dot{x} \ddot{x}}{A}$$

if  $\dot{x} = 0$

$$\frac{dP_1}{dt} - \frac{dP_2}{dt} = \frac{M}{A} \ddot{x} + \frac{a_2}{A} \ddot{x} \quad (3.13)$$

if  $\dot{x} < 0$

$$\frac{dP_1}{dt} - \frac{dP_2}{dt} = \frac{M}{A}\ddot{x} + \frac{a_2}{A}\dot{x} - \frac{2a_1\dot{x}\ddot{x}}{A}$$

which is the same as:

$$\frac{dP_1}{dt} - \frac{dP_2}{dt} = \frac{M}{A}\ddot{x} + \frac{a_2}{A}\dot{x} + \frac{2a_1\dot{x}\ddot{x}}{A} \operatorname{sgn}(\dot{x}) \quad (3.14)$$

Substituting Eqs. (3.12) and (3.14) into Eq. (3.8):

$$D_p \omega_p - \operatorname{sgn}(P_1 - P_2) Q_{L0} \quad (3.15)$$

$$\begin{aligned} &= \frac{MV_0}{A\beta}\ddot{x} + \frac{a_2V_0 + M\beta L_t}{A\beta}\dot{x} + \frac{A^2 + a_2L_t}{A}\dot{x} \\ &+ \frac{2a_1V_0\dot{x}\ddot{x} + \beta L_t(a_1\dot{x}^2 + a_3)}{A\beta} \operatorname{sgn}(\dot{x}) \end{aligned}$$

Eq. (3.15) is the nonlinear model of the EHA developed by Song, [4]. The detailed nonlinear model and all parametric values, are provided in Chapter 5.

## Chapter 4

### Control Strategies

For the purpose of achieving better EHA fault tolerance, several controllers are considered and applied in this research. These controllers were implemented and tested on the EHA prototype and the simulation/experimental results obtained on EHA setup are compared and analyzed. Firstly, two approaches of sliding mode control (SMC) are considered, that were proposed by Misawa, [5, 6], and Slotine and Li, [7]. Then a new controller strategy based on SMC (i.e., using the two SMC structures) is proposed that applies the interacting multiple model (IMM) frame work with two model based estimation techniques: the Smooth Variable Structure Filter (SVSF) and the Kalman Filter (KF). These are applied to the EHA prototype. The proportional-integral-derivative (PID) and the PID with added feedforward compensation are also applied and presented for comparative studies in this chapter.

#### **4.1. Existing controller: Misawa Based Sliding Mode Control Strategy**

El-Sayed et al., [28], proposed a new sliding mode control (SMC) strategy to increase the tracking accuracy of the EHA. Their design was based on the original SMC developed by E.A. Misawa, [5, 6], and S. Wang et al. [41]. Misawa's controller designs can be applied to both linear and nonlinear systems. S. Wang et al., [41], extended Misawa's strategy and applied it for trajectory tracking of EHA systems. His study showed that the SMC succeeded in providing accurate tracking results, with lower chatter in velocity and

acceleration, by using a higher boundary layer thickness while trading off a reduction in position precision. The basic control strategy used by M.A. El Sayed et al. builds on Misawa's and Wang's work and is provided in [28]. For a single input dynamical system represented by:

$$x_{k+1} = F * x_k + G * u_k + w_k \quad (4.1)$$

where  $k$  and  $k + 1$  are time steps,  $F$  and  $G$  are system and input matrices,  $x$  is the state,  $u$  is the input, and  $w$  is the uncertainties in the system. The uncertainties represented by  $w$  are assumed to be bounded:

$$Y \geq |C * w| \quad (4.2)$$

$C$  is a sliding surface parameter vector. The goal of a sliding mode control, is to keep the system trajectory to follow a desired trajectory  $x_d$ , by keep the tracking error  $e_k = x_{d,k} - x_k$  close to zero, which is defined as:

$$\Sigma = \{e_k | s_k = C * e_k = 0\} \quad (4.3)$$

The sliding boundary layer keeps the tracking trajectory sliding within the boundary layer:

$$\Psi = \{e_k | |s_k| = |C * e_k| \leq \psi\} \quad (4.4)$$

According to E. A. Misawa's SMC structure, [5, 6], M. A. El Sayed, et al., [28] designed the control input of an EHA system as:

$$u_k = u_{eq,k} - (C * G)^{-1} * s_k + (C * G)^{-1} * K_c * sat\left(\frac{s_k}{\psi}\right) \quad (4.5)$$

$u_{eq}$  is the equivalent control term, and the rest of the terms are switching control terms.

$K_c$  is the control gain, and  $\epsilon$  is an arbitrary constant. Each term is defined as following:

$$u_{eq,k} = (C * G)^{-1} * C * (x_{d,k-1} - F * x_k) \quad (4.6)$$

$$K_c = \gamma + 2\epsilon, \psi \geq \gamma + \epsilon \quad (4.7)$$

$$Sat\left(\frac{S_k}{\psi}\right) = +1 \text{ if } S > \psi \quad (4.8)$$

$$= \left(\frac{S}{\psi}\right) \text{ if } |S| \leq \psi$$

$$= -1 \text{ if otherwise}$$

The disadvantage of E.A. Misawa's theory is that the uncertainties,  $w$ , are bounded by a constant, [5, 6], which is conservative. M.A. El-Sayed, et al., [28] designed a new variable system gain  $K_c$ , and a variable boundary layer  $\psi$ :

$$K_c = C * F_{max} * |e_k| + C * F_{max} * |x_{d,k}| + C * G_{max} * u_{max} + C * v_{max} + 2\epsilon \quad (4.9)$$

$$\psi = C * F_{max} * |e_k| + C * F_{max} * |x_{d,k}| + C * G_{max} * u_{max} + C * v_{max} + \epsilon \quad (4.10)$$

$F_{max}$  and  $G_{max}$  are the upper bounds on uncertainties in the system matrix and input matrix,  $u_{max}$  is the maximum allowable input to the system, and  $v_{max}$  is the maximum noise amplitude. Eqs. (4. 1) to (4. 10) are the SMC applied by M.A. El-Sayed, et al., [28].

## 4.2. New Design: Slotine and Li Based SMC Strategy

By studying the existing design of SMC, a new SMC is proposed based on J.E. Slotine and W. Li's sliding mode control method, [7]. The purpose of this design is to improve the controller's performance for EHA position tracking and fault tolerance. The new SMC design steps are as follows.

First, defining a single input, dynamic system is assumed as:

$$x^{(n)} = f(x) + b(x) * u \quad (4.11)$$

with trajectory tracking errors defined as:

$$[e \ \dot{e} \ \ddot{e}] = [x \ \dot{x} \ \ddot{x}] - [x_d \ \dot{x}_d \ \ddot{x}_d] \quad (4.12)$$

$\mathbf{x} = [x \ \dot{x} \ \ddot{x}]$  and  $u$  are the state and control input.  $f(\mathbf{x})$  and  $b(\mathbf{x})$  are a system and input vectors similar to (4.1), they are not exactly known, but are bounded by a known function of  $\mathbf{x}$ . Slotine and Li ignore measurement errors and noise; as such they define  $\mathbf{x} = [x \ \dot{x} \ \ddot{x}]$  and  $\mathbf{x}_d = [x_d \ \dot{x}_d \ \ddot{x}_d]$  as the measured and desired position, velocity and acceleration, and  $\mathbf{e} = [e \ \dot{e} \ \ddot{e}]$  are the tracking errors between the measured and desired values. The control goal is to make sure state  $\mathbf{x}$  to track  $\mathbf{x}_d$  (i.e.  $\mathbf{x} \equiv \mathbf{x}_d$ ) with model imprecision on  $f(\mathbf{x})$  and  $b(\mathbf{x})$ .

According to Eq. (7.3) in [7], the sliding surface, or time-varying surface  $S(t)$  is defined as:  $s(\mathbf{x}; t) = (\frac{d}{dt} + C)^{n-1} * e$ , where  $C$  is a strictly positive constant, and  $n$  is the order of the system. For  $n = 2$ :

$$s = C * e + \dot{e} \quad (4.13)$$

$$\dot{s} = C * \dot{e} + \ddot{e} \quad (4.14)$$

$s$  is treated as a weighted sum of the position and velocity error. The control goal clearly is to keeping  $s$  as closed as possible at zero.

In another form, by replacing the  $n^{th}$ -order tracking problem with a  $1^{st}$ -order stabilization problem, the objective is to keep  $s$  as closed as possible to zero by choosing a proper control input  $u$ , so that outside of  $S(t)$ :

$$\frac{1}{2} \frac{d}{dt} s^2 = s\dot{s} \leq -\eta|s| \quad (4.15)$$

where  $\eta$  is a strictly positive constant. The above equation is the sliding condition, which makes sure the  $\frac{1}{2} \frac{d}{dt} s^2 = s\dot{s}$  is decreasing and moving towards the surface  $S(t)$ .

Eqs. (4. 13) to (4. 15) define the behavior of tracking error  $s$  on the surface  $S(t)$  and outside this surface.

For a system of the form  $\ddot{x} = f - b * u$ , by rearranging and combing with Eq.(4. 14) under expectation  $\dot{s} = 0$ , the equivalent control  $u_{eq}$  is obtained as:

$$u_{eq} = \frac{-\hat{f} + \ddot{x}}{\hat{b}} = \frac{-\hat{f} + \ddot{x}_d - C * \dot{e}}{\hat{b}} \quad (4. 16)$$

where  $\hat{f}$  and  $\hat{b}$  are the best estimations of  $f$  and  $b$ .  $u_{eq}$  is the best estimate of the equivalent control. Then by adding a discontinuous term to  $u_{eq}$  across surface  $s = 0$ :

$$u = u_{eq} - k * \text{sgn}(s) \quad (4. 17)$$

where  $k$  is the bounded value between equivalent input and maximum input, defined as:

$$k = |u_{max} - u_{eq}| \quad (4. 18)$$

and  $u_{max}$  is the defined maximum input. Substituting Eqs.(4. 16) to (4. 18) into (4. 15):

$$\begin{aligned} s\dot{s} &= s(C * \dot{e} + \ddot{x} - \ddot{x}_d) \\ &= s[(f - b * \hat{b}^{-1} \hat{f}) + (b * \hat{b}^{-1} - 1)(\ddot{x}_d - C * \dot{e})] - b|u_{max} - u_{eq}||s| \\ &\leq -\eta|s| \end{aligned}$$

$u_{max}$  can be properly chosen in order to satisfy the above mentioned sliding condition.

The high frequency of switching in  $s$  causes chattering. In order to achieve smooth control, a smoothing boundary layer  $B(t) = \{x, |s(x; t)| \leq \psi\}$  (Eq. 7.25 in [7]) is introduced.  $\psi$  is the thickness of the boundary layer. Outside of  $B(t)$ , the control law is as

usual; within the boundary layer  $B(t)$ , the  $sgn(s)$  term in Eq.(4. 16) is replaced by  $\frac{s}{\psi}$ .

Saturation functions are defined as:

$$sat\left(\frac{s}{\psi}\right) = \frac{s}{\psi}, \text{ if } \left|\frac{s}{\psi}\right| \leq 1; \quad (4. 19)$$

$$sat\left(\frac{s}{\psi}\right) = sign\left(\frac{s}{\psi}\right), \text{ otherwise.}$$

Rewriting the overall control input of Eq. (4. 17) as:

$$u = u_{eq} - k * sat\left(\frac{s}{\psi}\right) \quad (4. 20)$$

Eqs. (4. 11) to (4. 20) are the basic equations of Slotine and Li based SMC. Table 4. 1 summarizes the two approaches of SMC with different terms and values listed. It should be noted that the parameters in Table 4. 1 do not represent a direct comparison and are based on different assumptions pertaining to model complexity and structure.

**Table 4. 1: Comparison of Two SMC Controllers, including All Constant Terms**

	<b>Misawa Based SMC</b>	<b>Slotine and Li Based SMC</b>
<b>Error</b>	$e = x_d - x, \dot{e} = \dot{x}_d - \dot{x}, \ddot{e} = \ddot{x}_d - \ddot{x}$	
<b>Sliding surface gain</b>	$C = [20000 \ 100 \ 1]$	$C = 500$
<b>Error sum</b>	$s = C_1 * e + C_2 * \dot{e} + C_3 * \ddot{e}$	$s = C * e + \dot{e}$
<b>Equivalent input</b>	$u_{eq,k} = (C * G)^{-1} * C * [e_{k+1} \ \dot{e}_{k+1} \ \ddot{e}_{k+1}]$	$u_{eq} = \frac{-f + \ddot{x}_d - C * \dot{e}}{b}$
<b>Boundary layer</b>	$\psi = C * F_{max} *  e_k  + C * F_{max} *  x_{d,k}  + C * G_{max} * u_{max} + C * v_{max} + \epsilon$	$\Psi = 0.425$
<b>Gain</b>	$K_c = C * F_{max} *  e_k  + C * F_{max} *  x_{d,k}  + C * G_{max} * u_{max} + C * v_{max} + 2\epsilon$	$k =  u_{eq} - u_{max} $
<b>Saturation</b>	$sat(\frac{S_k}{\psi}) = +1$ if $S > \psi$ ; $sat(\frac{S_k}{\psi}) = (\frac{S}{\psi})$ if $ S  \leq \psi$ ; $sat(\frac{S_k}{\psi}) = -1$ if otherwise.	
<b>Control input</b>	$u_k = u_{eq,k} - (C * G)^{-1} * s_k + (C * G)^{-1} * K_c * sat(\frac{S_k}{\psi})$	$u = u_{eq} - k_c * sat(\frac{S}{\psi})$
<b>Constant values</b>	$F_{max} = [0 \ 0 \ 0; 0 \ 0 \ 0; 0 \ 8.6695 \ 0.3099];$ $G_{max} = 0;$ $u_{max} = 0;$ $\epsilon = 0$	$u_{max} = 600$

### 4.3. IMM with SMC Strategy

M.A. El-Sayed et al. [28] have proposed a new control strategy on the EHA for trajectory tracking that combines the SMC (section 4.1 and 4.2) and the IMM (section 2.3.3). The basic idea is to add an IMM block into the controller-system loop. The IMM algorithm calculates the estimated model probability based on the current system model information. The basic algorithm of the SMC-IMM is shown in Figure 4.2:

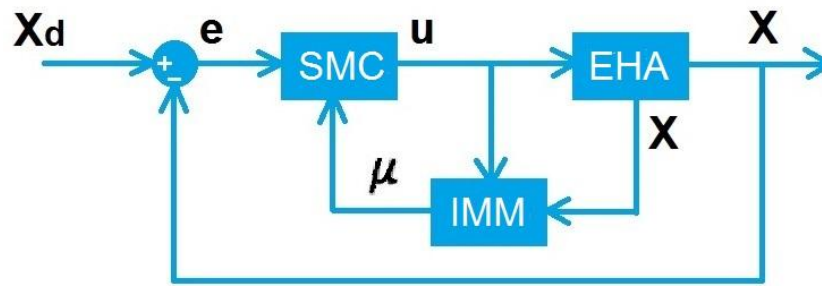


Figure 4.2: SMC-IMM Basic Structure

where  $x$  is the actual system states of the EHA actuator,  $x_d$  is the desired states,  $e$  is the differences between  $x$  and  $x_d$ ,  $u$  is the input, and  $\mu$  is the mode probability.

IMM takes this  $u$  and the system state  $x$  in order to calculate the mode probability  $\mu$ . The basic IMM algorithm is described in Section 2.3.3. Some important parametric values are given here.

The initial state estimation  $\hat{x}_{0|0}$  and initial error covariance  $\hat{p}_{0|0}$  (Eqs. (2. 63) and (2. 64)) are defined as:

$$\hat{x}_{0|0} = [0 \ 0 \ 0 \ 0]^T$$

$$\hat{p}_{0|0} = \begin{bmatrix} 20 & 0 & 0 & 0 \\ 0 & 20 & 0 & 0 \\ 0 & 0 & 20 & 0 \\ 0 & 0 & 0 & 20 \end{bmatrix}$$

The EHA system is assumed to have a probability of 85% operating normally at the start, and have equally 5% of operate under different fault conditions (leakage, friction, and combined). This starting condition probability is represented by the initial mode probability  $\mu_{i,0}$  (Eqs. (2. 61) and (2. 62)) as:

$$\mu_{i,0} = [0.85 \ 0.05 \ 0.05 \ 0.05]$$

After the initialization, the EHA system has the probability of switching between different modes, this is represent by a transition matrix  $p_{ij}$  (Eqs. (2. 61) and (2. 62)):

$$p_{ij} = \begin{bmatrix} 0.97 & 0.01 & 0.01 & 0.01 \\ 0.01 & 0.97 & 0.01 & 0.01 \\ 0.01 & 0.01 & 0.97 & 0.01 \\ 0.01 & 0.01 & 0.01 & 0.97 \end{bmatrix}$$

The diagonal elements of  $p_{ij}$  indicate that the system has a 97% probability of staying in the same condition. The non-diagonal elements indicate that the system has a 1% probability of switch to a different mode.

The SMC takes the tracking error  $e$  and the mode probability  $\mu$  (all the values are between 0 and 1) as inputs. The SMC will run  $r$  (number of models/conditions, i.e.  $r = 4$ ) times parallel for each iteration and calculates  $r$  number of system and input matrices  $F$  and  $G$  (each represents the system model for each conditions). Next each the system model is multiplied by the corresponding mode probability  $\mu$  and sum together to form a weighted system input  $u$ . Finally SMC will output this value to IMM and EHA system.

The actual control equations are modified as follows.

For Misawa based SMC (Section 4.1), the  $F$  and  $G$  terms in Eqs. (4.5) and (4.6) are replaced by  $F_{i,k}$  and  $G_{i,k}$  :

$$u_k = u_{eq,k} - (C * G_{i,k})^{-1} * s_k + (C * G_{i,k})^{-1} * K_c * sat\left(\frac{x_k}{\psi}\right) \quad (4. 21)$$

$$u_{eq,k} = (C * G_{i,k})^{-1} * C * (x_{d,k+1} - F_{i,k} * x_k) \quad (4.22)$$

where  $F_{i,k} = \sum_{i=1}^r \mu_{i,k} F_i$  and  $G_{i,k} = \sum_{i=1}^r \mu_{i,k} G_i$  are the sum of all modes multiplied by their corresponding mode probabilities.

The similar concept is applied to Slotine and Li based SMC (Section 4.2). The  $\hat{f}$  term in Eq. (4.16) is replaced by  $\hat{F}_{l,k}$ :

$$u_{eq} = \frac{-\hat{F}_{l,k} + \ddot{x}}{\hat{b}} = \frac{-\hat{F}_{l,k} + \ddot{x}_d - C * \dot{e}}{\hat{b}} \quad (4.23)$$

where  $\hat{F}_{l,k} = \sum_{i=1}^r \mu_{i,k} \hat{f}_i$  is the weighted sum of the  $\hat{f}_i$  terms, that control the actual dynamic of system under different operation conditions.

### Flowchart Explanation

By expanding Figure 4.2 into Figure 4.3, the algorithm can be further explained. The SMC block in Figure 4.2 is representing by several blocks inside the red box in Figure 4.3. The EHA and IMM-SVSF/KF blocks are the same.

Desired input/states are used for estimated system vectors  $\hat{f}_i$  calculation. For each EHA operating condition, there is a corresponding  $\hat{f}_i$  term, for four EHA operating condition, there are four  $\hat{f}_i$  terms.

Next, during the mixing stage  $\hat{F}$  is calculated from  $\hat{F}_{l,k} = \sum_{i=1}^r \mu_{i,k} \hat{f}_i$ . IMM-SVSF/KF calculation of  $\mu_i$  is actually going to the mixing stage block.

The weighted sum  $\hat{F}$  is used for the SMC calculation that is described by equations in Section 4.2. And the EHA actual states are going into SMC calculation block.

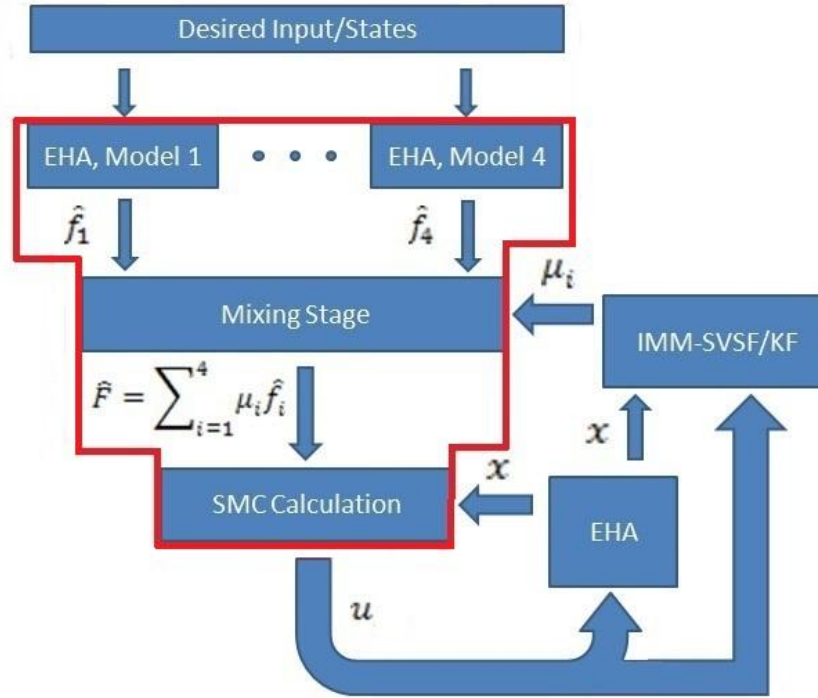


Figure 4.3: IMM-SMC Flowchart

#### 4.4. PID Control

According to M. Araki, [42], proportional, integral and derivative (PID) controllers are widely used; 90% of controllers used in industry are PID. A basic PID controller and modified PID controller were applied to the EHA. The PID controllers calculate a controlled input,  $u$ , based on the feedback error from the actuator's position values. The PID control strategy was applied to the EHA. The control gains were obtained as follows, [43, 44]. From Bone, [44], the transfer function for a PID controller has one of the forms:

$$G_c(s) = K_p + \frac{K_i}{s} + K_d s \quad (4.24)$$

$$G_c(s) = \frac{K_i(\tau_1 s + 1)(\tau_2 s + 1)}{s} \quad (4.25)$$

where  $\tau_1 > \tau_2$ ,  $K_d = K_i \tau_1 \tau_2$  and  $K_p = K_i(\tau_1 + \tau_2)$ .

The gains are calculated using the following steps:

Solving  $\tau_1$  by using:

$$\omega_c = \frac{10}{\tau_1} \quad (4.26)$$

where  $\omega_c$  is the desired cut-off frequency.

The Phase shift of PID controller is calculated by:

$$\Phi_{PID} = (\text{Desired } \Phi_m) + 5 - (\Phi_m \text{ at } \omega_c) \quad (4.27)$$

where  $\Phi_m$  is the desired phase margin. If  $\Phi_{PID} > 70$ , this specification is not valid, otherwise:

$$\log(\tau_2 \omega) = \frac{(\Phi_{PID} - 45)}{45} \quad (4.28)$$

$$\tau_2 = \frac{10^{\log(\tau_2 \omega)}}{(\text{Desired } \omega_c)} \quad (4.29)$$

Gain shift for desired  $\omega_c$  is: gain shift = 0-(dB at desired  $\omega_c$ )

If  $\Phi_{PID} > 45$ :

$$\log(K_i \tau_1) = \frac{(\text{gain shift} - 20 \log(\tau_2 \omega))}{20} \quad (4.30)$$

else:

$$\log(K_i \tau_1) = \frac{\text{gain shift}}{20} \quad (4.31)$$

$$K_i = \frac{10^{\log(K_i \tau_1)}}{\tau_1} \quad (4.32)$$

Calculate  $K_d$  and  $K_p$ :

$$K_d = K_i \tau_1 \tau_2 \quad (4.33)$$

$$K_p = K_i (\tau_1 + \tau_2) \quad (4.34)$$

The control gains are subsequently tuned manually on the system based on the observed time response of the system.

#### 4.5.1. PID for EHA

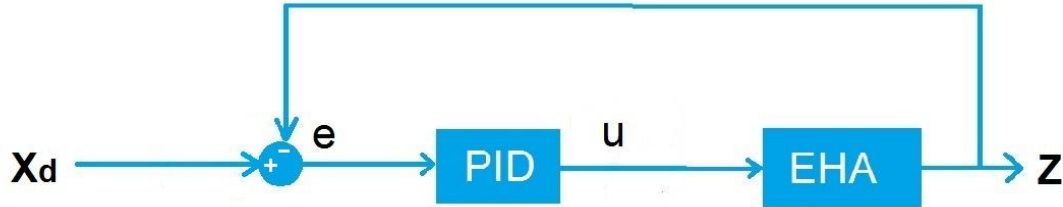


Figure 4.4: PID Control

Figure 4.3 is the basic control loop of a PID controller for the EHA. The error  $e$  between desired input and measured output feeds into the PID controller, and a calculated input  $u$  from the PID goes to the EHA system.

According to M.A. El-Sayed et al., [43], the EHA open loop transfer function can be simplified in a linear form as:

$$G_{EHA} = \frac{22.34}{p(p^2 + 3526p + 6.542 * 10^4)} \quad (4.35)$$

For desired  $\omega_c = 30 \text{ rad/s}$ ,  $\Phi_m = 50$ , and  $G_m = 8\text{dB}$ , the PID gains can be obtained according to the above mentioned process and the controller is derived as:

$$G_{PID} = \frac{4.71 * 10^3 p^2 + 9.44 * 10^4 p + 2.41 * 10^5}{p} \quad (4.36)$$

#### 4.5.2. PID with Equivalent Control

Another alternative control strategy is to combine the PID control (from Section 4.4), with the equivalent control term  $u_{eq}$  (from Section 4.1 and 4.2) that is effectively a form of feedforward compensation as shown in Figure 4.4.

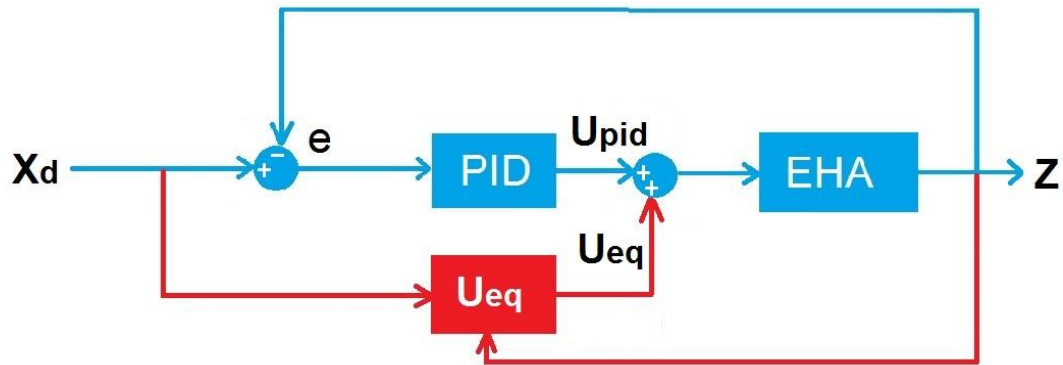


Figure 4.5: PID with Equivalent Control

In this chapter, five controllers were introduced (two SMC, IMM-SMC, PID, and PID with equivalent control). All the control strategies will be demonstrated on the EHA prototype for position tracking in the next chapter.

## Chapter 5

### Experiment Results

This chapter contains the experimental results obtained from five different control strategies applied to the EHA prototype under normal and fault conditions. The results for each control strategy are compared. These five control strategies are divided into two groups. The first group consist of the PID and the PID with the added equivalent control term. The second group is the sliding mode control (SMC), and the SMC with interactive multiple model (IMM) using two estimators that are the smooth variable structure filter (SVSF) and the Kalman filter (KF) as follows:

Group 1:

- PID
- PID with equivalent control

Group 2:

- SMC
- IMM-SMC-SVSF
- IMM-SMC-KF

#### 5.1. Initial Experiment Setup

For the purpose of consistency, all experiments were performed with the same input profiles and under the condition, as outlined in this section.

### 5.1.1. EHA Input and its Simulated Fault Conditions

Figure 5.1 shows the EHA input for all tests. The input corresponds to a triangular motor angular velocity with a peak magnitude of  $\pm 103.5 \text{ rad/s}$ , changing direction every two seconds. At the same time, different faults are physically simulated as listed in Table 5.1. The input profile of Figure 5.1 essentially results in steady state operation in terms of trajectory following of the acceleration term. This profile was used to allow simplification of the EHA's dynamic model. This is the only profile which can be used with the control strategies proposed in this thesis, posing a severe restriction at the application of the concepts proposed.

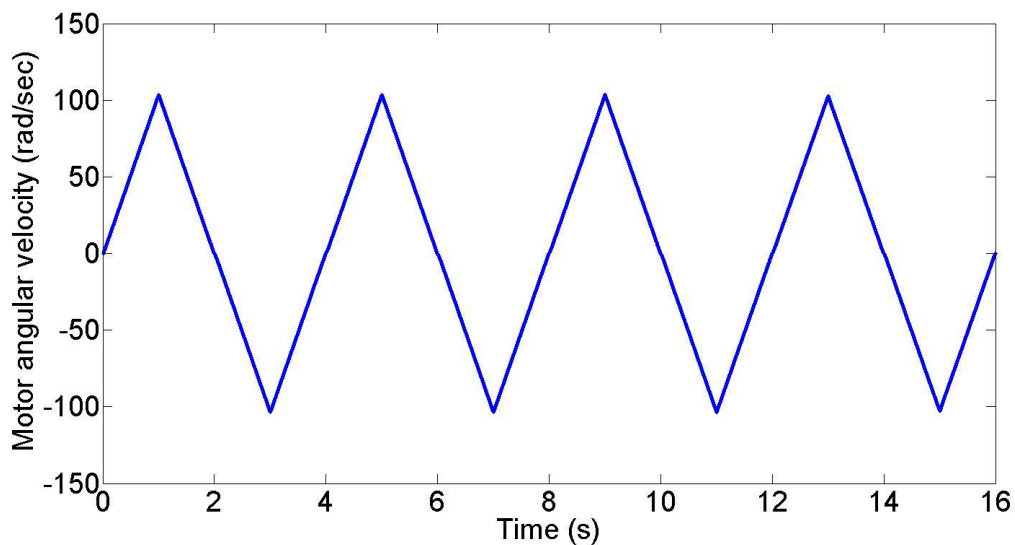


Figure 5.1: EHA Input Motor Angular Velocity

Table 5.1: EHA Fault Conditions

Running Conditions	Time (s)
Normal	0 – 4
Leakage fault	4 – 8
Friction fault	8 – 12

The leakage fault is described in Section 3.3.1, and leakage model coefficients are provided in 5.1.2.

The friction fault is described in Section 3.3.2, with friction model coefficients listed in 5.1.2.

Combined fault means leakage and friction fault introduced at the same time.

### 5.1.2. EHA Mathematic Models

Two EHA mathematical models are studied: a linear and a nonlinear models. The two models are used for IMM probability calculations and SMC implementations.

#### 5.1.2.1. EHA Nonlinear Model:

The EHA nonlinear model was derived by S.A. Gadsden et al., [29].  $x_1, x_2, x_3, x_4$  represent actuator position, velocity, acceleration and pressure,  $u_k$  is the EHA input, and  $T$  is the time step. This model has a fourth state as pressure measurement, which provides more system dynamics. Model with parameters and coefficients are listed below.

$$x_{1,k+1} = x_{1,k} + T * x_{2,k}$$

$$x_{2,k+1} = x_{2,k} + T * x_{3,k}$$

$$x_{3,k+1} = \left[ 1 - T * \left( \frac{a_2 * V_0 + M * \beta * L_t}{M * V_0} \right) \right] * x_{3,k} - \left[ T * \frac{(A^2 + a_2 * L_t) * \beta}{M * V_0} * x_{2,k} \right] \\ - \left[ T * \frac{2 * a_1 * V_0 * x_{2,k} * x_{3,k} + \beta * L_t * (a_1 * x_{2,k}^2 + a_3)}{M * V_0} * \text{sign}(x_{2,k}) \right] \\ + \left[ T * \frac{A * \beta}{M * V_0} * u_k \right]$$

$$x_{4,k+1} = \left[ \frac{M}{A} * x_{3,k} + \frac{a_2 * x_{2,k} + (a_1 * x_{2,k}^2 + a_3) * \text{sign}(x_{2,k})}{A} \right] * 10^{-6}$$

$$u_{k+1} = u_k * D_p - \text{sign}(x_2) * Q_b$$

Table 5.2: EHA Nonlinear Model Parameters

Parameters	Value	Description
$V_0$	$1.08 * 10^{-3} m^3$	Initial cylinder volume
$M$	$7.378 kg$	Actuator mass
$\beta$	$2.1 * 10^8 Pa$	Effective bulk modulus
$A$	$1.52 * 10^{-3} m^2$	Piston area
$D_p$	$5.57 * 10^{-7} m^3/s$	Gear pump volumetric displacement

Table 5.3: EHA Nonlinear Model Leakage Coefficients

Condition	Leakage coefficient ( $L_t$ )	Leakage offset ( $Q_b$ )
Normal	$4.7837 * 10^{-12} \frac{Pa * m^3}{s}$	$2.4125 * 10^{-6} \frac{m^3}{s}$
Leakage	$6.0057 * 10^{-11} \frac{Pa * m^3}{s}$	$1.4646 * 10^{-5} \frac{m^3}{s}$

Table 5.4: EHA Nonlinear Model Friction Coefficients

Condition	$a_1$	$a_2$	$a_3$
Normal	$8.3108 * 10^4$	$2.0998 * 10^3$	511
Friction	$2.0373 * 10^6$	$2.3475 * 10^3$	535

### 5.1.2.2. EHA Linear Model:

This EHA linear model was developed by M.A. El-Sayed et al., [28].  $F$  and  $G$  are the state and the input matrices respectively. The fault condition coefficients are provided in Tables 5.5 and 5.6. This model neglect higher order dynamics of the EHA and as such

contains inaccuracies pertaining both to parametric values as well as model structure.

Readers are referred to references [36, 29] for more accurate models of EHA.

$$x_{k+1} = F * x_k + G * u_k$$

$$F = \begin{bmatrix} 1 & T & 0 \\ 0 & 1 & T \\ 0 & \left[ -T * \frac{(A^2 + B * L_t) * \beta}{M * V_0} \right] & \left[ 1 - T * \left( \frac{B * V_0 + M * \beta * L_t}{M * V_0} \right) \right] \end{bmatrix}$$

$$G = \left[ 0; \quad 0; \quad \left( T * \frac{A * D_p * \beta}{M * V_0} \right) \right]$$

Table 5.5: EHA Linear Model Leakage Coefficients

Condition	$L_t$
Normal	$2.9030 * 10^{-11} \frac{Pa * m^3}{s}$
Leakage	$1.7418 * 10^{-10} \frac{Pa * m^3}{s}$

Table 5.6: EHA Linear Model Friction Coefficients

Condition	$B$
Normal	$2.8569 * 10^4$
Friction	$3.9997 * 10^4$

### 5.1.2.3. Model Accuracy Test

The accuracy of the two EHA models were tested under different fault conditions. By giving the same input signal and fault conditions as shown in Figure 5.1 and Table 5.1, the EHA's measured response is compared to its simulated response using the two models as shown in Figure 5.2 to Figure 5.4.

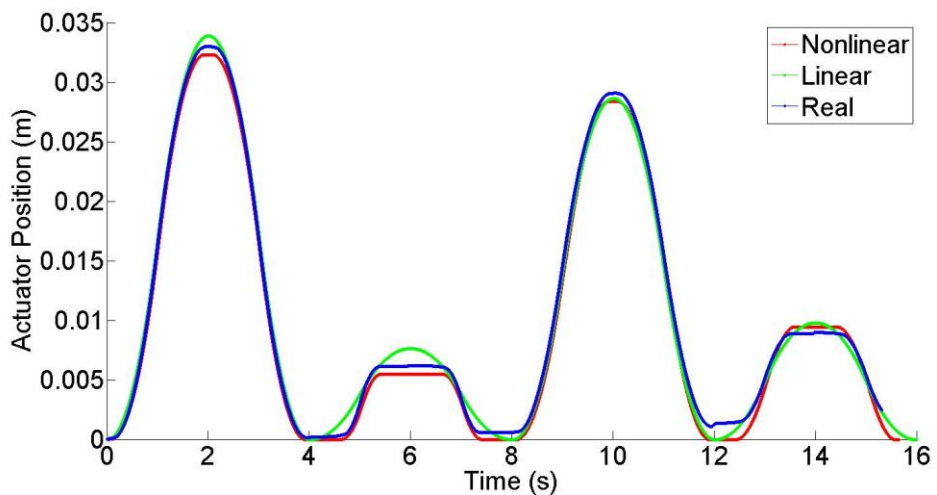


Figure 5.2: Position Plot

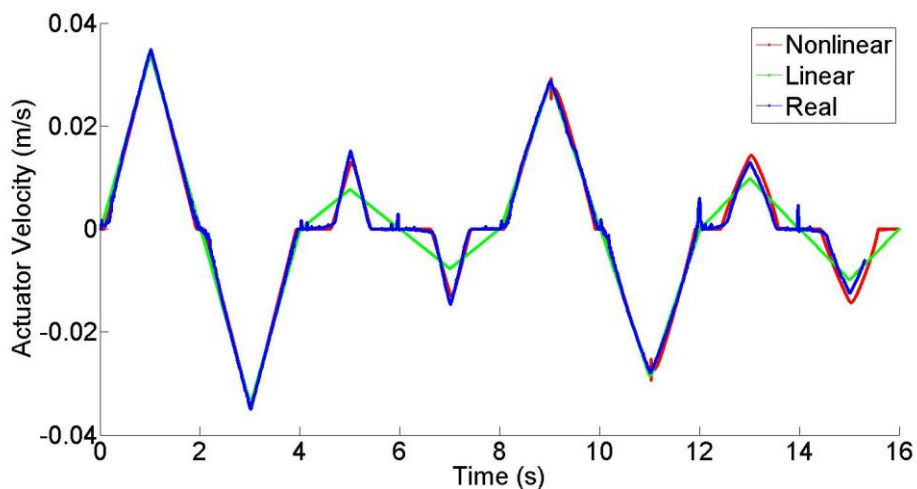


Figure 5.3: Velocity Plot

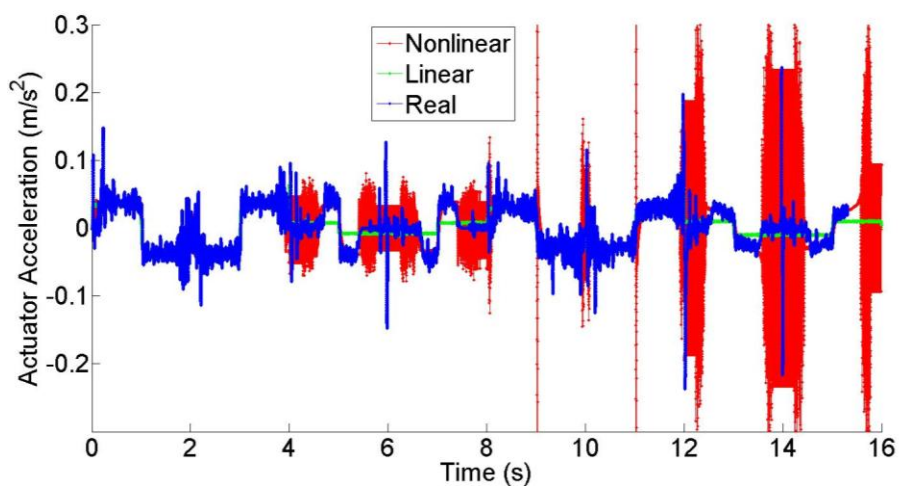


Figure 5.4: Acceleration Plot

Referring to Figure 5.2 to Figure 5.4, both EHA models can simulate the EHA's actual performance under different conditions. From Figure 5.4 containing the acceleration plot, high chattering can be observed with the EHA's nonlinear model. Since velocity and acceleration are not directly measured and are obtained by taking the first and the second derivatives of the position measurement, differentiation noise is observed.

## 5.2. IMM Implementation

The above two EHA mathematical models were used with the IMM strategy. Four different combinations of IMM were implemented:

- IMM-KF with nonlinear model
- IMM-SVSF with nonlinear model
- IMM-KF with linear model
- IMM-SVSF with linear model

The EHA's motor input as shown in Figures 5.1 was used with the four operating conditions listed in Table 5.1; The open-loop faulty response of the EHA is shown in Figure 5.2 to Figure 5.4. Figures 5.5 to 5.12 show the IMM probability outcomes with the different filters and model combinations.

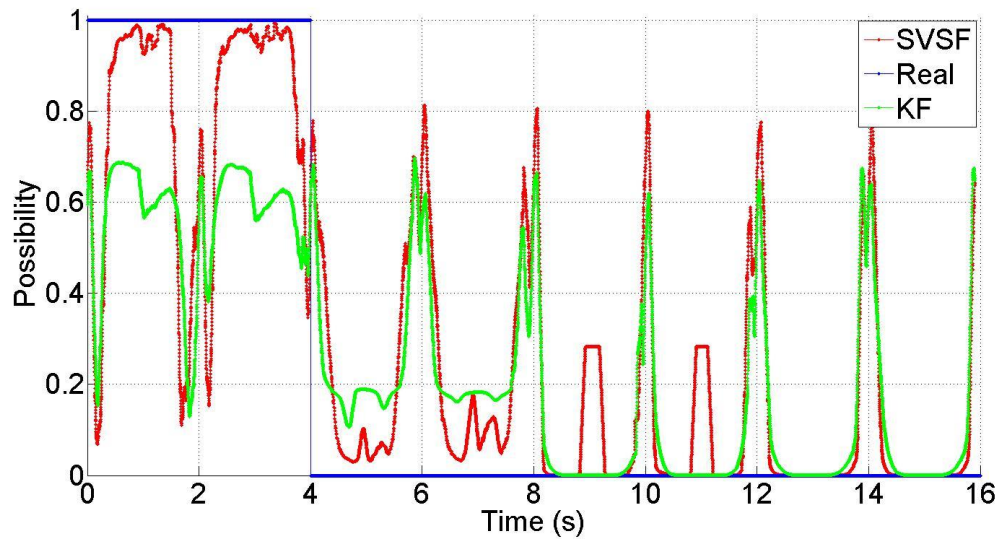


Figure 5.5: Normal Condition with Nonlinear Model

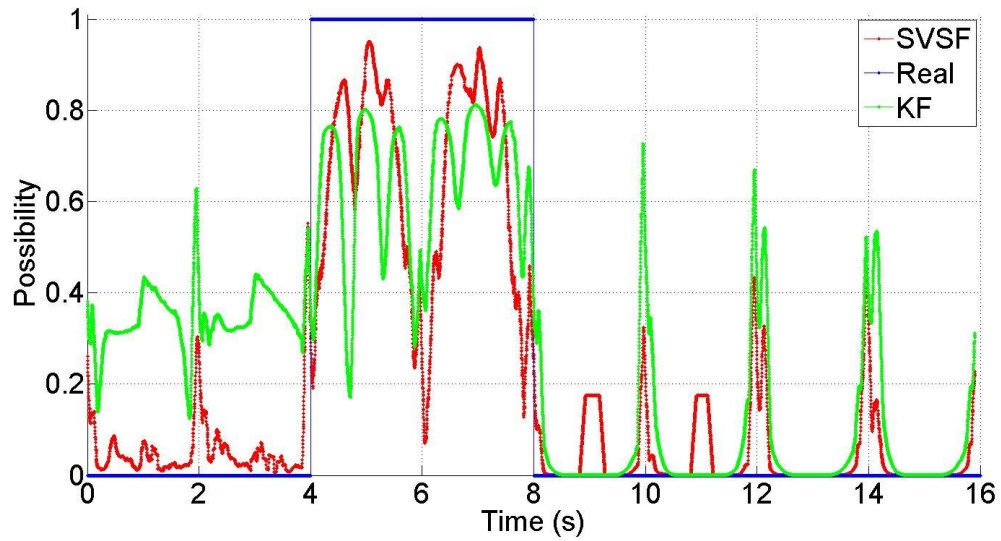


Figure 5.6: Leakage Condition with Nonlinear Model

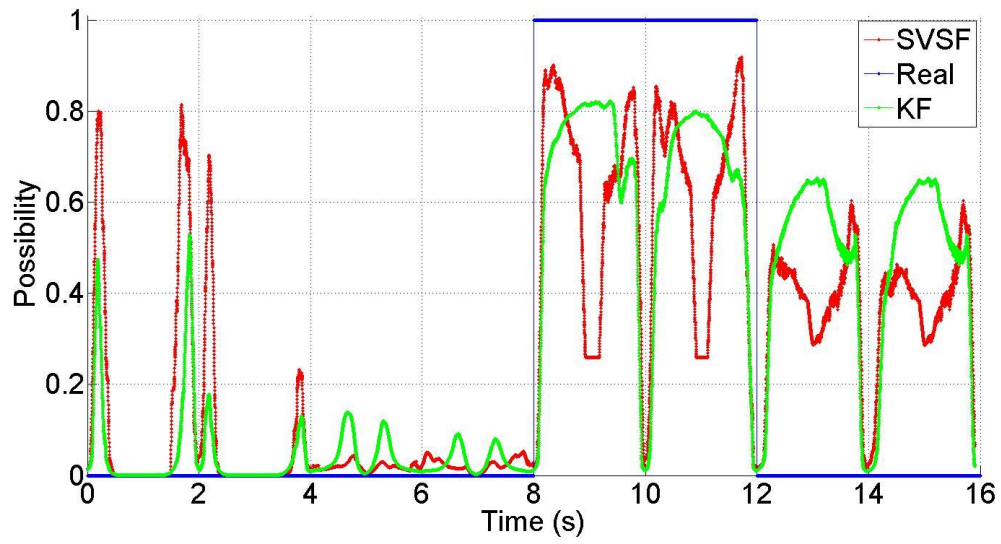


Figure 5.7: Friction Condition with Nonlinear Model

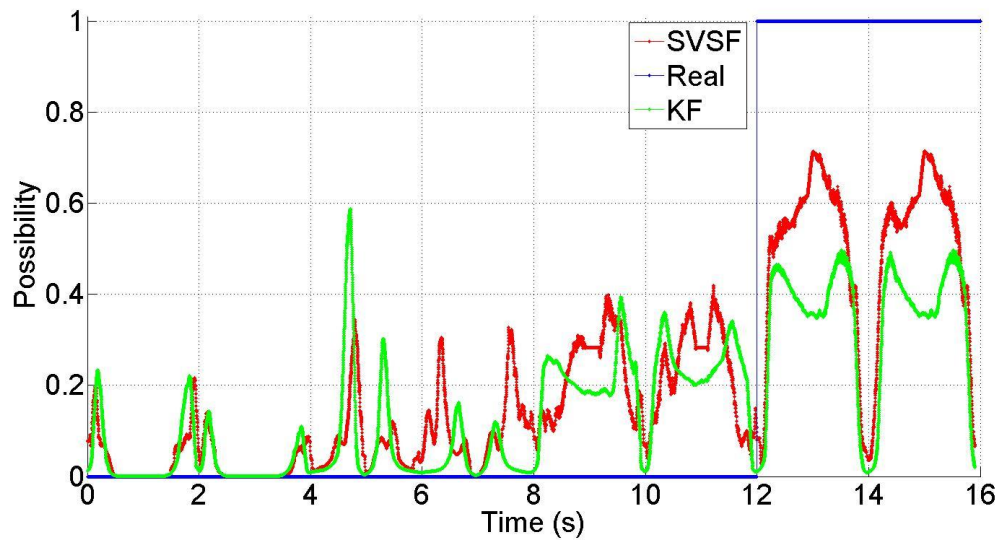


Figure 5.8: Combined Condition with Nonlinear Model

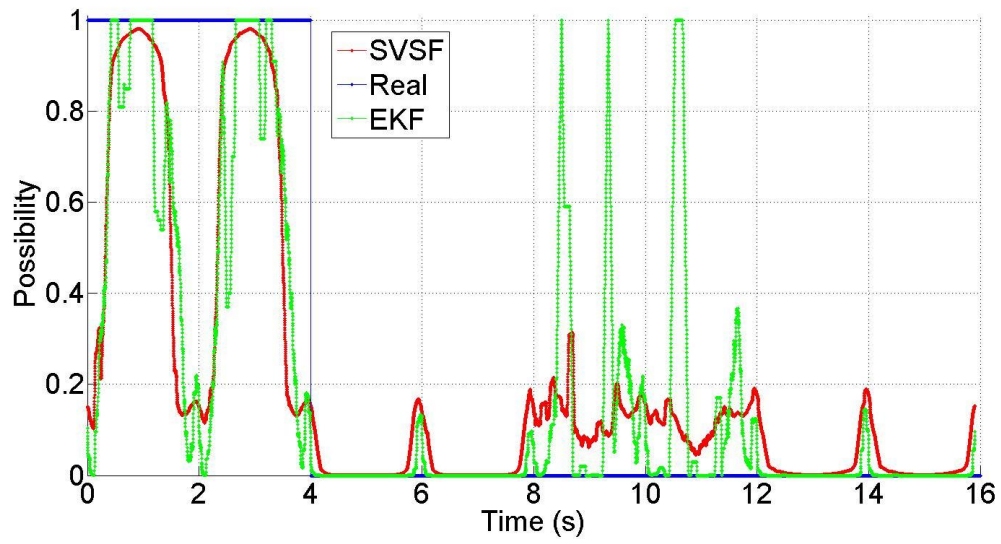


Figure 5.9: Normal Condition with Linear Model

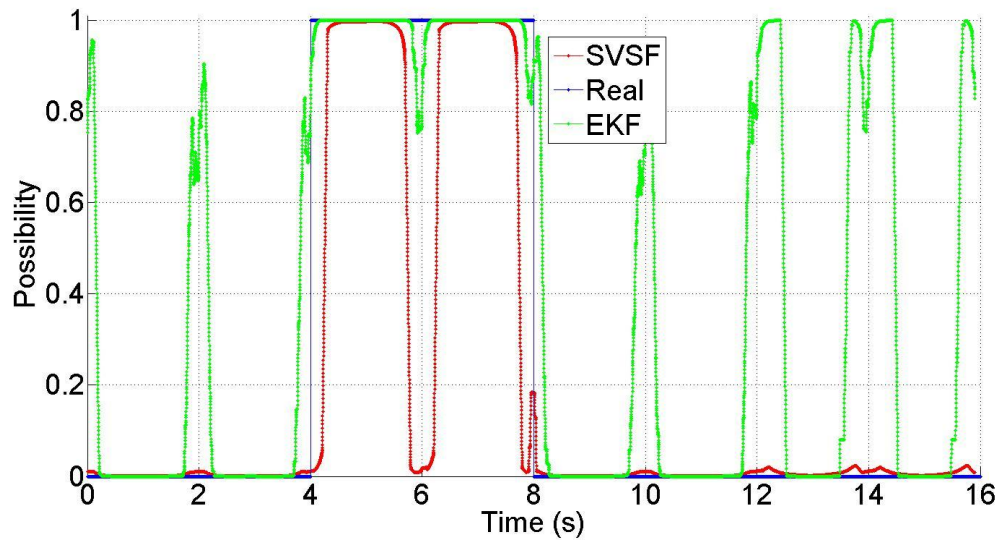


Figure 5.10: Leakage Condition with Linear Model

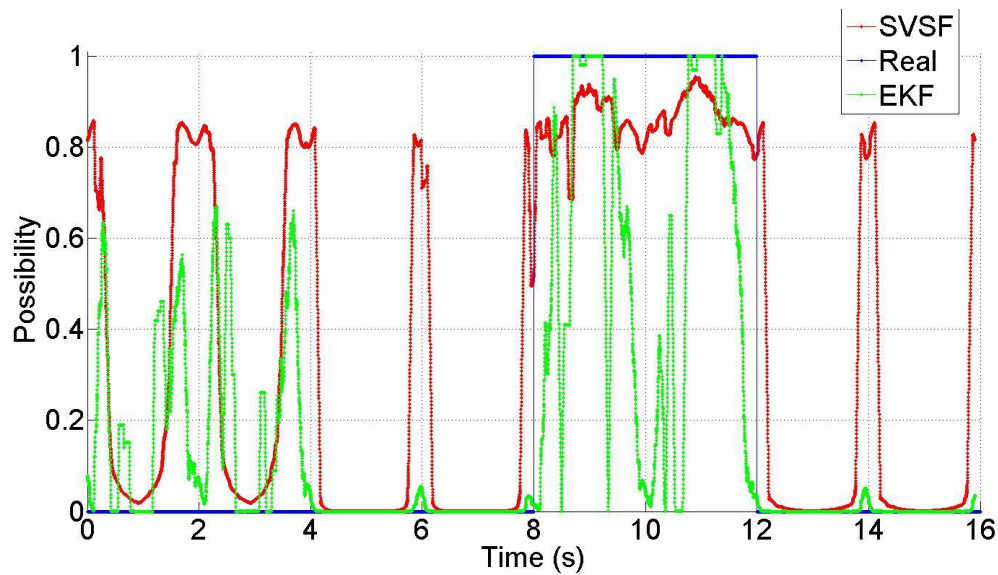


Figure 5.11: Friction Condition with Linear Model

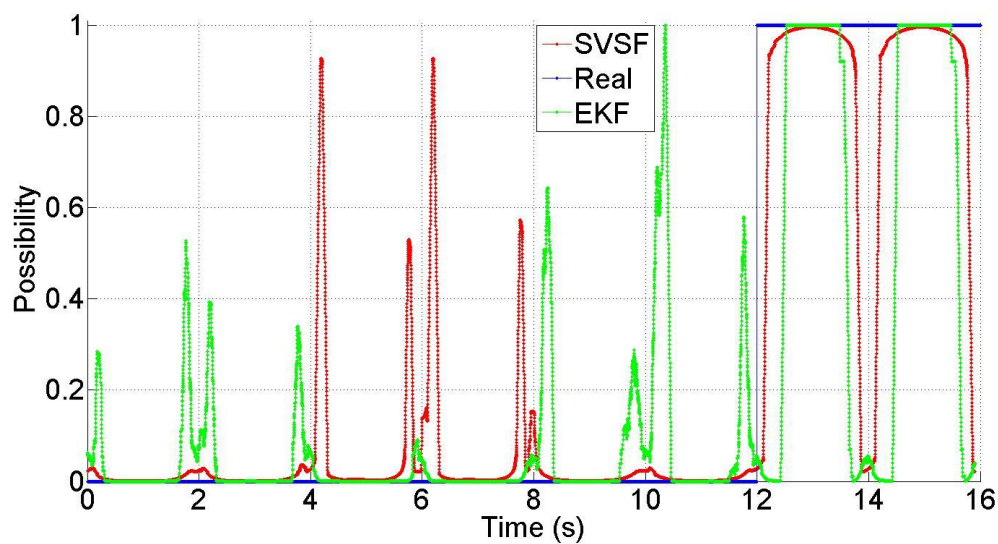


Figure 5.12: Combined Condition with Linear Model

According to the results, all four methods can successfully detect the correct system operation condition. For the purpose of comparing their performance more directly, the mean probabilities of each method under different operating conditions are shown in confusion matrices in Table 5.7 to Table 5.10. In these tables, the first row shows the real

working condition that the EHA was operating, and the first column shows the IMM prediction.

According to the results, IMM-EKF with nonlinear EHA model has a poor capability in detecting the correct mode, especially at the combined fault condition (34.25%); IMM-SVSF with nonlinear EHA model has higher detection rate than EKF. IMM-KF with the linear EHA model has a slightly increased correct detection rate, especially for the leakage fault condition (98.20%); IMM-SVSF with the linear EHA model has the best detection rate, it has correct detection rates of above 60% in all conditions.

Table 5.7: IMM-EKF with Nonlinear Model Performance

IMM-EKF with Nonlinear Model		Operating Condition			
		Normal	Leakage	Friction	Combined
IMM Prediction	Normal	<b>56.76%</b>	25.95%	7.75%	10.55%
	Leakage	34.59%	<b>64.05%</b>	7.14%	8.43%
	Friction	5.21%	3.53%	<b>63.68%</b>	46.77%
	Combined	3.44%	6.47%	21.44%	<b>34.25%</b>

Table 5.8: IMM-SVSF with Nonlinear Model Performance

IMM-SVSF with Nonlinear Model		Operating Condition			
		Normal	Leakage	Friction	Combined
IMM Prediction	Normal	<b>77.77%</b>	24.28%	13.51%	9.59%
	Leakage	5.97%	<b>64.48%</b>	5.51%	3.82%
	Friction	12.94%	2.19%	<b>58.53%</b>	36.58%
	Combined	3.33%	9.05%	22.45%	<b>50.01%</b>

Table 5.9: IMM-EKF with Linear Model Performance

IMM-EKF with Linear Model		Operating Condition			
		Normal	Leakage	Friction	Combined
IMM Prediction	Normal	<b>58.82%</b>	0.76%	18.60%	0.78%
	Leakage	14.63%	<b>98.20%</b>	15.10%	41.81%
	Friction	21.26%	0.35%	<b>54.65%</b>	0.32%
	Combined	5.29%	0.70%	11.65%	<b>57.02%</b>

Table 5.10: IMM-SVSF with Linear Model Performance

IMM-SVSF with linear Model		Operating Condition			
		Normal	Leakage	Friction	Combined
IMM Prediction	Normal	<b>61.04%</b>	2.45%	12.79%	2.91%
	Leakage	0.25%	<b>73.92%</b>	0.69%	0.84%
	Friction	38.01%	13.80%	<b>85.45%</b>	14.96%
	Combined	0.71%	98.32%	1.07%	<b>81.29%</b>

### 5.3. Controllers Simulation Results

Before experimenting with the EHA prototype, computer simulations were used to evaluate the controllers. The basic simulation setups are as the same as described in Sections 5.1 and 5.2. All the simulations were performed in Matlab. Six controllers as described in Chapter 4 were considered for the simulation analysis in the following order:

- Misawa based:

1. SMC
2. IMM-SMC-KF
3. IMM-SMC-SVSF
  - Slotine and Li based:
4. SMC
5. IMM-SMC-KF
6. IMM-SMC-SVSF

Simulations are performed to evaluate the control strategies. For consistency with experiments, all simulation trials are performed with the same input and operating conditions as outlined in Section 5.1.1. The EHA simulation model was the linear one described in section 5.1.2.2 with the parametric values given in Figure 5.1 and Table 5.1, and Figure 5.13 to Figure 5.18 show the simulation results of the above mentioned controllers (namely: Misawa based SMC, Misawa based IMM-SMC-KF, Misawa based IMM-SMC-SVSF, Slotine and Li based SMC, Slotine and Li based IMM-SMC-KF, and Slotine and Li based IMM-SMC-SVSF). It should be noted that each figure contains 3 subplots representing the EHA position, velocity and acceleration, respectively. Blue lines represent desired EHA trajectories under different operating conditions, and red lines represent actual EHA trajectories under the same operation conditions.

According to simulation results, all the control strategies achieved excellent position tracking. Their differences are not clear on EHA position trajectories; however, by looking at velocity and acceleration plots, the differences became clear. The KF based IMM controllers (two IMM-SMC-KF) have chattering with high frequency and amplitude on acceleration plots as shown in Figure 5.14 and Figure 5.17. The two

approaches of SMC (Misawa based / Slotine and Li based) have acceleration chattering at the last few seconds as shown in Figure 5.13 and Figure 5.16. The two SVSF based IMM (two IMM-SMC-SVSF) performed well in all experiments as shown in Figures 5.15 and 5.18.

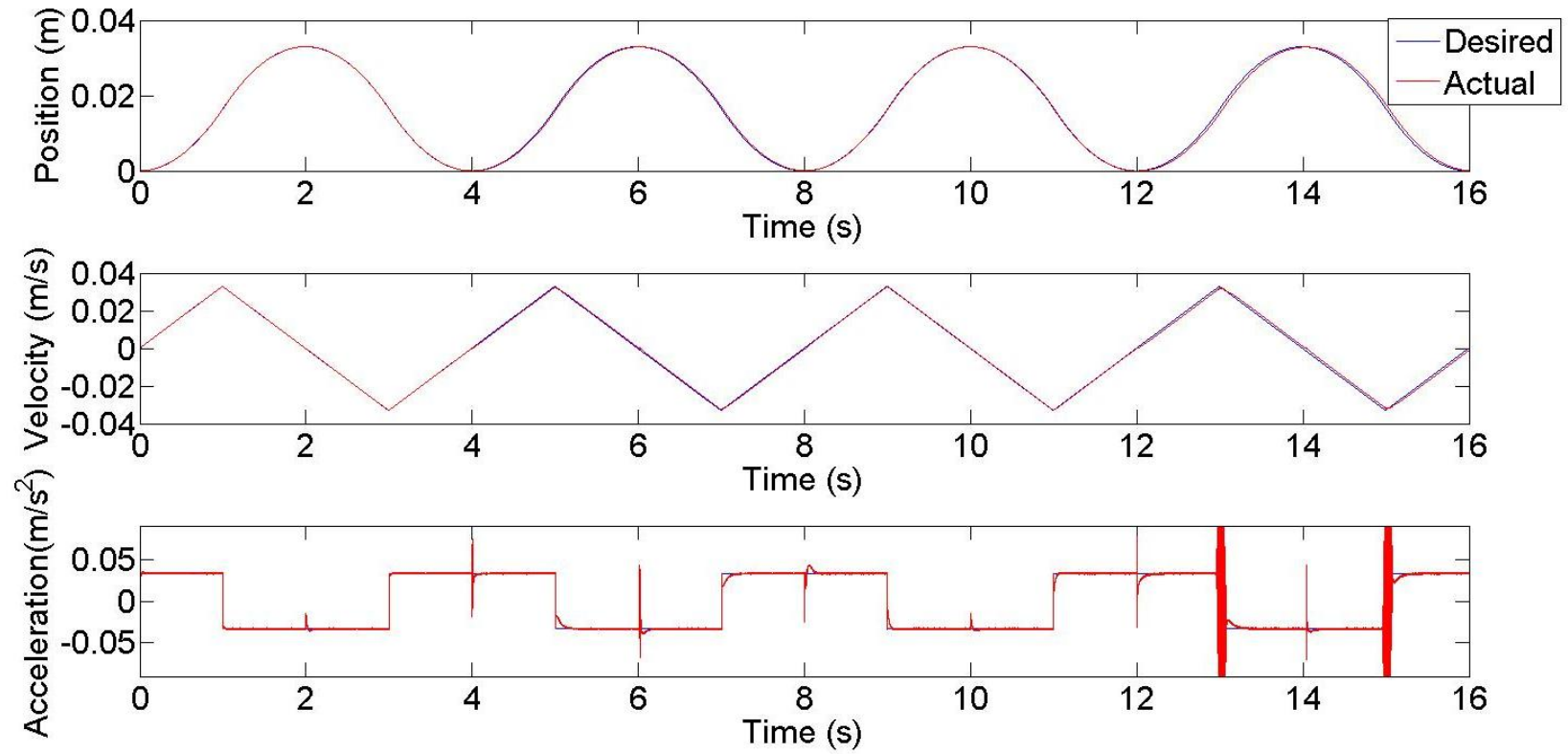


Figure 5.13: Misawa based SMC Simulation

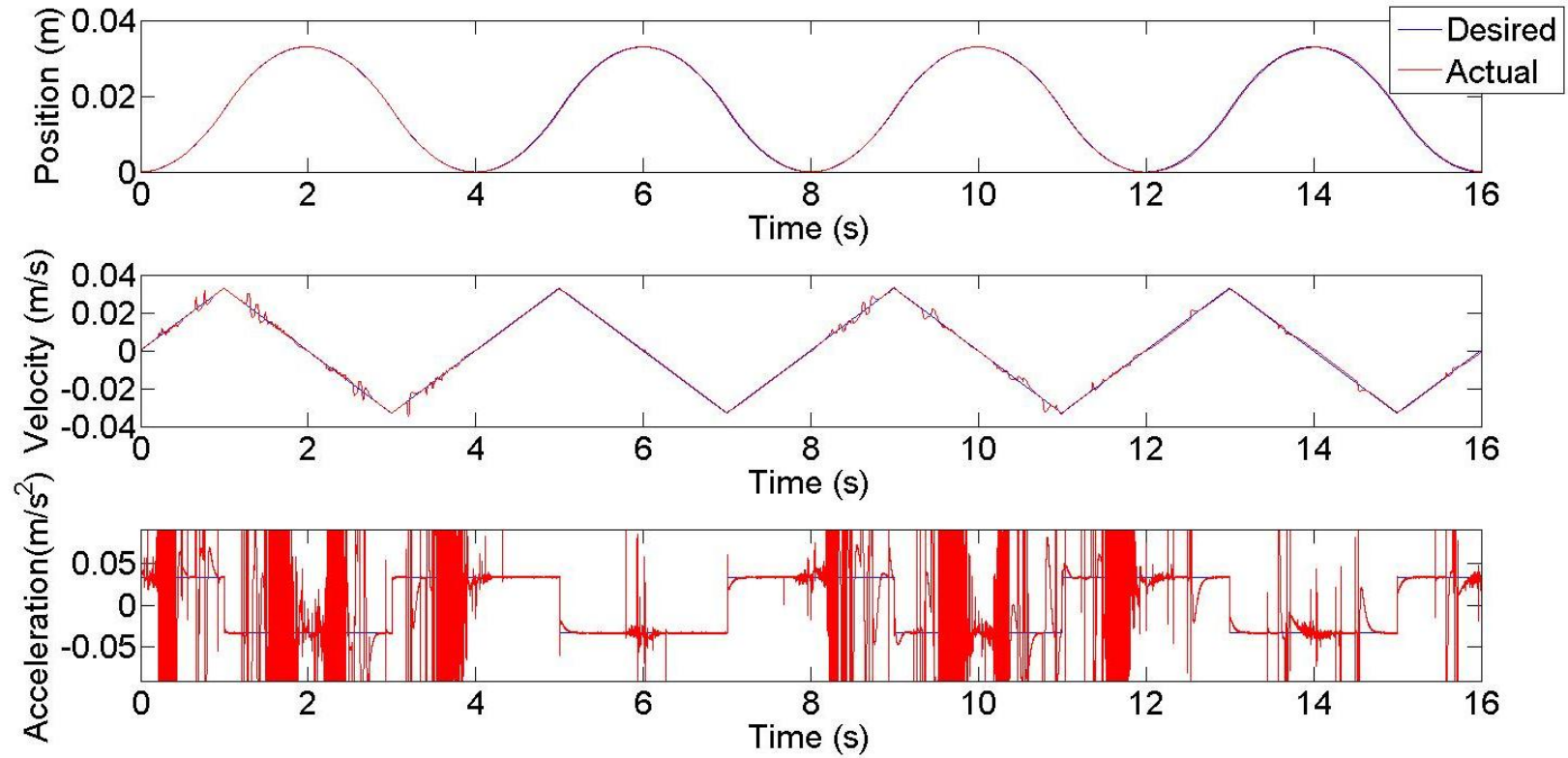


Figure 5.14: Misawa based IMM-SMC-KF Simulation

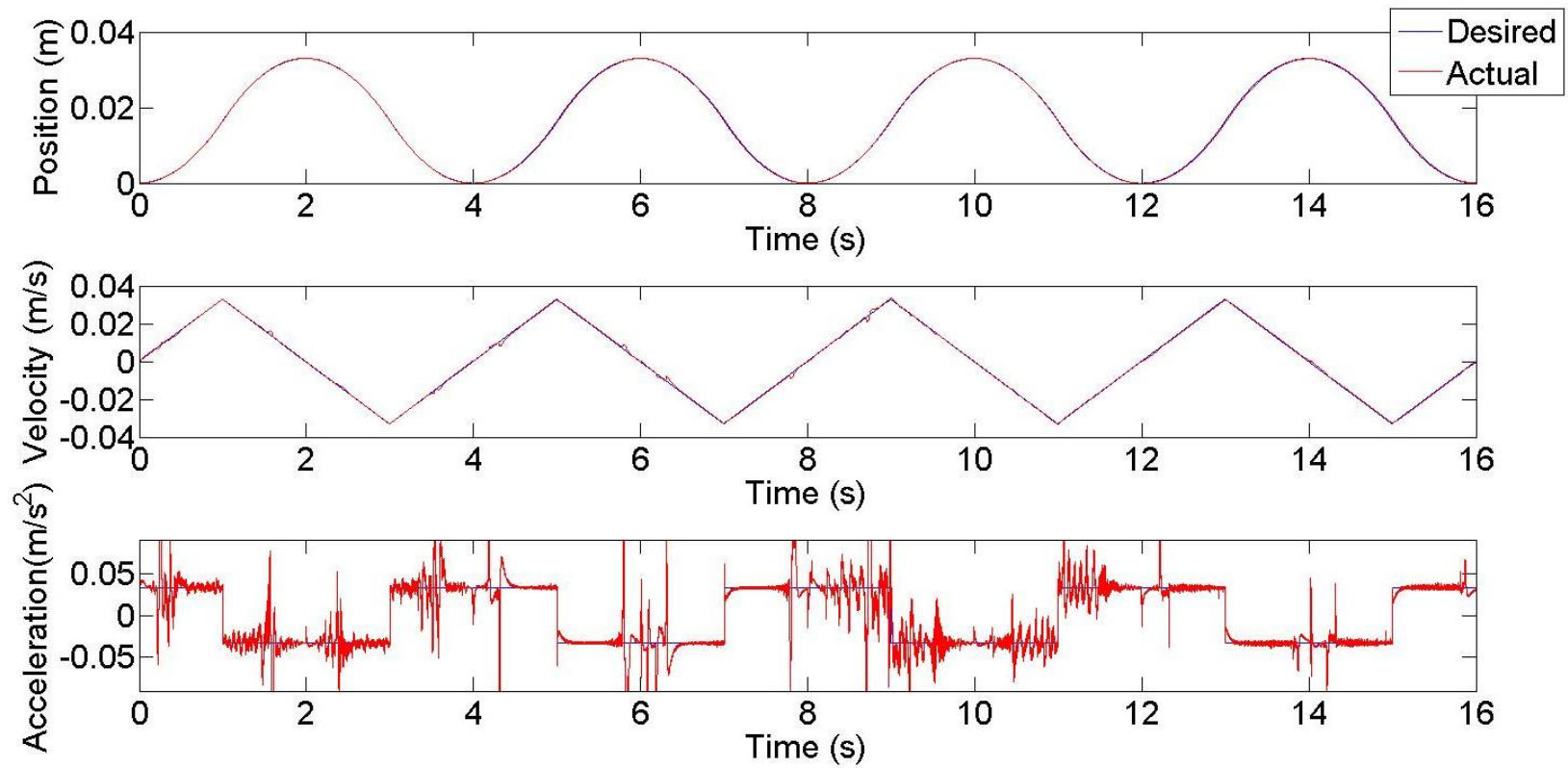


Figure 5.15: Misawa based IMM-SMC-SVSF Simulation

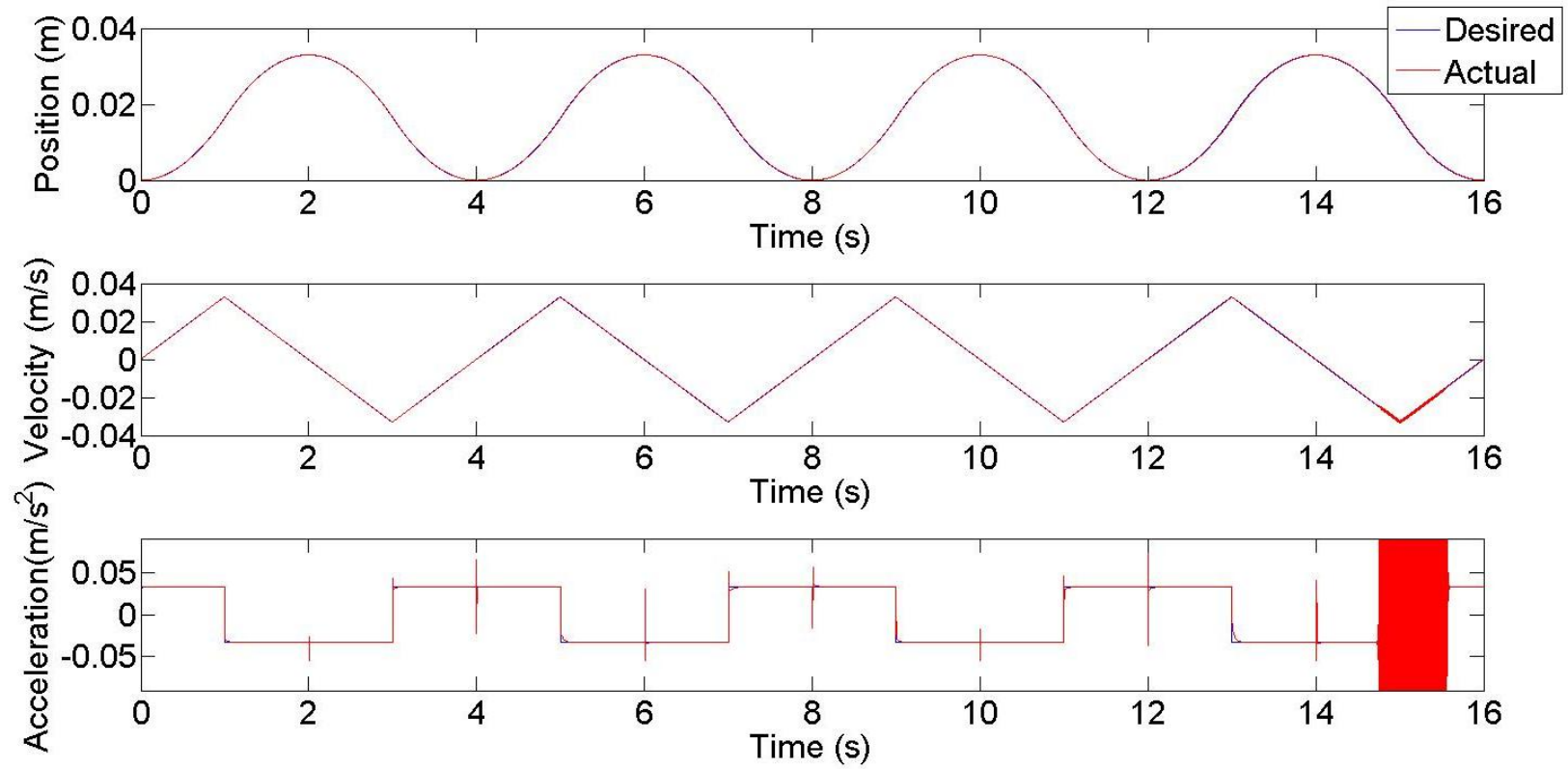


Figure 5.16: Slotine and Li based SMC Simulation

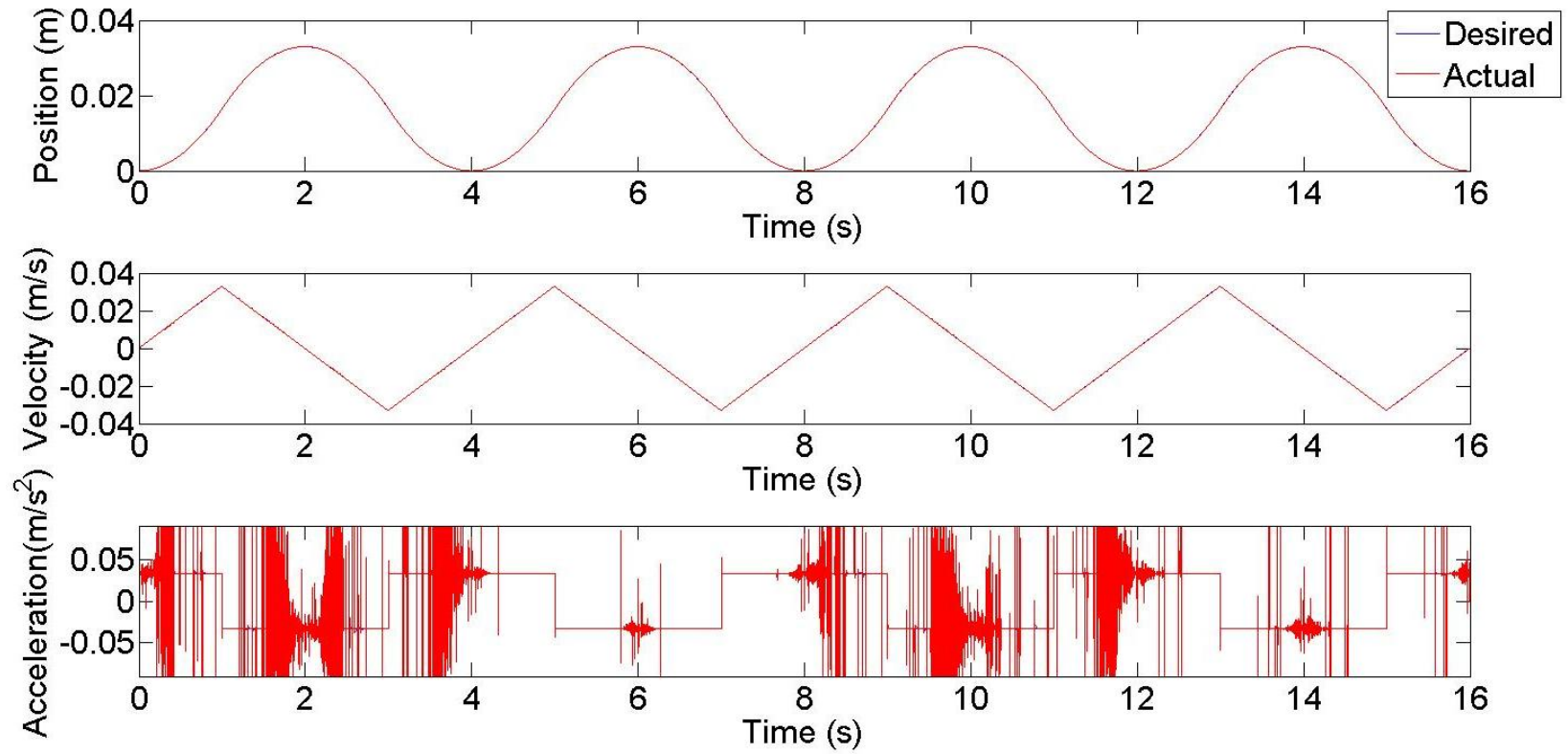


Figure 5.17: Slotine and Li based IMM-SMC-KF Simulation

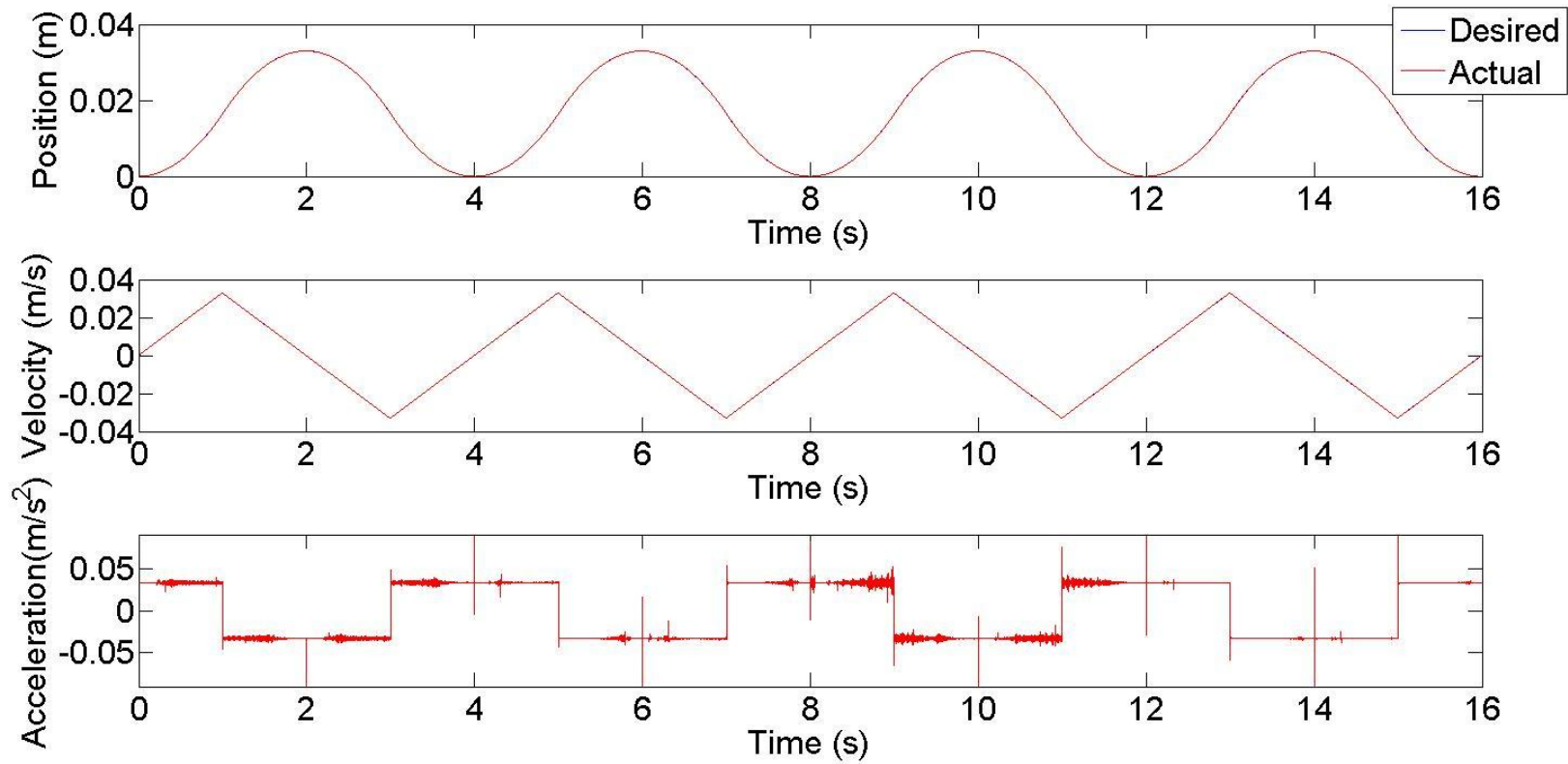


Figure 5.18: Slotine and Li based IMM-SMC-SVSF Simulation

In order to verify the tracking accuracy of above controllers, position error plots and root mean square error tables are provided in this section. Figure 5.19 and 5.20 show the position error plots of the SMC, IMM-SMC-KF and IMM-SMC-SVSF. Table 5.11 shows the root mean square errors of all controllers under different conditions for position, velocity and acceleration.

It is very clear that IMM-SMC can perform more accurately in position tracking than SMC alone. In both plots and tables, the SVSF and KF based IMM-SMC have comparable performances; however, recall pervious section's results, SVSF based IMM-SMC acceleration plot has less chattering than KF based one (Figure 5.15 compared to Figure 5.14, and Figure 5.18 compared to Figure 5.17). Next step is to verify this conclusion with real experiment.

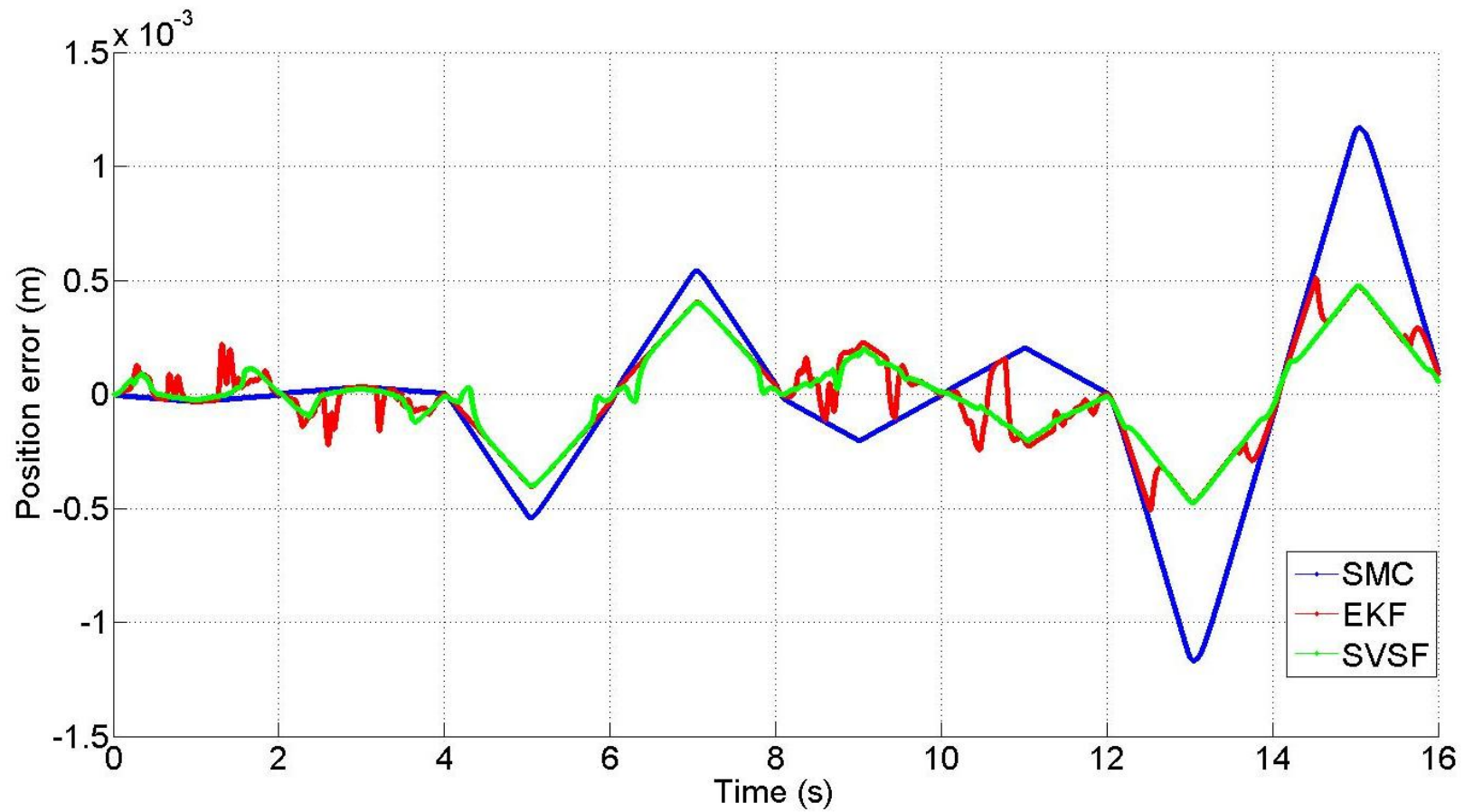
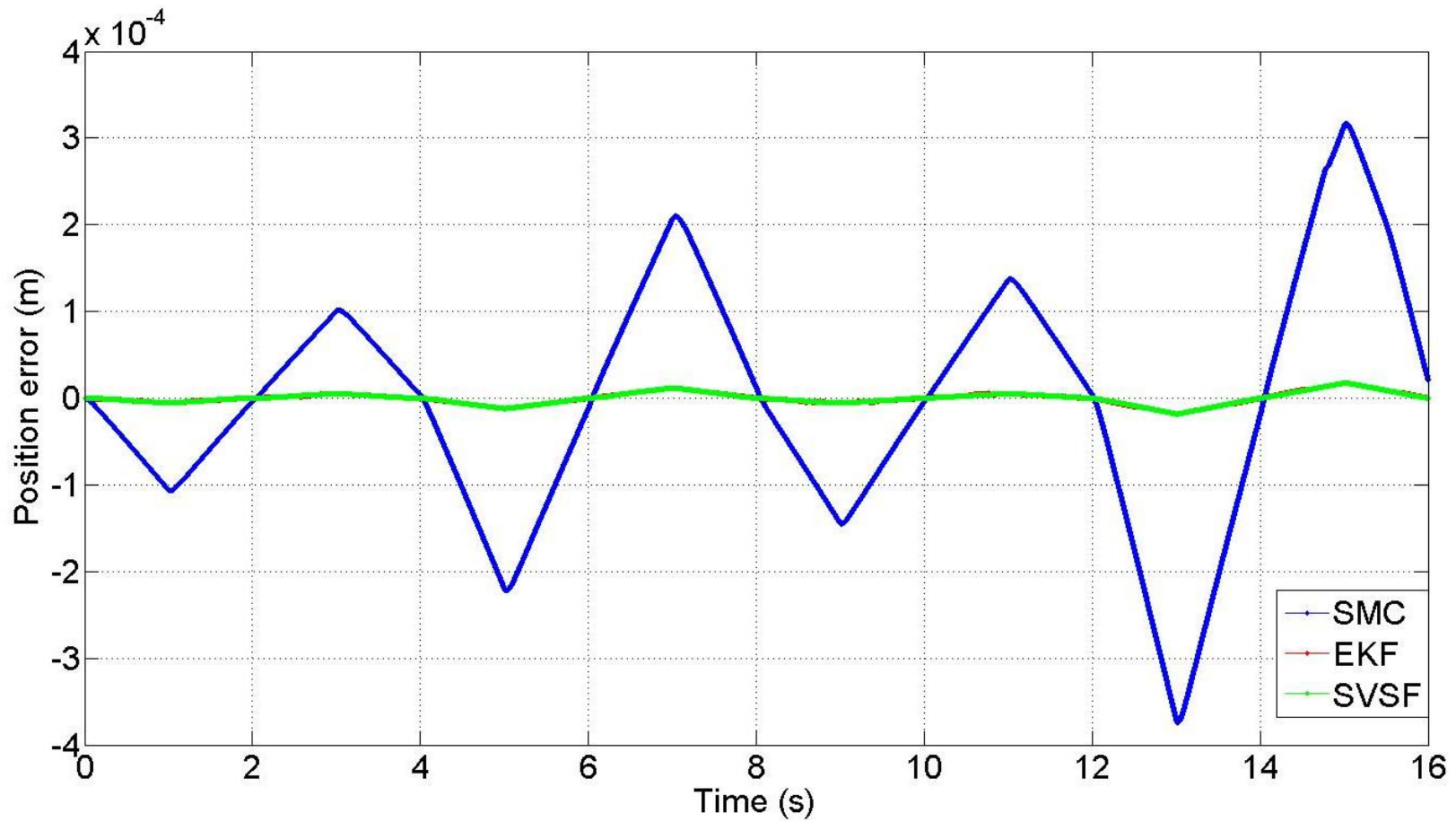


Figure 5.19: Simulation Position Errors of Misawa based SMC, IMM-SMC-KF and IMM-SMC-SVSF



Figure

5.20: Simulation Position Errors of Slotine and Li based SMC, IMM-SMC-KF and IMM-SMC-SVSF

Table 5.11: Simulation Root Mean Square Errors

	Normal			Leakage			Friction			Combine		
	Pos.	Vel.	Acc.									
<b>Misawa Based</b>												
<b>SMC</b>	1.94E-08	1.34E-07	5.51E-08	2.24E-07	2.71E-06	1.94E-07	2.91E-08	9.91E-07	1.58E-06	5.15E-07	6.14E-06	1.10E-06
<b>IMM_KF</b>	4.81E-09	2.83E-07	9.22E-05	1.91E-07	1.95E-06	1.77E-05	6.19E-09	6.56E-08	3.25E-05	4.43E-07	5.35E-06	1.10E-05
<b>IMM_SVSF</b>	3.95E-08	1.08E-06	3.84E-05	1.07E-07	7.11E-07	6.20E-06	4.55E-08	5.75E-07	4.76E-05	2.88E-07	3.60E-06	1.50E-05
<b>Slotine and Li Based</b>												
<b>SMC</b>	1.72E-08	4.83E-07	6.97E-07	6.20E-08	1.06E-06	6.71E-07	2.06E-08	6.74E-07	7.06E-07	1.06E-07	1.84E-06	6.40E-07
<b>IMM_KF</b>	4.00E-10	1.20E-09	6.98E-07	7.67E-10	4.64E-08	9.24E-06	5.49E-10	1.32E-08	6.37E-07	1.02E-09	6.97E-08	8.59E-07
<b>IMM_SVSF</b>	1.06E-09	1.70E-09	5.18E-08	7.94E-11	2.99E-08	4.59E-07	1.25E-09	1.17E-08	9.33E-08	3.61E-10	6.96E-08	1.43E-08

## 5.4. Controllers Experimental Results

Experimental results from the implementation of the control strategies on the EHA prototype are presented in this section. All the experiments run under the same input and fault conditions specified in Table 5.1 and Figure 5.1. In order to ensure repeatability, each test was run multiple times. Figure 5.21 to Figure 5.28 show the EHA desired and actual position, velocity and acceleration responses of each of the following controllers.

1. PID based:

- PID
- PID with equivalent control

2. Misawa based:

- SMC
- IMM-SMC-KF
- IMM-SMC-SVSF

3. Slotine and Li based:

- SMC
- IMM-SMC-KF
- IMM-SMC-SVSF

As expected, all controllers performed well as concluded from simulation results in previous section. The chattering levels are significant less than in the simulation. Since all plots are visually very similar, the performance differences between controllers need to be compared by trajectory errors.

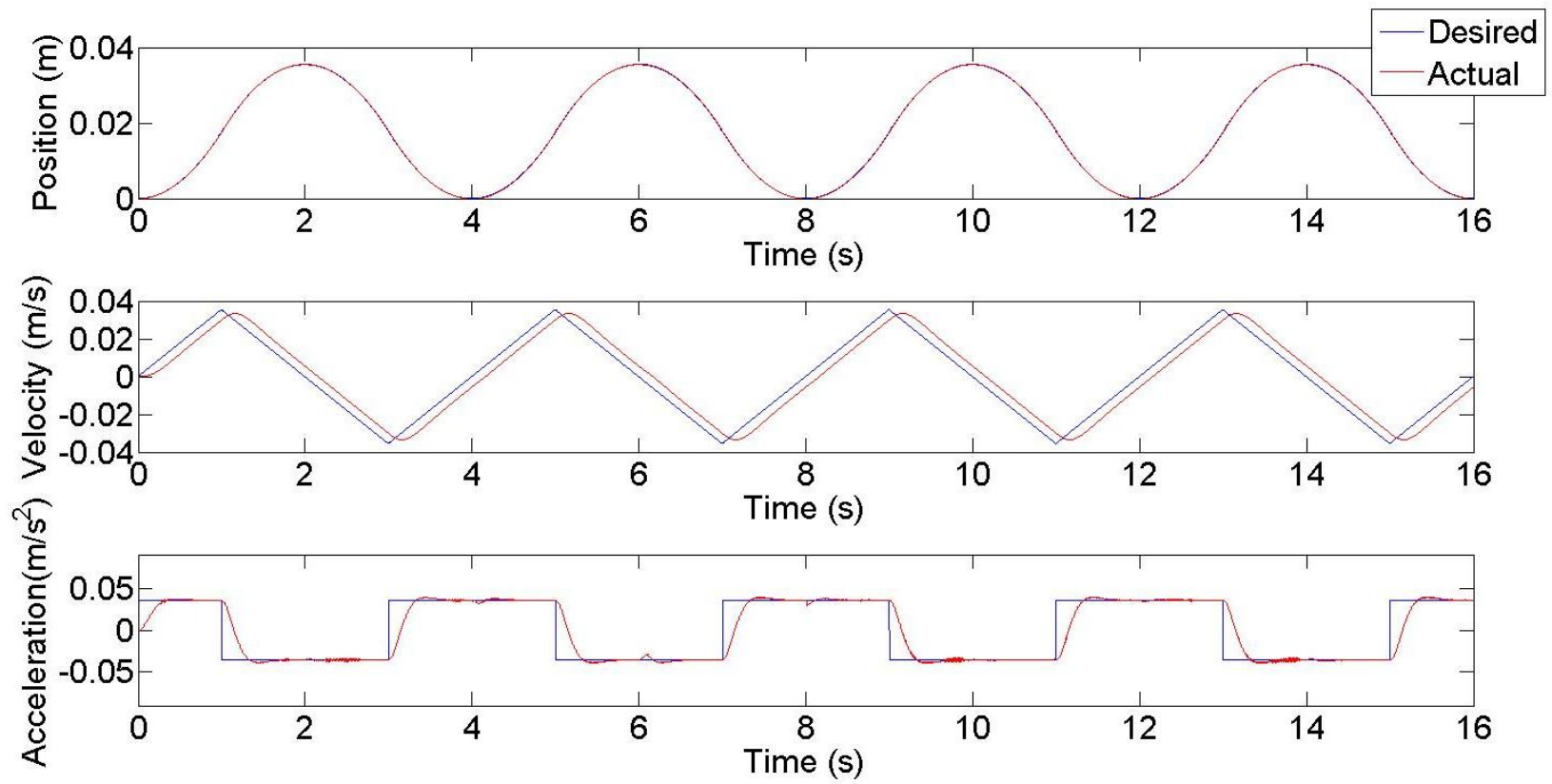


Figure 5.21: PID Controller

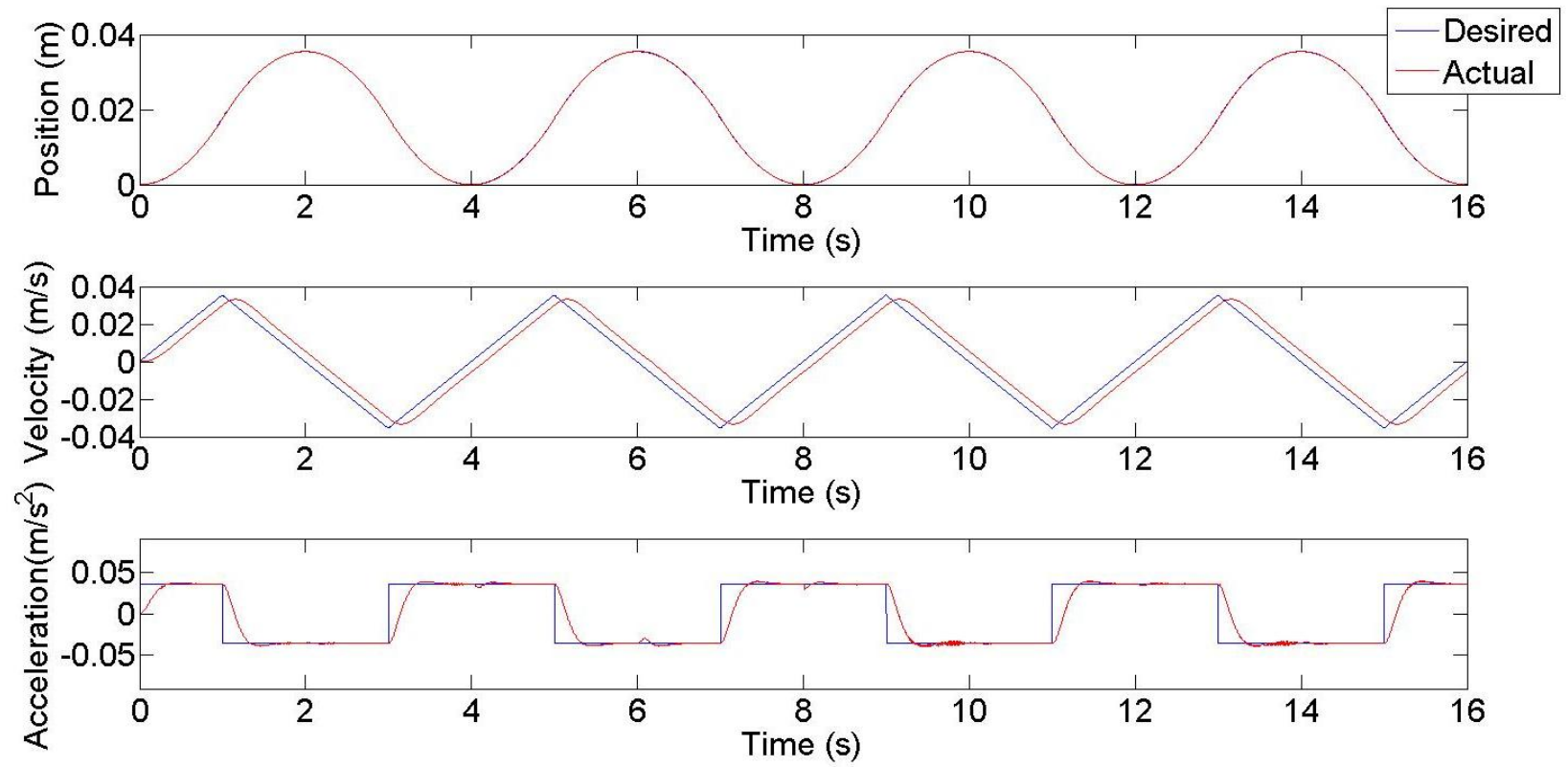


Figure 5.22: PID Controller with Equivalent Control

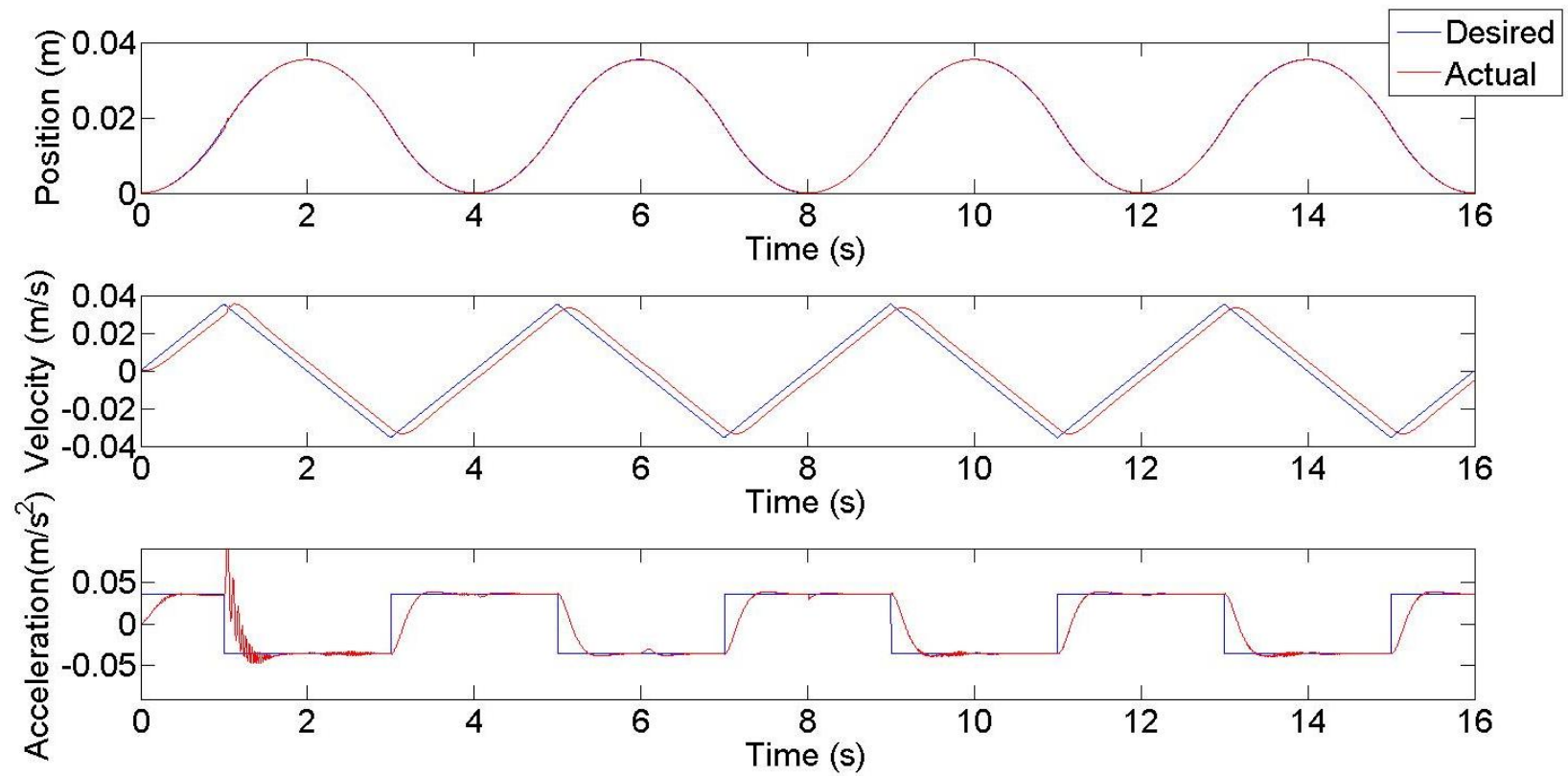


Figure 5.23: Misawa Based SMC Experimental Result

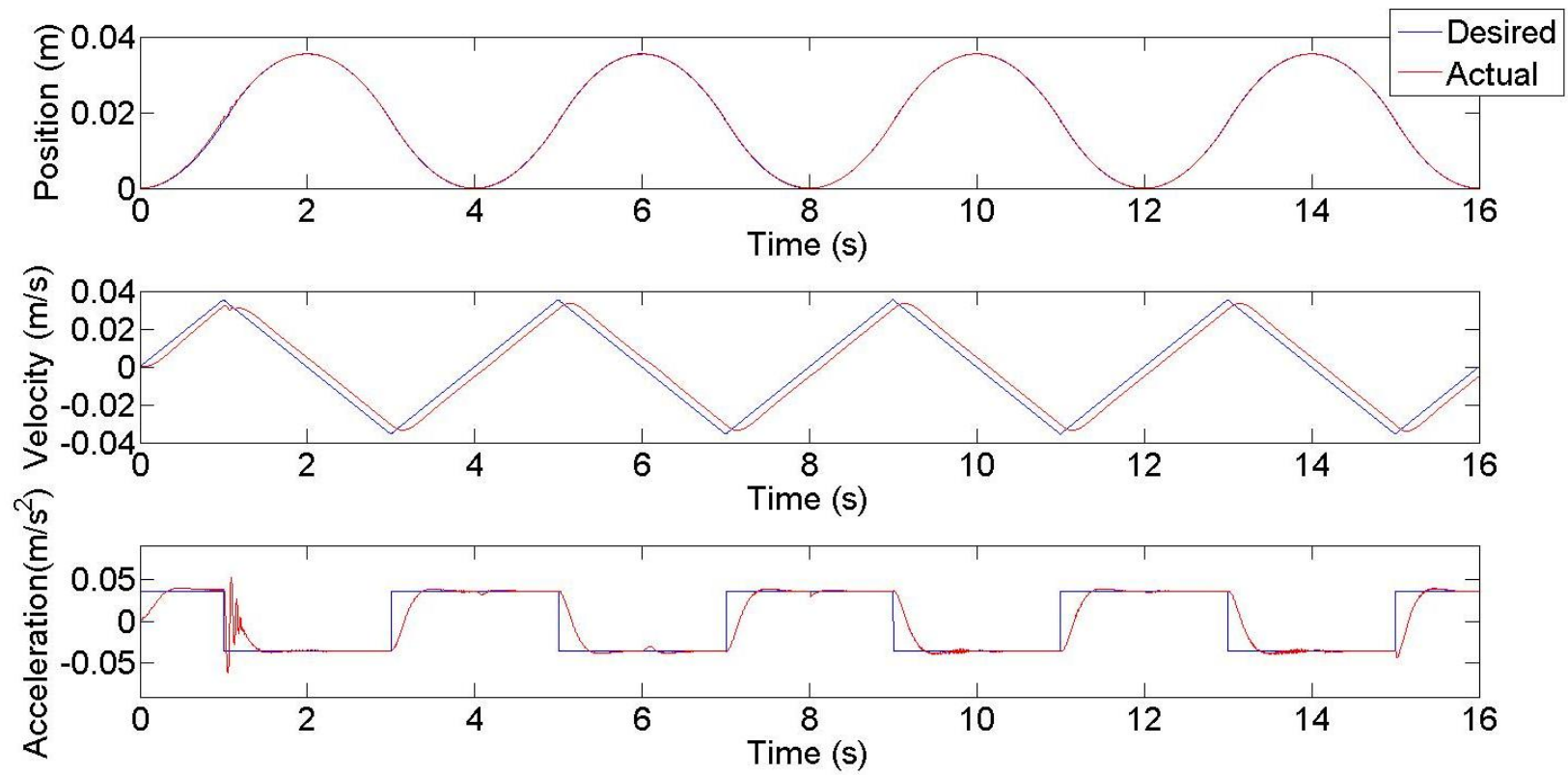


Figure 5.24: Misawa Based IMM-SMC-KF Experimental Result

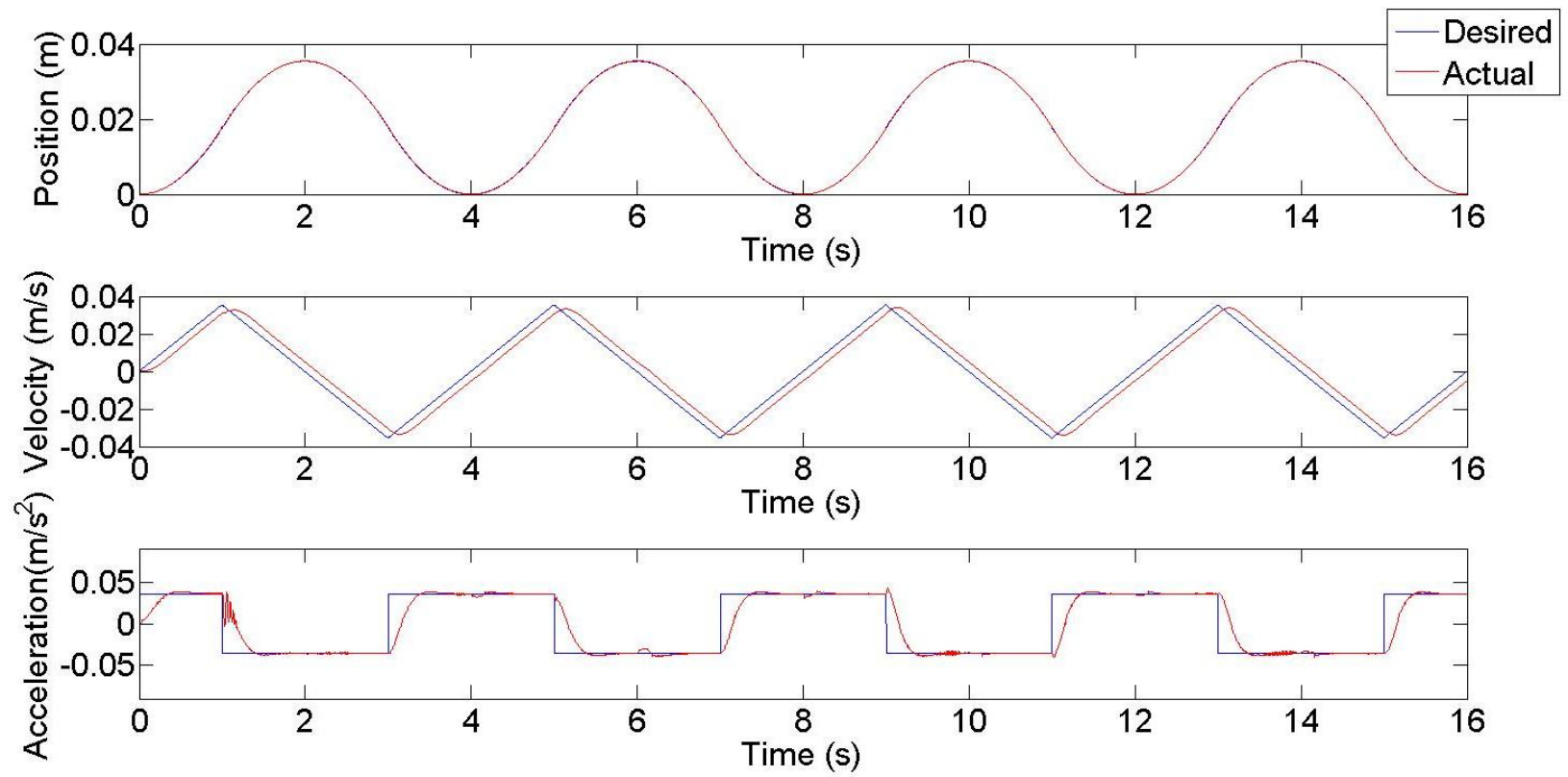


Figure 5.25: Misawa Based IMM-SMC-SVSF Experimental Result

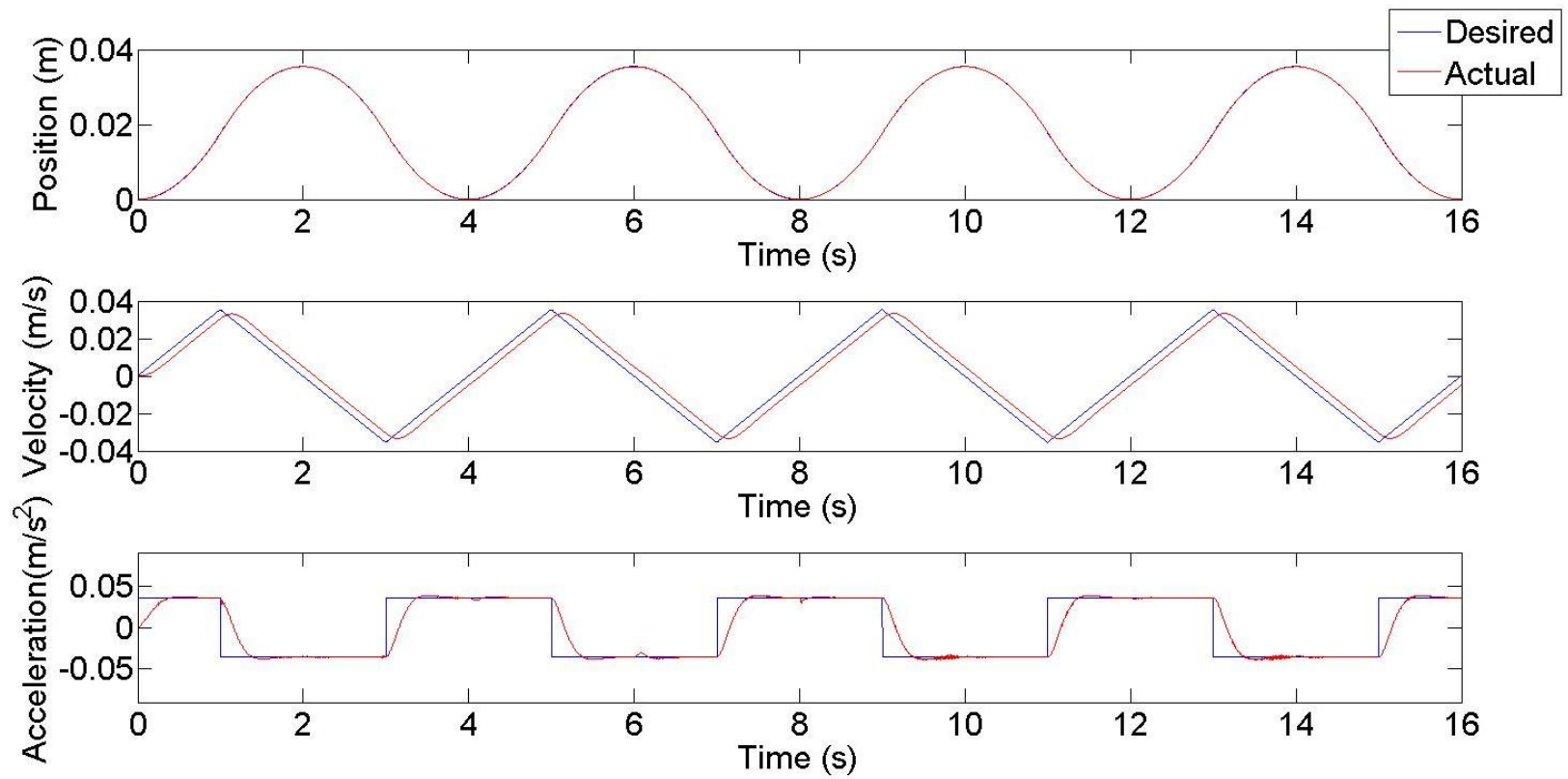


Figure 5.26: Slotine and Li Based SMC Experimental Result

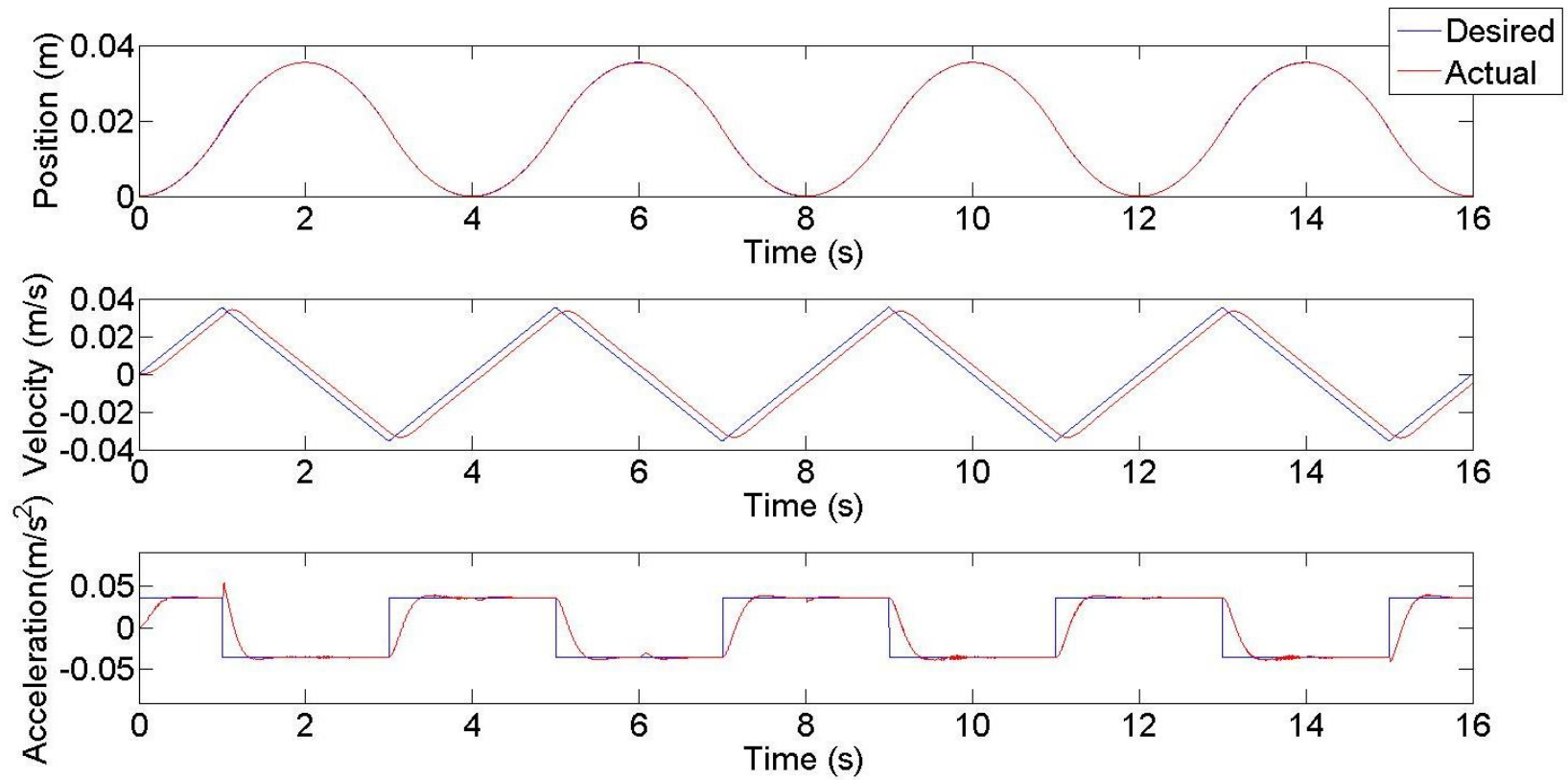


Figure 5.27: Slotine and Li Based IMM-SMC-KF Experimental Result

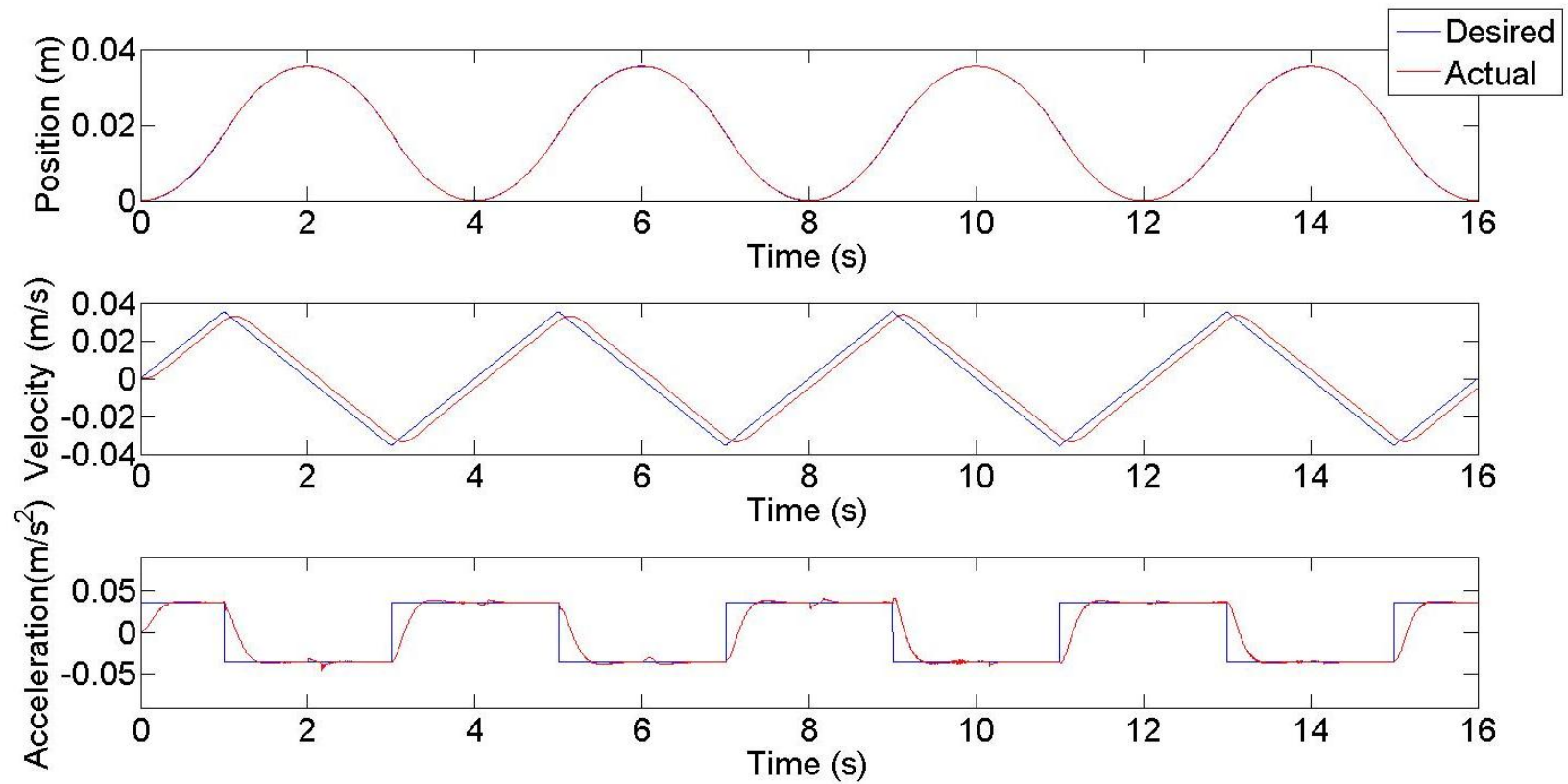


Figure 5.28: Slotine and Li Based IMM-SMC-KF Experimental Result

The EHA experimental position tracking accuracy of above controllers, with position error plots and root mean square error tables are displayed in Figure 5.29 to Figure 5.31. Table 5.12 shows the root mean square errors for position, velocity and acceleration for each of the controllers.

Figure 5.29 compares the performance of the PID, PID with equivalent control, the Misawa based SMC, and the Slotine and Li based SMC.

Figure 5.30 demonstrates Misawa based controller's performance, including SMC, IMM-SMC-KF and IMM-SMC-SVSF. IMM-SMC-SVSF has the least error amongst all. It proved IMM-SMC can further improve EHA position tracking and fault tolerance performance than SMC.

Figure 5.31 shows Slotine and Li's based new SMC, IMM-SMC-KF and IMM-SMC-SVSF plots. The new IMM-SMC-SVSF has the best performances as shown.

Table 5.12 lists the root mean square errors which supports the above conclusions.

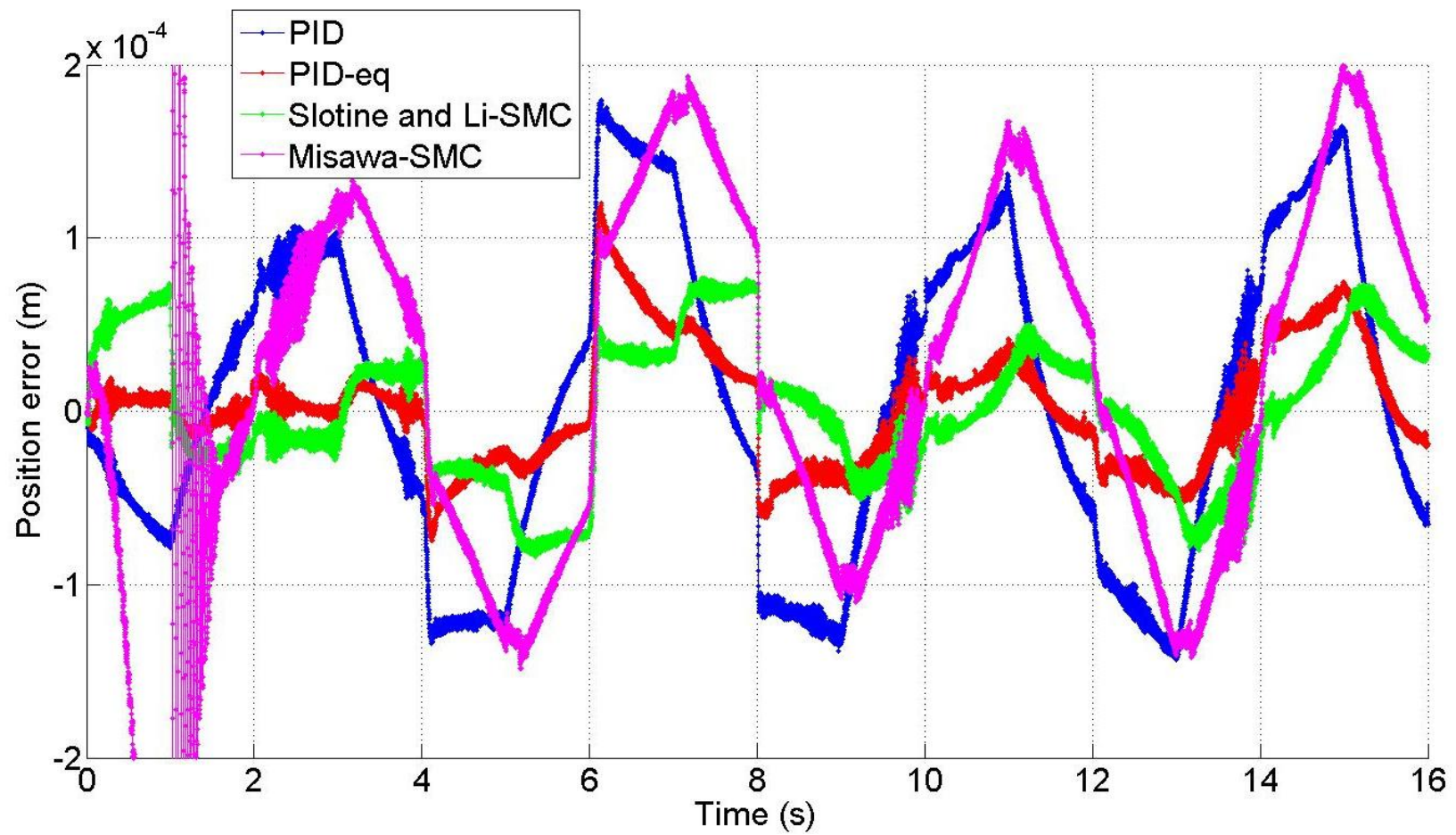


Figure 5.29: Position Errors of PID, PID Equivalent Control and SMCs

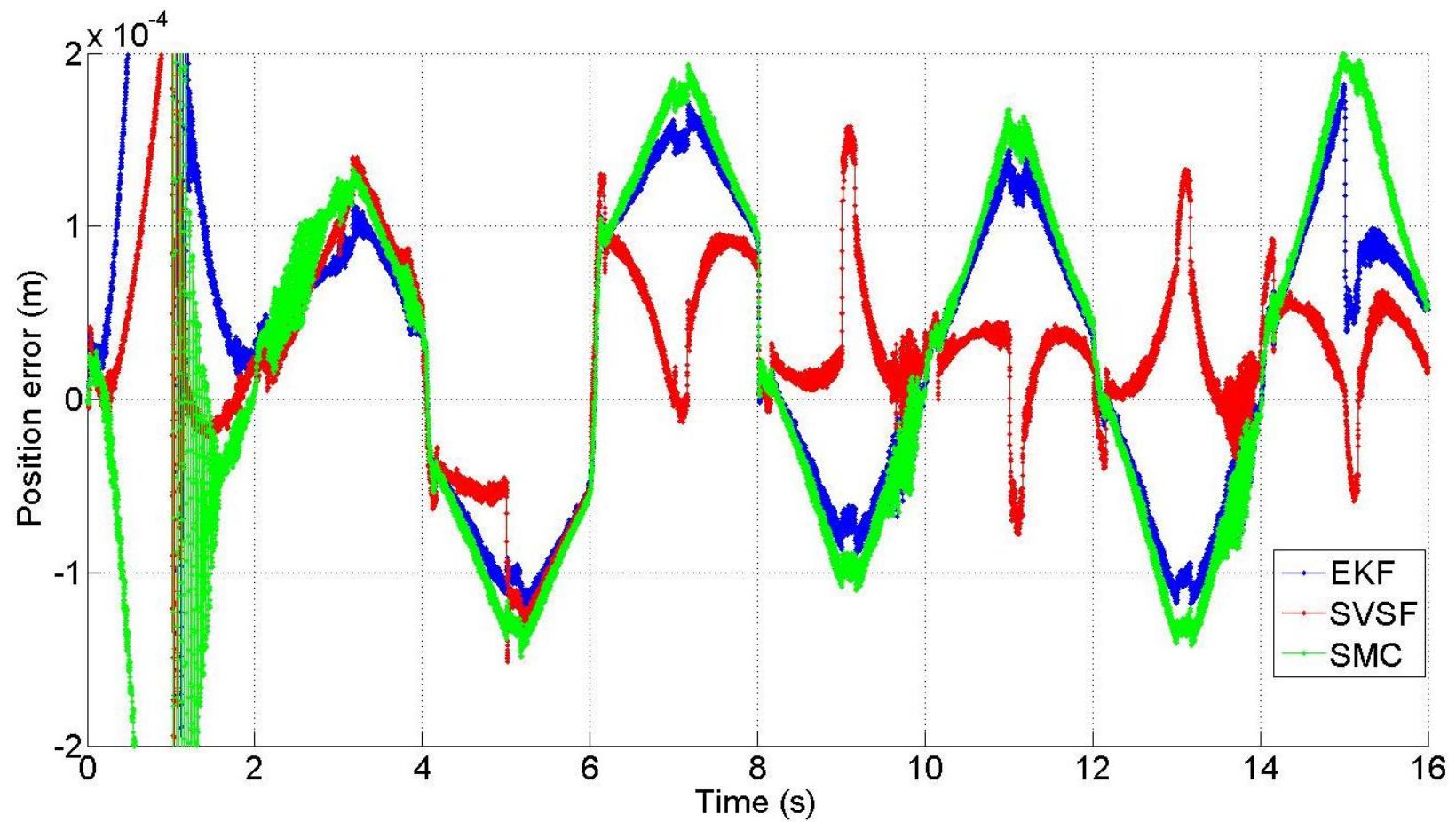


Figure 5.30: Position Errors of Misawa Based SMC, IMM-SMC-KF and IMM-SMC-SVSF

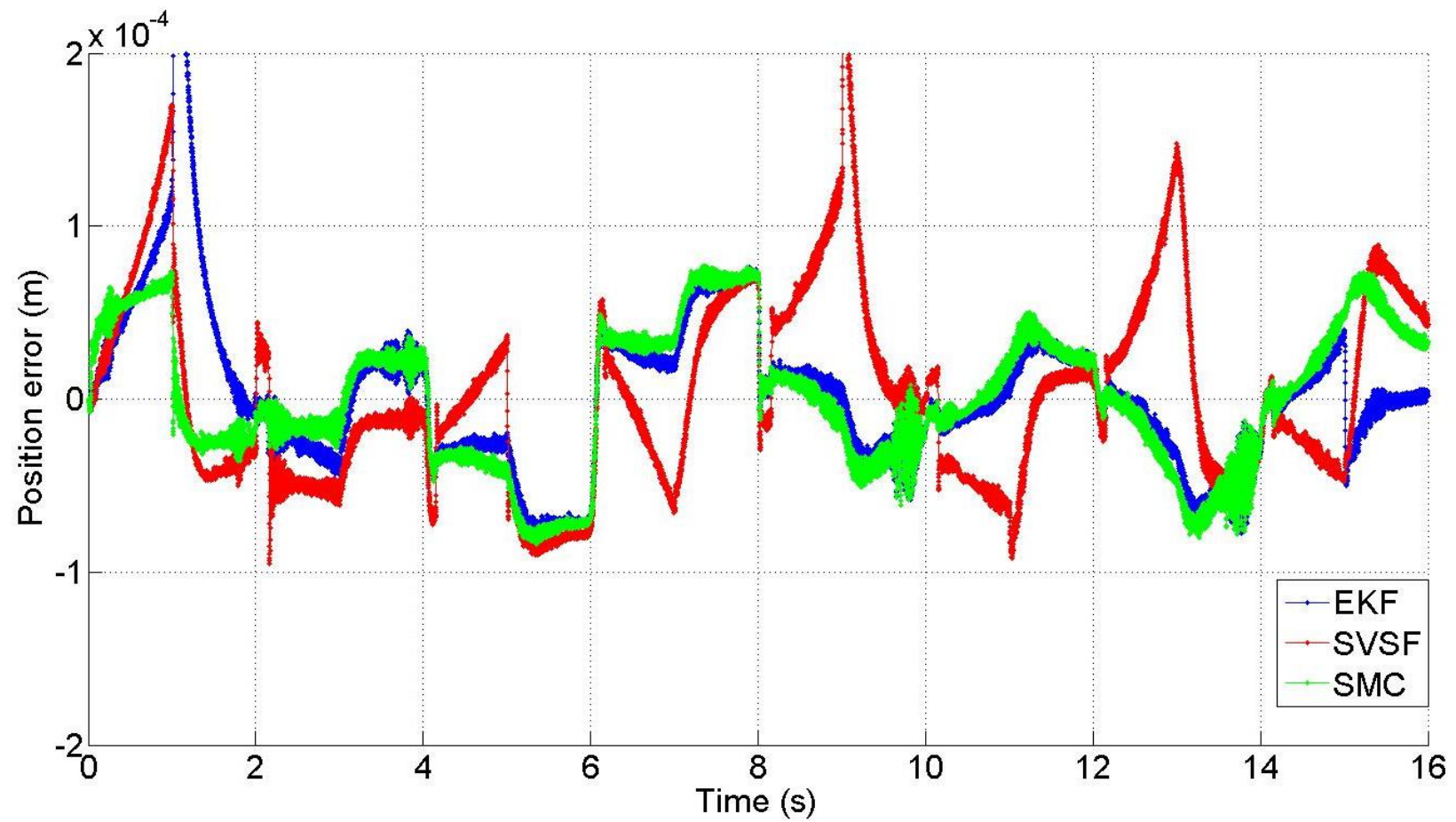


Figure 5.31: Position Errors of Slotine and Li Based SMC, IMM-SMC-KF and IMM-SMC-SVSF

Table 5.12: Experimental Root Mean Square Errors

	<b>Normal</b>			<b>Leakage</b>			<b>Friction</b>			<b>Combine</b>		
	<b>Pos</b>	<b>Vel</b>	<b>Acc</b>									
<b>PID</b>	7.33E-07	8.95E-05	3.05E-06	5.48E-07	8.97E-05	3.23E-06	9.38E-07	8.95E-05	4.73E-06	1.02E-06	8.97E-05	1.82E-06
<b>PID_Eq</b>	<b>3.16E-08</b>	8.83E-05	3.66E-06	<b>2.13E-07</b>	8.85E-05	4.64E-06	<b>1.50E-07</b>	8.83E-05	2.37E-06	<b>2.73E-07</b>	8.86E-05	2.07E-06
<b>Misawa Based</b>												
<b>SMC</b>	6.91E-07	8.10E-05	4.32E-06	1.49E-06	8.10E-05	3.73E-06	6.56E-07	8.12E-05	2.96E-06	8.61E-07	8.15E-05	2.17E-06
<b>IMM_KF</b>	<b>5.85E-07</b>	8.10E-05	5.44E-06	1.44E-06	8.09E-05	4.26E-06	5.85E-07	8.12E-05	4.75E-06	8.06E-07	8.06E-05	4.83E-06
<b>IMM_SVSF</b>	7.78E-07	8.10E-05	4.93E-06	<b>1.18E-06</b>	8.02E-05	9.88E-06	<b>3.08E-07</b>	8.03E-05	8.41E-06	<b>2.84E-07</b>	8.09E-05	5.33E-06
<b>Slotine and Li Based</b>												
<b>SMC</b>	3.35E-07	7.93E-05	3.85E-06	1.22E-06	7.92E-05	4.93E-06	3.38E-07	7.95E-05	2.65E-06	5.18E-07	7.99E-05	2.39E-06
<b>IMM_KF</b>	3.25E-07	7.94E-05	5.23E-06	1.23E-06	7.92E-05	5.22E-06	3.60E-07	7.95E-05	4.14E-06	<b>5.03E-08</b>	7.92E-05	3.16E-06
<b>IMM_SVSF</b>	<b>2.74E-07</b>	7.82E-05	1.29E-05	<b>1.07E-06</b>	7.91E-05	7.32E-06	<b>2.11E-07</b>	7.94E-05	5.60E-06	5.45E-07	8.02E-05	3.48E-06

## 5.5. Conclusion

Eight controllers as described in Chapter 4 were tested for EHA position tracking: PID based (PID, and PID with equivalent control), Misawa based SMC, IMM-SMC-KF, and IMM-SMC-SVSF, and Slotine and Li based SMC, IMM-SMC-KF, and IMM-SMC-SVSF. The same test signal was used for all experiments spanning four operating conditions (normal, leakage, friction, and combined).

A direct comparison of the performance cannot however be made as the assumption concerning model complexity was not consistently applied in the design of controllers.

## Chapter 6

### Remark Conclusions and Future Work

Electro-hydrostatic actuator (EHA) is a displacement control type of hydraulic actuation system, and it is being increasingly used in aircraft flight surface control. EHA has several advantages over traditional hydraulic systems such as compactness, better energy efficiency and modularity. An EHA prototype was produced at McMaster University, and this prototype was used for experimental studies in this research.

This research considered and developed a new control strategy for the EHA position tracking. Several control strategies were also studied and compared. The control strategies studied and implemented on the EHA prototype included:

Group 1:

- PID
- PID with equivalent control

Group 2:

- SMC
- IMM-SMC-SVSF
- IMM-SMC-KF

The following observations were made from experimental evaluation of the above mentioned control strategies:

- By combining SMC with IMM, the IMM-SMC demonstrated a better performance compared to SMC alone.

- By comparing two filtering techniques: smooth variable structure filter (SVSF) and Kalman filter (KF), SVSF combined with IMM-SMC performed better than the KF on model selection.

In designing the control strategies, different assumptions were made pertaining to the model complexity, making a direct comparison between the controllers invalid. Furthermore a saw tooth input profile was used in order to reduce the effect of high order dynamics that were subsequently ignored. These are severe limitations of the results reported in this thesis and restrains the conclusions and observation to the profile in this thesis. The controller implementations studied in this thesis can only be considered as a first step in developing an effective fault tolerant control strategy using the IMM concept. In particular, a more realistic model should have been used.

### **Future Work Recommendation**

A more comprehensive consideration and design of control strategies is require, by considering the full model of the EHA as reported in [36], in order to validate the observations reported in this thesis. Furthermore all controllers were tested under 4 different operating conditions as follows: normal operation, leakage fault, friction fault, and combined leakage-friction fault.

Future studies should consider more fault conditions such as defining different levels of severity on leakage and friction faults and their combination.

## Bibliography

- [1] "HULC," Lockheed Martin, [Online]. Available:  
<http://www.lockheedmartin.com/us/products/hulc.html>.
- [2] "Exoskeleton Suits for Wheelchair Users," Wheelchair, [Online]. Available:  
<http://www.newdisability.com/exoskeletonsuit.htm>.
- [3] K. McCullough, "Design and Characterization of a Dual Electro-Hydrostatic Actuator," McMaster University, Hamilton, January 2011.
- [4] Y. Song, "Electro-hydrostatic Actuator Fault Detection and Diagnosis," McMaster University, Hamilton, September 2012.
- [5] E. Misawa, "Discrete Time Sliding Mode Control for nonlinear System with Unmatched Uncertainties and Uncertain Control Vector," *ASME Journal of Dynamic System, Measurement and Control*, vol. 119, no. 3, pp. 503-512, 1997.
- [6] E. Misawa, "Discrete Time Sliding Mode Control: The Linear Case," *ASME Journal of Dynamic System, Measurement and Control*, vol. 119, no. 4, pp. 819-821, 1997.
- [7] Jean-Jacques E. Slotine and Weiping Li, *Applied Nonlinear Control*, New Jersey: Prentice-Hall International, Inc., 1991.
- [8] S. J. Zhu, "Modeling, System Identification and Control of A Belt Drive System," McMaster University, Hamilton, March 2011.
- [9] V. Utkin, "Variable Structure System with Sliding Modes," *IEEE Transactions on Automatic Control*, vol. 22, pp. 212-222, 1977.
- [10] W. B. Gao and J. C. Hung, "Variable Structure Control of Nonlinear Systems: A New Approach," *IEEE Transactions on Automatic Control*, vol. 40, pp. 45-55, 1993.
- [11] W. B. Gao, "Foundation of Variable Structure Control," China Press of Science and Technology, Beijing, 1990.

- [12] H. Asada and J.-J. E. Slotine, *Robot Analysis and Control*, New York: Massachusetts Institute of Technology, 1986.
- [13] E. Bailey and A. Arapostathis, "Simple Sliding Mode Control Scheme Applied to Robot Manipulator," *Journal of Control*, pp. 1197-1209, 1987.
- [14] C. Dorling and A. Zinober, "Robust Hyperplane Design in Multivariable Variable Structure Control System," *Journal of Control*, pp. 2043-2054, 1988.
- [15] C. Dorling, *The Design of Variable Structure Control System*, University Sheffield, 1985.
- [16] S. R. Habibi and R. J. Richards, "Sliding Mode Control of an Electrically Powered Industrial Robot," *IEE Proceedings-D*, vol. 139, no. 2, March 1992.
- [17] W. B. Gao and J. C. Hung, "Variable Structure Control of Nonlinear Systems: A New Approach," *IEEE Transactions on Industrial Electronics*, pp. 45-55, 1993.
- [18] M. Chaouki and G. Moncef, "Robust Decentralized Sliding Mode Control for Large Scale Uncertain Systems," *Control Conference*, pp. 76-81, 2007.
- [19] N. S. Nise, *Control System Engineering*, 4 ed., John Willy and Sons, 2004.
- [20] K. Ogata, *Modern Control Engineering*, 3 ed., Prentice-Hal, 1997.
- [21] G. Welch and G. Bishop, "An Introduction to the Kalman Filter," *Department of Computer Science*, Vols. NC 27599 - 3175, September 1997.
- [22] M. S. Grewal and A. P. Andrew, *Kalman Filtering: Theory and Practice Using Matlab*, 3 ed., A John Wiley & Sons, Inc, 2008.
- [23] S. Schmidt and L. McGee, "Discovery of the Kalman Filter as a Practical Tool for Aerospace and Industry," *NASA*, vol. Technical Memo 86847, 1985.
- [24] S. A. Gadsden, "Smooth Variable Structure Filtering: Theory and Applications," McMaster University, 2011.
- [25] S. R. Habibi and R. Burton, "The Variable Structure Filter," *Journal of Dynamic Systems, Measurement, and Control (ASME)*, vol. 125, pp. 287-293, September 2003.

- [26] S. R. Habibi, "The Smooth Variable Structure Filter," *Proceeding of the IEEE*, vol. 95, no. 5, pp. 1026-1059, 2007.
- [27] Y. Bar-Shalom, X. R. Li and T. Kirubarajan, *Estimation with Applications to Tracking and Navigation*, New York: John Wiley and Sons, Inc., 2008.
- [28] M. A. El Sayed, S. A. Gadsden, and S. R. Habibi, "A Sliding Mode Controller Based on the Interacting Multiple Model Strategy," 2012.
- [29] S. A. Gadsden, Y. Song and S. R. Habibi, "Novel Model-Based Estimators for the Purposes of Fault Detection and Diagnosis," *IEEE/ASME Transactions on Mechatronics*, vol. 18, no. 4, August 2013.
- [30] "Flight Controls," [Online]. Available: [http://www.faa.gov/regulations\\_policies/handbooks\\_manuals/aviation/pilot\\_handbook/media/PHAK%20-%20Chapter%2005.pdf](http://www.faa.gov/regulations_policies/handbooks_manuals/aviation/pilot_handbook/media/PHAK%20-%20Chapter%2005.pdf). [Accessed May 2014].
- [31] "Control Surface," [Online]. Available: <http://rcmentor.com/glossary/>.
- [32] "Fully Powered Flight Controls," November 2012. [Online]. Available: <http://edallcoin.fatcow.com/ecollege/index.php/aero-sem4/102-aero-sem-4->. [Accessed May 2014].
- [33] "Flight Control Systems," May 2014. [Online]. Available: <http://www.daerospace.com/FlightControlSystems/Irreversible.php>.
- [34] R. Navarro, "Performance of an Electro-Hydrostatic Actuator on the F-18 Systems Research Aircraft," *NASA/TN-97-206224*, October 1997.
- [35] Y. A. Chinniah, "Fault Detection in the Electrohydraulic Actuator Using Extended Kalman Filter," University of Saskatchewan, Saskatchewan, 2004.
- [36] S. Habibi, R. Burton and E. Sampson, "High Precision Hydrostatic Actuation Systems for Micro and Nano Manipulation of Heavy Loads," *ASME Journal of Dynamic Systems, Measurement, and Control*.
- [37] S. Habibi and A. Goldenberg, "Design of a New High Performance Electro - Hydraulic Actuator," *IEEE/ASME Transactions on Mechatronics*, vol. 5(2), pp.

158-164, 2000.

- [38] M. Sepasi and F. Sassani, "On-line Fault Diagnosis of Hydraulic System Using Unscented Kalman Filter," *International Journal of Control, Automation, and Systems*, vol. 8, no. 1, pp. 149-156, 2010.
- [39] W. Igers and T. Papatheodrous, "Fluid-power efficiency on the rise," *Machine Design*, vol. 82, no. 20, pp. 42-45, November 2010.
- [40] X. B. Tran, N. Hafizah and H. Yanada, "Modeling of Dynamic Friction Behaviors of Hydraulic Cylinders," *Mechatronics*, vol. 22, no. 1, pp. 65-75, February 2012.
- [41] S. Wang, S. R. Habibi and R. Burton, "Sliding Mode control for a Model of an Electrohydraulic Actuator System with Discontinuous Nonlinear Friction," *American Control Conference*, p. 38, 2006.
- [42] M. Araki, "Control Systems, Robotics, and Automation," *Encyclopedia of Life Support System, ELOSS*, vol. 2, 2011.
- [43] M. A. El Sayed, "Multiple Inner-loop Control of An Electro-hydrostatic Actuator," McMaster University, Hamilton, 2012.
- [44] G. Bone, Mech Eng 751 Course Notes, Hamilton: McMaster University, 2014.